Nicholas Alonzo Frost
MD/PhD

University of Maryland School of Medicine
Program in Neuroscience

EDUCATION

2012	MD University of Maryland School of Medicine Baltimore, Maryland
2012	PhD, Neuroscience University of Maryland School of Medicine Baltimore, Maryland Advisor: Dr. Thomas Blanpied
2003	Florida State University Tallahassee, Florida B.S. “With Honors” in Biochemistry B.A. Foreign Language (Spanish)

OTHER RESEARCH TRAINING

Imaging Structure and Function in the Nervous System, summer course (2008)
Cold Spring Harbor Laboratory

Cancer Research Training Award, Laboratory of Dr. Stuart Yuspa.
National Cancer Institute, National Institutes of Health, Bethesda, Maryland

Summer Internship, Pfizer Pharmaceuticals, Ann Arbor Michigan (2001)

RESEARCH FUNDING

NIMH F30 Kirschstein-NRSA MH086185-01 Regulation of Actin Polymerization at Functional Subdomains within Dendritic Spines (2009-2012), National Institutes of Mental Health

Membrane Training Program T32 GM008181 (2007-2008), University of Maryland School of Medicine

Leslie B. Barnett, M.D. Memorial Student Fellowship in Neurology (2007), University of Maryland School of Medicine

Summer Training in Aging Research Topics – Mental Health Fellowship (2006), University of California, San Diego & The National Institute of Mental Health

Fischer Fellowship for Undergraduate Research (2002), American Cancer Society

AWARDS

American Academy of Neurology Medical Student Prize for Excellence in Neurology (2012), American Academy of Neurology

PhD Scholar Award (2009), University of Maryland School of Medicine

Section Winner, Poster Presentation, Graduate Research Conference (2007), University of Maryland School of Medicine

First Place Poster Presentation, Medical Student Research Day (2006), University of Maryland School of Medicine

"Honors," Host Defense and Infectious Disease (2006), University of Maryland School of Medicine

"Honors," Functional Systems (2006), University of Maryland School of Medicine

Bess Ward Scholarship for International Scholastics (2001), Florida State University

National Merit Scholarship, Full Tuition, Room and Board (1999-2003)

POSITIONS HELD

Curriculum Committee, MD/PhD Program (2011-2012)
Interview Committee, MD/PhD Program (2009-2010)
Translational Research in Medicine Journal Club, Founder (2006-2009)
Medical School Student Government President (2006-2007)
United Student Government Association Representative (2005-2006)

PUBLICATIONS AND PRESENTATIONS

Peer Reviewed Publications

"CaMKII dynamics and localization in spines and dendrites resolved by single-molecule tracking PALM." Hsiangmin E Lu, **Nicholas A. Frost**, and Thomas A. Blanpied; In Preparation.

"Optimization of cell morphology measurement via single-molecule tracking PALM." **Nicholas A. Frost**, Hsiangmin E. Lu, Thomas A. Blanpied. In Press.

"Unique Vesicular Trafficking Mechanisms Underlies the Proximal Localization of Kv2.1 Channels in Neurons." Camilla S. Jensen, Hanne B. Rasmussen, Nicole Schmitt, Søren-Peter Olesen, **Nicholas A. Frost**, Thomas A. Blanpied, and Hiroaki Misonou. In Revision.

"Outer membrane targeting, Ultrastructure, and single molecule localization of BfpB, the Enteropathogenic Escherichia coli Type IV Pilus Secretin." Joshua Lieberman, **Nicholas A Frost**, Michael Hoppert, Paula Fernandes, Stephanie Vogt, Tracy Raivio, Thomas A Blanpied, Michael Donnenberg; Journal of Bacteriology, 2012, 194(7):1646. DOI: 10.1128/JB.06330-11.

"Single-Molecule Discrimination of Discrete Perisynaptic and Distributed Sites of Actin Filament Assembly within Dendritic Spines." **Nicholas A. Frost**, Hari Shroff, Huihui Kong, Eric Betzig, Thomas A. Blanpied; Neuron, 67(1): 86-99, 2010.

"PTH transiently increases the mobile fraction of Npt2a in OK cells as determined by FRAP." Edward j. Weinman, Deborah Steplock, Boyoung Cha, **Nicholas A. Frost**, Rochelle Cunningham, Shirish Shenolikar, Thomas A. Blanpied, Mark Donowitz; Am J Physiol Renal Physiol. 2009 Dec;297(6):F1560-5.

"AP-1 activity regulates epithelial tumor cell identity." Michael J. Gerdes, Maxim Myakishev, **Nicholas A. Frost**, Vikas Rishi, Jaideep Moitra, Asha Acharya, Michelle R. Levy, Sang-won Park, Adam Glick, Stuart H. Yuspa, and Charles Vinson; Cancer Research, 66 (15): 7578, 2006.

Reviews

"A network of networks: cytoskeletal control of compartmentalized function within dendritic spines." **Nicholas A. Frost**, Justin M. Kerr, Hsiangmin E. Lu, Thomas A. Blanpied; Current Opinions in Neurobiology, doi:10.1016/j.conb.2010.06.009.

Book Chapters

"Live-cell PALM of intracellular proteins in neurons." **Nicholas A. Frost**, Harold MacGillavry, Hsiangmin E. Lu, Thomas A Blanpied; In Press.

Selected Abstracts and Posters

"Uncoupling illumination duration from acquisition for increasing localization precision of rapidly moving molecules in the neuronal membrane." **Nicholas A. Frost**, Hsiangmin E Lu, and Thomas A Blanpied; Society for Neuroscience, Washington DC (2011).

"CaMKII dynamics and localization in spines and dendrites resolved by single-molecule tracking PALM." Hsiangmin E Lu, **Nicholas A. Frost**, and Thomas A. Blanpied; Society for Neuroscience, Washington DC (2011).

"A Case of Magnesium-Responsive Paraneoplastic Non-convulsive Status Epilepticus." Robert Shin, Anna Rosenbaum, **Nicholas A. Frost**; Annual meeting of the American Neurological Association, San Diego (2011).

"Sub-cellular Localization of the Enteropathogenic *Escherichia coli* Type IV Pilus Secretin, BfpB using Photo-Activation Localization Microscopy." Joshua Lieberman, **Nicholas A. Frost**, Thomas Blanpied, Michael Donnenberg; American Society for Microbiology, 2011.

"Single-Molecule Discrimination of Discrete Perisynaptic and Distributed Sites of Actin Filament Assembly within Dendritic Spines." **Nicholas A. Frost**, Hari Shroff, Huihui Kong, Eric Betzig, Thomas A. Blanpied; Gordon Conference: Cellular Biology of the Neuron, Waterville, NH (2010).

"Local dynamics of actin polymerization resolved within dendritic spines by single-particle tracking PALM." **Nicholas A. Frost**, Hari Shroff, Huihui Kong, Eric Betzig, Thomas A. Blanpied. Society for Neuroscience Annual Meeting; 421.12/D26, Chicago, 2009.

"Local dynamics of actin polymerization resolved within dendritic spines by single-particle tracking PALM." **Nicholas A. Frost**, Hari Shroff, Huihui Kong, Eric Betzig, Thomas A. Blanpied. Gordon Conference: Excitatory Synapses; Les Diableret, Switzerland, 2009.

"Spatial Regulation of Dendritic Spine Actin by Cortactin." **Nicholas A. Frost**, Justin Kerr, Steven Zhan, Thomas A. Blanpied. Society for Neuroscience Annual Meeting, San Diego, (November 2008).

"Localization and Kinetics of Actin Dynamics in Dendritic Spines Controlled by Protein Interactions at the Postsynaptic Density." **Nicholas A. Frost**, Steven Zhan, Thomas A. Blanpied. Summer Topics in Aging Research – Mental Health Conference, University of California, San Diego, (August 2006).

"Disruption of AP-1 Activity Alters Epidermal Lineage Commitment and Carcinogenesis." **Nicholas A. Frost**, Michael J. Gerdes, Michelle R. Levy, Ashanti Woods, Jaideep Moitra, Adam B. Glick, Charles Vinson, Stuart H. Yuspa. American Association for Cancer Research, (April 2004).

"AP-1 Transcriptional Activity Determines Keratinocyte Lineage Commmitment During Tumorigenesis." Michael J. Gerdes, **Nicholas A. Frost**, Michelle R. Levy, Ashanti Woods, Jaideep Moitra, Adam B. Glick, Charles Vinson, Stuart H. Yuspa. Society of Investigative Dermatology LXV (2004).

"Cloning of the Human Kallikreins," **Nicholas A. Frost**, Sachiko I Blaber, and Michael Blaber, FLACS LVI, 19 (2003).

Undergraduate Thesis:
"Cloning of the Human Kallikreins." Advisor: Dr. Michael Blaber, Florida State University, (2003).

Abstract

Excitatory synapses within the brain occur on dendritic spines. Within the spine the branching, filamentous network of the actin cytoskeleton anchors receptors in the postsynaptic density and is critical to the regulation of synaptic transmission. The mechanisms whereby actin regulates synaptic function are vague and may consist of direct interaction with receptors in the synaptic or extrasynaptic membrane, propulsive forces at the base or sides of the postsynaptic density (PSD), enhancement of local recycling, or selective filtering of membrane protein mobility through the spine neck. Furthermore, it is unclear where polymerization takes place within spines, and whether regulation of the network occurs *en bloc* as it has been measured in the past or if specific subregions of the network may be regulated in response to local demands. I propose a model in which actin networks within individual dendritic spines have multiple points of control at distributed locations, allowing regulation of parts of the network within specific spine subdomains.

The submicron dimensions of spines have limited examination of actin dynamics within spines and prevented live-cell discrimination of perisynaptic actin filaments. To overcome this I used Photoactivated Localization Microscopy (PALM) to localize with a high degree of accuracy and track single polymerized actin molecules within dendritic spines. I use Monte Carlo simulations to test the effect of diffusion on localization accuracy, demonstrating that motion blur from rapidly moving molecules negatively impacts localization accuracy. In addition, when imaging freely diffusing molecules, the distance molecules travel during the course of excitation affects their localized position with respect to the edge of a bounded region, again necessitating very short excitation

pulses to accurately measure morphology. On the other hand, slowly moving molecules, such as polymerized actin are mostly spared from these effects. Thus, this motion blur provides a mechanism to specifically track polymerized actin molecules by using long exposures in which freely diffusing molecules are blurred.

Using PALM I show that the velocity of single actin molecules along filaments, an index of filament polymerization rate, was highly heterogeneous within individual spines. Most strikingly, molecular velocity was elevated in discrete, well-separated foci occurring not principally at the spine tip, but in subdomains throughout the spine, including the neck. Whereas actin velocity on filaments at the synapse was substantially elevated, those at the endocytic zone showed no enhanced polymerization activity. I conclude that actin subserves spatially diverse, independently regulated processes throughout spines. Perisynaptic actin forms a uniquely dynamic structure well suited for direct, active regulation of the synapse.

Actin dynamics at nanometer domains within individual dendritic spines.

by
Nicholas A. Frost

Dissertation submitted to the Faculty of the Graduate School
of the University of Maryland, Baltimore in partial fulfillment
of the requirements for the degree of
Doctor of Philosophy
2012.

To Sara Lux

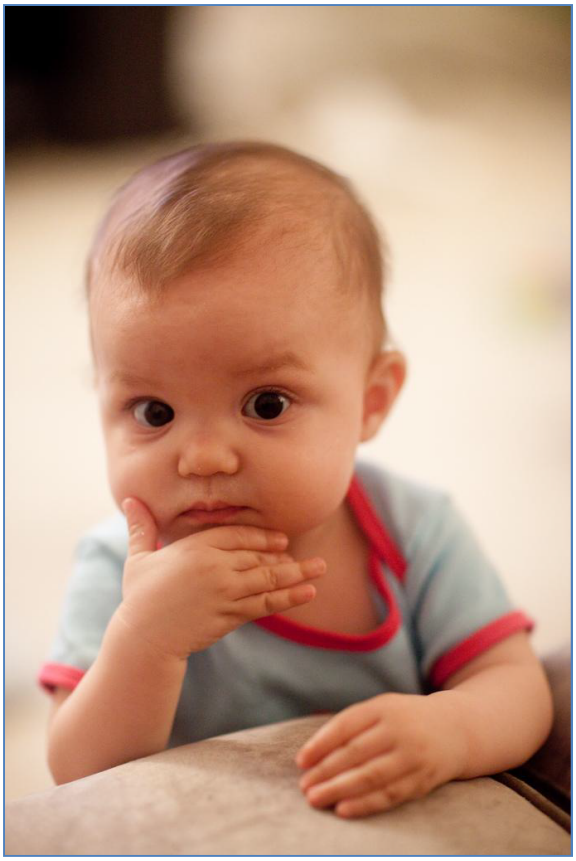

ACKNOWLEDGEMENTS

I thank my thesis committee consisting of Dr. Brad Alger, Dr. Robert Bloch, Dr. Terry Rogers, and Dr. Scott Thompson for their support and suggestions regarding this work and Dr. Thomas Blanpied for his guidance and mentorship throughout my time in Baltimore.

I thank the following for supplying plasmids: S. McKinney (mEos2-actin), B. Imhof (GFPactin), G. Patterson (PA-GFP), M. Rizzo (cerulean), J. Lippincott-Schwartz (tdEos-paxillin), D. Bredt (PSD-95-GFP), R. Y. Tsien (tdTomato, mCherry), G. Feng (GKAP), and M. Davidson (Dronpa). I thank also J. Kerr, H. Lu, and H. MacGillavry for helpful discussions, and M. Ehlers, J. Bear, and S. Thompson for comments on manuscripts. Support was provided by a Summer Training in Aging Research Topics - Mental Health (Start-MH) fellowship, Training Grant NIGMS T32GM008181, and NRSA F30MH086185 (NAF), and NIMH R01MH080046, The Dana Foundation, and the Katherine D. and Theodore J. Carski Foundation (TAB).

Table of Contents:

Chapter		Page
Preface	…….	iii
1.	Introduction …….	1
	a. The Dendritic Spine …….	1
	b. The Spine in Plasticity …….	8
	c. Spines as Compartmentalized Units …….	13
	d. The Spine Actin Cytoskeleton …….	18
	e. Regulating the Structure and Function of Actin Networks	22
	f. A network of networks: cytoskeletal control of compartmentalized function within dendritic spines……..	32
	g. Summary and Hypothesis …….	43
2.	Developing PALM for imaging neuronal morphology …….	48
3.	Independent Regulation of actin polymerization at discrete sites within the spine …….	88
4.	Spatial regulation of spine actin networks by cortactin …….	140
5.	Discussion …….	150
6.	Future Directions …….	152
7.	Appendix …….	156
8.	References …….	174

1. Introduction

a. The Dendritic Spine

Excitatory neurotransmission between neurons in the mammalian brain occurs on dendritic spines. Housing the postsynaptic machinery of the excitatory synapse, spines are micron-sized, bulbous structures which protrude from the neuronal dendrite. Directly apposed to the presynaptic terminal, the spine encloses a number of specialized structures thought to be critical to the efficient reception and transduction of synaptic input, including the postsynaptic density (PSD), the endocytic zone (EZ) (Blanpied, Scott et al. 2002; Blanpied, Scott et al. 2002), a recently described exocytic domain (Kennedy, Davidson et al. 2010), the spine apparatus (Deller, Korte et al. 2003; Deller, Orth et al. 2007), and the spine neck. These structures can be thought of as functional spine subdomains, as they perform spatially and temporally segregated roles governing the function of individual postsynaptic units.

Neurotransmitter receptors are positioned and anchored in the postsynaptic membrane by a thick, electron-dense web of scaffolding molecules known as the postsynaptic density (hereafter referred to as the PSD). The number and perhaps even the nanometer positioning (Raghavachari and Lisman 2004)) of neurotransmitter receptors within the synaptic membrane are critical for the consistent and reliable transduction of synaptic input. AMPA receptors open in response to the binding of released glutamate, allowing a depolarizing current to flow into the cell. This depolarization relieves the magnesium block on NMDA receptors, allowing calcium to enter the cell. Thus, increased AMPA

receptor numbers at the synapse permits greater depolarization in response to vesicle release, and indirectly increases the activation of NMDA receptors.

The importance of subsynaptic receptor positioning depends largely on the relative saturation of the synaptic receptors by single vesicle release. The low affinity of AMPA receptors for glutamate means that in many cases (Liu, Choi et al. 1999; McAllister and Stevens 2000), individual synapses are not saturated by quantal release. As the width of the postsynaptic scaffold far exceeds the width of the synaptic cleft, the concentration of glutamate following release is not even across the synapse. This spatial heterogeneity of glutamate concentration potentially restricts activation to a subset of postsynaptic receptors; modeling has demonstrated that while receptors directly apposed to the release site may be activated, receptors randomly distributed within the PSD may not be activated (Raghavachari and Lisman 2004). Furthermore, as the relative rates of activation to inactivation increase for highly ligand-bound channels, receptors near the release site are likely to be open immediately following vesicle release, whereas channels outside the glutamate “hotspot” exhibit an increased likelihood of becoming inactivated. Thus, subsynaptic regulation of receptor density may have important physiological consequences for the strength of the synapse.

This concept is difficult to test experimentally, but indirect supporting evidence comes from the observation that perturbations that increase the mobility of AMPA receptors within the synapse also reduce the degree of paired pulse depression observed (Heine, Groc et al. 2008; Frischknecht, Heine et al. 2009; Opazo, Labrecque et al. 2010).

Thus, cross-linking AMPA receptors with antibodies slows their effective motion and also increases paired-pulse depression (Heine, 2008). Increasing the degree to which receptors are stabilized within the PSD by CaMKII-mediated phosphorylation of stargazin (Opazo, Labrecque et al. 2010) mirrors this effect. Conversely, increasing the mobility of extracellular AMPA receptors by enzymatic removal of extracellular matrix had the opposite effect (Frischknecht, Heine et al. 2009). The authors of these studies conclude that paired pulse depression in their system is due to the local inactivation of receptors following stimulation, and that the degree of paired pulse depression can be reduced if these inactivated receptors can freely exchange with other non-inactivated receptors within the PSD. These studies have several caveats. First, they assume that consecutive vesicles are released from the same release site at individual synapses within a very short amount of time (50 ms). Secondly, the conclusion seems to disregard the potential that receptors outside the "hotspot," which supposedly exchange with activated and subsequently inactive AMPA receptors within the "hotspot," have a higher likelihood of being inactivated. Nevertheless, these studies as a group make a strong case that AMPA receptor mobility within the synapse has the potential to affect synaptic signaling.

Although the regulation of subsynaptic receptor distribution is largely theoretical, the regulation of receptor number at individual synapses has been observed in a number of contexts ((Matsuzaki, Honkura et al. 2004; Bagal, Kao et al. 2005; Lee, Yasuda et al. 2010). This regulation likely requires the coordinated activity of several spine subdomains. Although the relative contribution may be context-dependent, the principle

mechanisms proposed to regulate synaptic receptor number are receptor ‘trapping’ or retention within the PSD and regulation of surface receptor numbers.

Imaging studies using single particle tracking (Heine, Groc et al. 2008) have demonstrated that AMPA receptors at the cell surface exchange freely between extrasynaptic and synaptic membrane, with behavior approaching Brownian motion within extrasynaptic spaces. At the synapse, the behavior of individual receptors is markedly different, with receptors pausing for extended periods of time, suggesting that some impediment to free diffusion exists while they are within the confines of the PSD. As a population, FRAP studies of super-ecliptic GFP tagged receptors reveal that synaptic receptors are much more stable than freely diffusing extrasynaptic receptors (Ashby, Maier et al. 2006). Taken together, this evidence suggests that stable receptors at the synapse are drawn from a pool of freely diffusing extrasynaptic receptors, with receptors able to exchange between the two pools. Thus, as all synapses draw from the same extrasynaptic receptor pool, individual synapses must be better able to retain their captured receptors to increase their strength relative to neighbors.

This retention or stability of receptors at the PSD depends on the quantity of binding partners in the postsynaptic density. In the brain of the adult rat, strong synapses are associated with increased PSD surface area and scaffold content. Large PSDs occur on spines with increased spine head volume (Harris and Stevens 1988; Harris and Stevens 1989) and there is a strong correlation between the size of the PSD and spine head with the size of the presynaptic terminal and the number of vesicles it contains. Larger PSDs

provide a greater number of interacting scaffold molecules, termed “slot proteins” (Hayashi, Shi et al. 2000; Ehrlich and Malinow 2004). The term slot protein refers to PDZ-domain containing proteins, such as PSD-95, which have the capacity to retain receptors at the synapse through interactions with either the receptor (Hayashi, Shi et al. 2000) or with AMPA receptor accessory protein, stargazin (Bats, Groc et al. 2007). Both of these interactions may be important for the retention of AMPA receptors at the synapse. Overexpression of PSD-95 recruits GluR1 to synapses and occludes LTP induction (Ehrlich and Malinow 2004; Ehrlich, Klein et al. 2007). CaMKII activity has been shown to lead to recruitment of AMPAR to the synapse in a PDZ binding-domain dependent manner (Hayashi, Shi et al. 2000). However, a later study demonstrated that stabilization of AMPAR at the synapse by CaMKII depended on stargazin, and not on the PDZ binding-domain of AMPAR (Opazo, Labrecque et al. 2010).

The molecular crowding within the synaptic membrane overlying the PSD provides yet another mechanism for the regulated retention of receptors at the synapse. Modeling experiments reveal that the tortuous path taken by receptors diffusing through a crowded space could result in extended dwell times within the PSD, even in the absence of binding interactions. Indeed, increased binding interactions actually increased the rate of diffusion experienced by receptors within the PSD (Santamaria, Gonzalez et al. 2010). Importantly, the dwell time of receptors was found to be extremely sensitive to small changes in the concentration of crowding molecules, indicating that receptor retention could be regulated by the addition or removal of a small percentage of the total molecules within the PSD.

Thus, the composition of the PSD is critical in regulating the rate of exchange of receptors to and away from the synapse. Away from the synapse, the coordinated activity of several other spine subdomains may influence synaptic receptor numbers by regulating extrasynaptic receptor number or delivery. The endocytic zone is a functionally-named structure found in the majority of mature spines (Blanpied, Scott et al. 2002) and is marked by the presence of clathrin at the spine membrane. The finding that recycling of AMPA receptors was actually necessary both for the delivery of AMPA receptors during LTP and for the maintenance of basal synaptic receptor numbers over time suggested that the endocytic zone may play an active role in local recycling of AMPA receptors at single spines (Park, Penick et al. 2004; Park, Salgado et al. 2006). Furthermore, treatment with thrombin for 4 hours to remove HA tags specifically from receptors located at the surface revealed that virtually all receptors delivered during glycine stimulation came from recycling endosomes and had been on the surface at least one time prior to the stimuli-driven insertion.

That the endocytic zone was located on the spine implied that recycling occurred locally; however numerous studies using tagged receptors to investigate the site of receptor insertion observed robust insertion along the neuronal dendrite, but not in the spine itself (Yudowski, Puthenveedu et al. 2007). Another recent study concluded that the location of insertion was irrelevant because sufficient numbers of receptors exist on the cell surface to supply all the added receptors during LTP (Makino and Malinow 2009). However, studies have now observed exocytosis occurring within the spine head (Kennedy, Davidson et al. 2010) in a syntaxin-4-dependent manner. Thus, individual

spines possess all the machinery required for the traffic and recycling of their own receptors. Further augmenting the ability of spines to self-regulate their surface protein composition is the presence of long, thin necks found on mushroom spines. Many spine necks within hippocampal spines are less than 100 nm in diameter, providing a mechanism whereby surface (Ashby, Maier et al. 2006) and cytosolic signaling molecules (Svoboda, Tank et al. 1996; Majewska, Tashiro et al. 2000; Bloodgood and Sabatini 2005) may be sequestered.

Finally, more than 80% of mushroom spines in the adult rat brain contain a mysterious structure known as the spine apparatus, which associates with the PSD and the actin cytoskeleton (Spacek and Harris 1997). Although its function is largely unknown, the spine apparatus has been proposed to function as a reservoir for internally stored calcium, which may augment synaptic calcium influx through NMDA channels (Emptage, Bliss et al. 1999).

Underlying all these structures is a dense, filamentous actin cytoskeletal network. The protrusive force of continuously polymerizing actin filaments is well-known to form the basis of spine morphology. In addition, the actin cytoskeleton plays critical roles in a number of processes thought to be important in the maintenance of synaptic function which will be covered later.

b. The Spine in Plasticity

The synapse is the point of communication between neurons, and therefore is a critical point of control for network activity activity in the brain. To maintain stable network activity, mechanisms must exist to maintain the function of individual synapses over timescales approaching the lifespan of an organism. On the other hand, synapses are plastic, and rapid, long-lasting changes in the strength of individual synapses are thought to underlie many forms of behavioral and developmental learning and memory formation. Thus, for the normal functioning of many neuronal circuits, mechanisms must exist which both preserve the stability and composition of synapses over long periods of time, while allowing rapid modification of the strength or efficacy of individual synapses within seconds or minutes.

Experimentally, a number of protocols have been devised whereby synaptic strength can be rapidly and persistently modified. Our ability to induce various forms of synaptic plasticity in specific preparations is not ubiquitous, and the underlying mechanisms may vary widely. To keep this discussion brief I will focus on plasticity of the hippocampal CA3-CA1 synapse. The hippocampus is well-studied due to its role in learning and memory, and because its laminar structure facilitates the isolation of a well-defined circuit. A number of experimental protocols lead to long term potentiation (LTP), which is characterized by a rapid and persistent increase in synaptic strength. Likewise, long term depression (LTD) is an experimental paradigm in which a net decrease in synaptic strength is induced.

While a number of mechanisms have been proposed to underlie various forms of activity-induced synaptic plasticity, increasing molecular and physiological evidence suggests that the locus for synapse modification within the CA3-CA1 synapse is postsynaptic. Entry of extracellular calcium through calcium channels at the presynaptic active zone is required to promote release of glutamate-containing synaptic vesicles, which binds postsynaptic AMPA receptors, depolarizing the postsynapse. Depolarization of the postsynaptic neuron releases the magnesium block of synaptic NMDA receptors, allowing the influx of calcium into the spine. Reduced extracellular magnesium facilitates NMDA receptor-dependent LTP induction, which can be prevented pharmacologically by inhibition of NMDA receptor currents by APV or chelation of intracellular calcium (Lynch, Larson et al. 1983). Downstream of calcium entry, plasticity is mediated by an intricate web of intracellular signaling molecules within the postsynaptic spine.

In general, induction of LTP requires the activation of intracellular kinases, including CaMKII (Lisman 1985; Malenka, Kauer et al. 1989; Malinow, Schulman et al. 1989; Malinow and Tsien 1990; Malinow and Tsien 1991; Otmakhov, Griffith et al. 1997) and PKA (Lee, Barbarosie et al. 2000; Malleret, Alarcon et al. 2010) whereas induction of LTD requires the activation of phosphatases such as PP1, Calcineurin/PP2B (Zhou, Homma et al. 2004) and protein phosphatase C (Dell'Acqua, Smith et al. 2006). In many cases the ultimate target of these proteins, including AMPA receptor subunits, are the same (Barria, Derkach et al. 1997; Barria, Muller et al. 1997; Lee, Barbarosie et al. 2000). Thus a careful balance of the phosphorylation state of AMPAR and other target proteins is essential to stability of synaptic strength.

This balance is achieved by a number of mechanisms. In the case of CaMKII, one possible mechanism is persistent autophosphorylation. Activated by calcium influx at the synapse, calmodulin binds and activates CaMKII. CaMKII bound to NMDA receptors at the synapse can then be maintained in an activated state by interactions with the NMDA receptor until neighboring subunits of the dodecameric complex phosphorylate the Thr286 site, leading to persistent activation of the kinase (Reviewed in (Lisman, Schulman et al. 2002)). A small population of CaMKII at the synapse could then theoretically (Miller, Zhabotinsky et al. 2005) remain activated for weeks or months. Indeed, CaMKII activity has been demonstrated to remain persistently activated for periods of an hour (Fukunaga, Stoppini et al. 1993; Fukunaga, Muller et al. 1995) and perhaps remain even longer (Lisman and Zhabotinsky 2001). In contrast, optical measurement of CaMKII activity by FRET following induction of LTP at single synapses (Lee, Escobedo-Lozoya et al. 2009), demonstrated that at the very least, the vast majority of CaMKII in individual spines becomes inactivated or leaves the spine within minutes of LTP induction, suggesting that CaMKII is not persistently activated at the synapse.

However, it is possible that the recruitment of large numbers of CaMKII molecules into the spine during LTP may mask of the activation state of a small number of NMDA receptor-bound or PSD-resident CaMKII in these experiments. Many of these CaMKII molecules may bind sites outside the PSD and their numbers are far in excess of synaptic NMDA receptors or other potentially important targets. These transient CaMKII molecules represent over 80% of the CaMKII in stimulated spines, where they are less stably localized, turning over with a time constant of approximately one minute (Lee,

Escobedo-Lozoya et al. 2009). This is in sharp contrast to another, more stable fraction of CaMKII molecules, representing nearly 50% of CaMKII in unstimulated spines, which turns over with a time constant nearly 20 times slower. Accordingly, it is quite possible that transient CaMKII may or may not share a common state of activation with a small number of stable, persistent CaMKII molecules localized in nanodomains at or near the synapse.

Another particularly intriguing possibility whereby the balance of phosphorylation may be regulated at the synapse is through positioning or localization of the signaling molecules themselves. As already mentioned, CaMKII is recruited to individual spines during LTP induction (Lee, Escobedo-Lozoya et al. 2009). CaMKII is one of the principal molecules of the postsynaptic density, and binds to a number of molecules at the synapse, including the NMDA receptor, and its activity may be influenced by this interaction. CaMKII dodecamers contain both CaMKII-alpha and CaMKII-beta, which also binds and bundles actin fibers (Okamoto, Bosch et al. 2009), suggesting a mechanism for its localization at sites away from the PSD. Likewise, PKA can be localized at the synapse through interactions with the PSD scaffold molecule AKAP79/150 (Horne and Dell'Acqua 2007). In both cases, the localization of these signaling molecules may position them in nanodomains where they are efficiently activated, and also potentially importantly, near the site of many of their physiological targets, including synaptic AMPA receptors. During LTD induction, AKAP79/150 translocates rapidly out of spines, and thus PKA targeting to the PSD is lost. This disrupts the balance between phosphorylation by synaptic PKA and dephosphorylation by PP1 in

the PSD, thus resulting in a net dephosphorylation of these proteins' targets within the PSD.

The principle outcome attributed to all this signaling is altered strength of the synapse. In the CA3-CA1 synapse this is primarily due to changes in synaptic AMPA receptor number. Parallel phosphorylation of AMPA receptors by PKA and CaMKII (Lee, Barbarosie et al. 2000; Esteban, Shi et al. 2003) are required for their insertion into the neuronal membrane and incorporation at the synapse. Receptors may be trapped within the synapse by interactions between the PSD scaffold and CaMKII phosphorylated stargazin (Opazo, Labrecque et al. 2010) or the receptors themselves.

In addition to changes in receptor number, a number of other changes occur within the spine in concert with synaptic plasticity induction. Perhaps most notably, in many cases spine morphological plasticity occurs with modification of synaptic function. Thus, LTP is often (Matsuzaki, Honkura et al. 2004; Harvey and Svoboda 2007) but not always (Bagal, Kao et al. 2005) accompanied by increases in spine volume, where LTD is often associated with spine shrinkage.

In short, alterations in synaptic strength can be induced experimentally that involve changes in the structure and function of the synapse postsynaptically. The fact that LTP can be induced by glutamate uncaging specifically at individual synapses, with no effect on neighboring synapses, strongly suggests that individual synapses are capable of autonomous self-regulation. Thus, it seems fair to say that the molecular machinery

required for induction of plasticity at individual synapses may be located very near the synapse, and indeed inside the spine.

c. Spines as Compartmentalized Units

Individual synapses can be regulated independently of neighboring synapses even as close as a micron away (Matsuzaki, Honkura et al. 2004; Bagal, Kao et al. 2005; Harvey and Svoboda 2007; Lee, Yasuda et al. 2010). This feature has both been demonstrated by multiple labs, and used as a tool to study many features of both Hebbian and homeostatic plasticity. LTP induction at single spines using glutamate uncaging activates NMDA receptors, leads to a recruitment of glutamate receptors (Matsuzaki, Honkura et al. 2004; Bagal, Kao et al. 2005) and in many cases initiates spine enlargement by modulation of actin dynamics.

For plasticity to be reliably expressed at one synapse independently of its neighbors, cross-talk between synapses must be minimized. This is a particularly startling feat, as synaptically induced depolarization of the cellular membrane passively spreads along the entire dendrite, and few spine necks are thin enough to electrically decouple the spine head from the parent dendrite (Harris and Stevens 1988; Harris and Stevens 1989). Passive spread of calcium may stretch up to 10 microns along the neuronal dendrite (Santamaria, Wils et al. 2006), where it may activate signaling cascades well away from the stimulated synapse. Finally, synaptic molecules such as PSD-95 and Shank are lost from the PSD with time constants of 20 to 30 minutes and upon being lost from one synapse may be redistributed among neighboring synapses (Gray, Weimer et al. 2006;

Tsuriel, Geva et al. 2006). Naturally, this occurs much more rapidly for molecules less tightly bound, such as actin which turns over with time scales less than a minute, and other signaling molecules including Ras (Harvey, Yasuda et al. 2008) which may redistribute within seconds.

Given that the basic components of synapses are being constantly redistributed and shared, how can an individual synapse maintain its identity, and moreover, how can a synapse tune itself in response to synaptic activity that it receives while remaining unaffected by input at other synapses? A set of papers by Harvey and Svoboda shed light on these questions by testing the distance rules over which synaptic input is effectively shared between neighboring synapses. In the first paper (Harvey and Svoboda 2007), two photon glutamate uncaging was used to induce LTP at single dendritic spines. By pairing an initial strong LTP stimulus with a subsequent weak stimulus at a neighboring synapse, the investigators demonstrated that information was indeed shared between the two spines, as the normally sub-threshold weak stimulus became sufficient to induce spine growth at the second synapse. In the second paper (Harvey, Yasuda et al. 2008), using two photon Fluorescence Lifetime Imagine FRET (FLIM) following LTP induction at single spines, they suggested that signaling molecules, in this case Ras, may diffuse freely along the dendrite, and that the activation radius is effectively limited by the lifetime of their activation.

On the other hand, the same approach to measure the spread of other LTP-activated signaling molecules has demonstrated that this phenomenon is not universal,

and indeed, that many activated molecules, including CaMKII and Cdc42, inactivate before leaving the spine (Lee and Yasuda 2009). Thus, while certain activated molecules may spread quickly enough along the dendrite to reach neighboring synapses, where they may facilitate the priming of LTP induction, it appears that these "promiscuous" molecules are not sufficient for induction of spine structural plasticity or LTP on their own. Thus, mechanisms must exist to keep the key players in the right place. Spines possess ample, stable binding partners for many of the signaling molecules thought to be important in regulating synaptic strength. In the case of CaMKII, which accumulates in spines during LTP induction, it is possible that the spine actually creates new binding sites to prevent activated CaMKII from escaping stimulated spines. The inactivation kinetics of activated CaMKII, while perhaps faster than originally thought (Lee and Yasuda 2009), still approach a minute; this is ample time for even a molecule as large (Kolodziej, Hudmon et al. 2000) as activated CaMKII (100 angstroms x 200 angstroms) to diffuse freely to neighboring spines.

The spine machinery has several mechanisms to prevent this from occurring. CaMKII may be hampered by the slender neck of many mushroom spines, which in many cases may be as small as 30-50 nm (Harris and Stevens 1988; Harris and Stevens 1989) and is often packed with smooth endoplasmic reticulum and actin filaments. The thinness of the spine neck thus makes it an effective barrier to the exchange of molecules between the spine head and dendritic shaft. The effect of the spine neck on diffusional coupling was first examined by Karel Svoboda in 1996. Fluorescent dextran was photobleached within the spine head and the lifetime of recovery was measured. Not

surprisingly, the length of spine necks was found to correlate with the timecourse of recovery (Svoboda, Tank et al. 1996). A similar correlation was found for calcium transients in spines following glutamate uncaging (Majewska, Tashiro et al. 2000). Interestingly, in this study the rate at which calcium transients persisted in the spine head was observed to change over time with direct relation to ongoing changes in the length of the spine neck. Bloodgood and Sabatini showed, using 2 photon photoactivation and imaging of photoactivatable GFP, that the coupling between spine heads and the parent dendrite could change spontaneously over time, and that the coupling ratio was rapidly altered in response to synaptic input. Intriguingly, the magnitude of the changes observed in this study suggested that something beyond mere lengthening or shortening of the spine neck may be responsible for the changes in coupling. Finally, it has been demonstrated that diffusional decoupling by the spine neck extends to surface receptors (Ashby, Maier et al. 2006) and membrane molecules (Richards, De Paola et al. 2004). Although no mechanism beyond mere lengthening of the neck have been conclusively demonstrated, Richards observed a correlation between the amount of ongoing actin-dependent spine “morphing” and the turnover of a membrane-bound red fluorescent protein.

Thus it is possible that the actin cytoskeleton plays a role in regulating diffusion within dendritic spines. Spine actin networks are rapidly and persistently stabilized following glutamate receptor activation (Star, Kwiatkowski et al. 2002; Okamoto, Nagai et al. 2004). Although the factors that control this stabilization are unknown, this would provide a mechanism whereby any actin binding protein, including activated CaMKII

containing CaMKII-beta, would be more stably bound within the spine, thus slowing the departure of activated signaling molecules until after they inactivate.

In regards to synaptic sharing of molecules, it is important to distinguish activated, information-containing signaling molecules, which may initiate signaling upon arriving at neighboring synapses, from inactivated, essentially naïve molecules which may function as simple building blocks when incorporated at a neighboring synapse. While it may be critical that the neuron sequester the former set of molecules to spatial domains where their activity is appropriate, continuous exchange of molecules under steady-state conditions with a pool of molecules located outside the synapse may be necessary for fidelity-checking of synaptic molecules. The matching of inactivation rates to molecular turnover within spines provides a mechanism whereby molecules may be continuously exchanged while still maintaining localized signaling gradients within appropriate domains near the synapse.

Thus, the actin cytoskeleton functions either as a diffusion barrier in the spine neck, interacts with membrane proteins in the spine head, or may determine the morphology of the spine neck itself. Actin filaments within the spine neck have long been thought of as being straight bundled filaments, as are seen in filopodia. However, the Arp2/3 complex has been shown to localize to within the neck, as well as the spine head (Hotulainen, Llano et al. 2009) and a recent study utilizing platinum replica electron tomography (Korobova and Svitkina 2009) demonstrated the existence of branched filaments within the neck. Thus, the actin cytoskeleton may play a determining role in the

length, and possibly the width of spine necks. As the morphology of the spine neck has been shown to effect the rate of exchange of a variety of molecules into and out of the spine (Svoboda, Tank et al. 1996; Majewska, Tashiro et al. 2000; Bloodgood and Sabatini 2005; Ashby, Maier et al. 2006), this raises the possibility that regulated actin polymerization within the spine neck may modulate compartmentalization of signalling molecules within the spine head.

d. The Spine Actin Cytoskeleton

Actin has long been recognized as the principle cytoskeletal component of dendritic spines (Caceres, Payne et al. 1983), where it is thought to be the primary determinant of spine morphology (Fischer, Kaech et al. 1998; Matus 2000). As in other biological systems in which cytoskeletal dynamics have been studied in great detail, actin in spines undergoes continuous treadmilling (Star, Kwiatkowski et al. 2002; Frost and Blanpied 2008; Honkura, Matsuzaki et al. 2008), driven by the preferential incorporation of free cytosolic monomers at plus ends of growing filaments; the cytosolic pool is constantly replenished by the removal and severing of monomers from the opposite end of the filament. Thus monomers polymerized into actin filaments move constantly away from sites of depolymerization at the tip and circumference of the spine head (Frost and Blanpied 2008; Honkura, Matsuzaki et al. 2008; Hotulainen, Llano et al. 2009).

This treadmilling drives spine motility (Fischer, Kaech et al. 1998; Fischer, Kaech et al. 2000), as the continuous remodeling of the spines cytoskeleton results in morphological changes of spine head shape and protrusions. Importantly, treatment of

neurons with jasplakinolide, which stabilizes actin filaments, also abrogates spine motion, indicating that polymerizing actin is necessary for the continuous restructuring of spine geometry.

In most cell types, extension of unbranched filaments is accomplished by the formin family, and in neuronal filopodia, the formin mDia2 appears to play a large role (Hotulainen, Llano et al. 2009). On the other hand, branching of filaments near their barbed end is catalyzed principally by the Arp2/3 complex, activated by the neural Wiskott Aldrych syndrome Protein (N-WASP). Because spines have a high degree of branched filaments (Fifkova and Delay 1982; Landis and Reese 1983), it is assumed that Arp2/3-mediated branching is particularly important there. Indeed, knockdown, pharmacological inhibition, or mutation of N-WASP drastically reduces the number of spines (Wegner, Nebhan et al. 2008), and RNAi-mediated suppression of the Arp2/3 complex selectively reduces mature, mushroom spine density (Hotulainen, Llano et al. 2009). Mechanisms of disassembling filaments appear broadly conserved as well. Depletion of cofilin via siRNA slows actin turnover (Hotulainen, Llano et al. 2009), and altering cofilin activity results in misshapen spines (Meng, Zhang et al. 2002), confirming the importance of this protein in spines. Thus, comparisons to other cell types reveal broadly conserved mechanisms of actin regulation that control spine morphology. However, rather than merely using these mechanisms to control spine shape, neurons spatially, temporally, and molecularly adapt them to coordinate a diverse array of actin-dependent processes within the microscopic confines of the spine.

Both polymerization-driven spine motility and the continuous treadmilling of spine actin filaments have been observed to halt rapidly following activation of glutamate receptors. Measurement of spine actin behavior has revealed that the spine actin network is stabilized following the activation of glutamate receptors. Using Fluorescence Recovery after Photobleaching (FRAP) of actin-GFP, Venky Murthy's lab showed first that actin filaments within individual spines turn over continuously with a time course of less than one minute (Star et al, 2002). This exchange of actin monomers could be abrogated by the actin stabilizing drugs jasplakinolide and cytochalasin D. Application of NMDA or electrical stimulation resulted in rapid stabilization of actin filaments within the spine. The Hayashi lab demonstrated that LTP-like stimuli result in an increase in FRET efficiency between –CFP and –YFP tagged actin monomers, whereas LTD inducing stimuli resulted in a decrease in FRET efficiency (Okamoto, Nagai et al. 2004). They concluded that spine morphological changes were due to changes in polymerization state of the actin cytoskeleton. Honkura further demonstrated that stabilization of actin tagged with photoactivatable GFPs could be induced through glutamate uncaging (Honkura, Matsuzaki et al. 2008).

These studies suggest that modulation of the structure of spine actin networks accompany the induction of synaptic plasticity. We know that actin polymerization is required for the maintenance phase of LTP (Fukazawa, Saitoh et al. 2003), as application of latrunculin A immediately after the induction of LTP has been observed to result failure to maintain expression of LTP over 30 minutes. This has been attributed to a role for actin in maintaining a perisynaptic pool of AMPA receptors that is required for LTP

expression (Yang, Wang et al. 2008). Whether the stable pool that is formed during LTP induction is the pool that is required for its maintenance remains unclear however, particularly since a number of studies have now shown that active remodeling of the spine actin cytoskeleton by Cofilin are required for LTP induction (Gu, Lee et al. 2010).

Activity-dependent stabilization of spine actin could potentially be explained by several mechanisms. In the lamellipodium of migrating cells, protrusive force generation by the actin cytoskeleton depends on the strength of the interactions between filaments undergoing retrograde flow and adhesion complexes. The strength of this interaction thus determines both the rate of protrusion of the cellular membrane at the leading edge and the migration rate of moving cells. Stabilization of the actin cytoskeleton through activation of a number of actin binding proteins could prevent severing by ADF/Cofilin. On the other hand, inhibition of polymerization-mediating factors could slow the addition of new monomers to existing actin filaments. Alternatively, release of filaments by proteins such as myosin II (Ryu, Liu et al. 2006) could dramatically influence the protrusive force generated by new monomer addition.

Besides altering the dynamics of individual filaments, activation of actin binding proteins has the potential to dramatically influence the structure of the actin network through cross-linking and bundling of filaments. Another interpretation of changes in FRET signal accompanying plasticity is that changes in the spine actin network structure may increase the interaction or proximity between neighboring filaments. One prominent molecular candidate which may mediate increased filament cross-linking is CaMKII,

which has been shown to cross-link actin filaments in vitro (Okamoto, Bosch et al. 2009). CaMKII is recruited to spines during LTP induction, where it may bind to actin filaments. In addition, CaMKII overexpression or knockdown has been shown to influence actin turnover rates in spines. The acute effect of CaMKII activation or inhibition on actin filament stability in spines has not been tested, so the possibility remains that CaMKII action on actin cytoskeletal dynamics is indirect through promotion of spine and synapse maturation.

e. Regulating the Structure and Function of Actin Networks

Actin

Actin exists in two forms: globular, monomeric G-actin which freely diffuses in solution and filaments composed of chains of polymerized monomers called F-actin. Regulatory mechanisms governing the structural dynamics of these filaments has been finely tuned, and the critical nature of this tuning is evidenced by the fact that the amino acid sequence of the 43 kD, 375 amino acid skeletal actin is virtually unchanged between chickens and humans (Reisler and Egelman 2007), and further by the many actin binding proteins that are also conserved.

Actin filaments are organized as two protofilaments which wrap around each other. Filaments may be branched through the action of Arp2/3, bundled by proteins such as alpha-actinin, organized into more complex structures such as stress fibers (Hotulainen and Lappalainen 2006), permitting their function in diverse roles including protrusive and

contractile force generation, obstruction of molecular diffusion and facilitation of myosin based transport of cargo over long distances within the cell.

A basic biochemical tenet of actin function is the preferential addition of monomers to the barbed end of filaments. Polymerization is diffusion-dependent, and therefore dependent on the concentration of free monomers. In the absence of filaments, polymerization is unfavorable, as actin dimers and trimers are unstable (Pollard and Borisy 2003). However, once polymerization is initiated it proceeds rapidly.

ATP-bound actin monomers have a 7-fold greater affinity for the barbed end of filaments then the pointed end, providing the physiological basis for “treadmilling” or motion of polymerized monomers along a filament driven by net addition of monomers to the barbed end and loss at the pointed end of the filament. Once incorporated into filaments, hydrolysis of ATP occurs with a time constant of about 2 seconds (Blanchoin and Pollard 2002). Inorganic phosphate dissociation is much slower (350 seconds; (Carlier and Pantaloni 1986)). Together, these processes may provide an internal timer for the age of actin filaments which may drive actin filament structural plasticity (Kueh and Mitchison 2009) and also regulate the binding of actin regulatory proteins such as Cofilin to points of varying distance from the site of polymerization. Finally, although the biochemical properties of the actin molecule itself support treadmilling in vitro, the presence of actin regulatory proteins may hasten this process by nearly two orders of magnitude making them indispensable for the physiological roles of the actin cytoskeleton within the cell.

Actin exists in three isoforms, which share 90% homology in their amino acid sequences. Alpha-actin is found mainly in muscle where it functions as part of the contractile apparatus. Beta and Gamma form the building blocks of cytoskeletal thin filaments in non-muscle cells. Hippocampal and cerebellar neurons express high levels of mRNA for both beta and gamma actin isoforms and the mature protein encoded by both genes are selectively targeted to the dendritic spine cytoplasm. In contrast, alpha actin is not expressed in neurons, and when exogenously expressed is not targeted to spines (Kaech, Fischer et al. 1997).

These proteins differ only in 4 residues at the C-terminus, which suggests that there is a great deal of functional redundancy between the two isoforms. Indeed, although mutation of the gene encoding gamma-actin has been linked to a progressive form of hearing loss (Zhu, Yang et al. 2003), mice in which the gamma-actin isoform has been genetically ablated are viable, and are able to compensate for this deficit in most cases through upregulation of the beta-actin isoform.

However, although hair cells develop stereocilia normally, the loss of gamma-actin leaves them unable to repair noise-induced damage to the core F-actin structure of the stereocilia, leading to progressive deafness (Belyantseva, Perrin et al. 2009). Protein carrying disease-causing mutations appears to be capable of incorporation into stress-fibers and into the lamellipodial cytoskeleton, although it can result in the formation of “a large cytoplasmic clump” of polymerized actin (Morin, Bryan et al. 2009). In addition, the ability of certain actin binding proteins, including tropomyosin, to bind gamma-actin

filaments is also altered. It is unclear whether pathology is due to sequestration of protein outside the stereocilia, or the inability of specific actin-binding proteins to interact with the mutant protein and initiate repair of damaged cilia. Moreover, although fluorescently tagged beta actin has been widely studied in spines of Hippocampal neurons, both the dynamics of gamma actin isoform and the effect of gamma-actin incorporation on beta-actin dynamics or synaptic function has is unknown.

However, the roles of a vast array of actin binding and regulating proteins have been extensively studied, and a selected group of these proteins will be discussed below. *In vitro*, actin polymerization and actin-based motility can be initiated by a core set of actin binding proteins. These proteins are actin, the Arp2/3 complex, profilin, capping protein, ADF/Cofilin, and an activator of the Arp2/3 complex such as Scar or Wasp (Pollard and Borisy 2003). These proteins will be discussed first.

Arp2/3

The Arp2/3 complex was originally identified in 1994 as a set of 7 closely associated proteins including actin related proteins 2 and 3, and 5 other proteins (p40, p34, p21, p20, and p16 (Machesky, Atkinson et al. 1994). This protein complex is a convergence point for many cellular signaling pathways and is required for the activation of actin polymerization by small guanine nucleotide binding protein cdc42 (Ma, Rohatgi et al. 1998) and for the recruitment of polymerizing actin to the surface of intracellular Listeria (Welch, Rosenblatt et al. 1998). It localizes to the lamellipodium of migrating cells, and

to the growth cone and dendritic spines of neurons (Racz and Weinberg 2008; Wegner, Nebhan et al. 2008; Hotulainen, Llano et al. 2009).

The complex dimerizes and thus is capable of binding to the pointed end of growing filaments and nucleating new branches, which diverge from parent filaments by a 70 degree angle. New branches grow rapidly once initiated by addition of monomers to their barbed end, and repeated branching can lead to the elaborate dendritic which is found within many cellular compartments where dynamic actin polymerization occurs, including the lamellipodium and dendritic spines. The Arp2/3 complex has been directly observed at these branch points by electron microscopy (Blanchoin, Amann et al. 2000; Cai, Marshall et al. 2007). Thus, the action of the Arp2/3 complex alters both the complexity of the actin network, and may increase and distribute the capability of the polymerizing actin network to generate force by dramatically increasing the number of barbed ends where new monomers may be incorporated. The presence and activation of the complex has been demonstrated to be critical to proper development and maturation of spines and synapses (Kim, Sung et al. 2006; Wegner, Nebhan et al. 2008). Accordingly, knockdown of Arp3 (Wegner, Nebhan et al. 2008) and its upstream activators n-Wasp, cdc42, and WAVE1 in young cultured neurons inhibited the development of spines as well as PSD95 puncta. Similar effects have been observed following the knockdown of the Arp2/3 complex subunit p34 (Hotulainen, Llano et al. 2009). In general, knockdown of all of these proteins in young neurons results in a distribution of less mature spines and synapses, with an increased number of filopodia and a decrease in the fraction of synapses that take place on mushroom spines. The role

of the Arp2/3 complex in maintaining developed synapses is less established, but should be aided by the recent development of specific pharmacological inhibitors (Nolen, Tomasevic et al. 2009).

WASP/WAVE

The Wiskott-Aldrich syndrome protein (WASP) family includes a number of members that promote polymerization of the actin cytoskeleton through activation of the Arp2/3 complex. The family, which includes WASP, neural-WASP (N-WASP, and the WASP-family verprolin homologous proteins (WAVEs), activates the initiation of new branched filaments by the Arp2/3 complex. Both WASP and N-WASP bind PIP2 through a pleckstrin homology domain, cdc42 through a GBD domain, a G-actin binding verprolin homology domain, and a C-terminal acidic segment, through which they bind and activate the Arp2/3 complex (Miki and Takenawa 2003). Coordinated cdc42 and PIP2 binding activates N-WASP, which releases an autoinhibitory domain, allowing it to bind and activate Arp2/3 (Rohatgi, Ma et al. 1999).

In neurons, N-WASP is thought to regulate the development of spines and synapses through activation of Arp2/3-mediated nucleation of branching filaments. N-WASP is targeted to dendritic spines and colocalizes with postsynaptic density proteins such as PSD-95. Knockdown of N-WASP or treatment of immature neurons with chronic application of wiskostatin, an N-WASP specific inhibitor, dramatically decreases the number of excitatory synapses that develop (Wegner, Nebhan et al. 2008). As with the Arp2/3 complex, the role of N-WASP in the maintenance of developed synapses has not

been studied. Furthermore, it is unclear what fraction of actin filaments are nucleated by Arp- and WASP-dependent mechanisms, and the precise location of these filaments within spines is unknown.

Profilin

Profilin, the first actin binding protein to be shown to associate with monomeric actin (Carlsson, Nystrom et al. 1977) exists in 4 isoforms, of which profilin II is expressed primarily in the brain. Profilins are 14-16 kDa proteins which are critical to the function of actin networks in cells through their ability to bind G-actin and enhance polymerization through the catalysis of ATP addition (Goldschmidt-Clermont, Machesky et al. 1990).The local activation of profilin mediated nucleotide exchange by PIP2, coupled with the competing stabilization by Thymosin beta 4 (Goldschmidt-Clermont, Furman et al. 1992) provides a general mechanism for the spatial regulation of actin dynamics within the cell.

Within neurons, Profilin interacts with postsynaptic scaffolding molecules at both inhibitory (Mammoto, Sasaki et al. 1998)) and excitatory synapses (Neuhoff, Sassoe-Pognetto et al. 2005). Notably, both profilins I and II are recruited into spines in an activity-dependent manner (Ackermann and Matus 2003; Neuhoff, Sassoe-Pognetto et al. 2005) where they may contribute to the temporary stabilization of actin filaments and spine enlargement that occur during LTP.

Capping Protein

Capping protein forms a heterodimeric complex that binds to the barbed end of growing actin filaments, preventing the loss of polymerized monomers from that end and effectively regulating assembly at bound filaments (Wear, Yamashita et al. 2003). Capping protein is one of the core factors necessary to reconstitute actin-based motility of listeria and shigella (Loisel, Boujemaa et al. 1999). As capping protein stabilizes actin filaments and prevents their growth, its requirement in actin-based motility and force generation at first seems contradictory, but there are a number of indirect mechanisms whereby capping of barbed ends is critical for the force generation of dynamics actin networks. One such mechanism is likely to be the inactivation and stabilization of barbed ends at secondary or unnecessary sites of polymerization. Replenishment of the pool of monomers through severing and removal of polymerized actin at the pointed end of filaments is also necessary for actin-based motility. It is likely therefore that capping of a large percentage of the barbed ends within a network prevents the incorporation of monomers into regions of the network where force generation is not needed. A second, less obvious but probably the most critical, relates to the opposing effects of the Arp2/3 complex and capping protein on the actin network. As the Arp2/3 complex functions through the nucleation of new branches with the resulting addition of a new barbed end with each branch, uncontrolled branching would rapidly result in an exponential increase in the number of barbed ends within the network, thereby exponentially decreasing the growth rate of individual filaments in a system where the supply of ATP-actin is rate-limiting (Pantaloni, Boujemaa et al. 2000).

Like the Arp2/3 complex, capping protein localizes to spine heads, and both are thought to play a role in the initiation of spine growth due to their presence in the majority of filopodial spine precursors (Korobova and Svitkina 2009). The presence of Arp2/3 and capping protein in dendritic filopodia (Svitkina, Bulanova et al. 2003) is interesting due to their exclusion from lamellipodial filopodia (Svitkina and Borisy 1999), suggesting that spine precursor filopodia are functionally distinct from other forms of filopodia. Regulation of actin dynamics within the spine head is likely to be important both in the spatial localization of active filament assembly as well as the rapid regulation of global assembly within the spine head. However, detailed investigation of the role of capping protein function on the maintenance of synaptic function or spine morphology has not been performed.

ADF/Cofilin

The actin depolymerizing factor and cofilin are two closely related filament severing agents present in dynamic actin networks. Cofilin is one of the core proteins necessary for actin based motility of shigella and listeria (Loisel, Boujemaa et al. 1999). Cofilin is inactivated through phosphorylation by LIMK, a serine/threonine kinase containing LIM and PDZ domains, at serine 3 (Yang, Higuchi et al. 1998; Yang, Higuchi et al. 1998). Dephosphorylation of this residue by phosphatases such as slingshot activates cofilin-mediated actin disassembly at the pointed end of actin filaments (Yuen, Liu et al. 2010). Cofilin activity thus is necessary for remodeling of the actin network, and is responsible for the replenishment of the cytoplasmic pool of free actin monomers. As such, expression of phosphomimetic inactive form of cofilin, with glutamate substituted for

Ser3 hinder actin-based motility, whereas constitutively active cofilin enhances actin polymerization, increasing the movement rate of migrating cells (Carlier, Laurent et al. 1997). Local activation of caged cofilin results in cytoskeletal remodeling which may determine the direction of cell migration (Ghosh, Song et al. 2004), likely through the local generation of free actin monomers.

In neurons, NMDA receptor stimulation results in transient activation of Cofilin through dephosphorylation of Ser3 that mediated by activation of slingshot by Calcineurin (Carlisle, Manzerra et al. 2008), thus inducing activity-dependent remodeling of the spine actin cytoskeleton. A number of observations have made it clear that this remodeling of the actin cytoskeleton necessary for activity-dependent synaptic plasticity. Loading postsynaptic neurons with phalloidin, an actin-stabilizing toxin has been reported to prevent the induction of NMDA receptor-mediated LTD. Furthermore, inhibitory peptides of cofilin, which would be expected to prevent cofilin-dependent remodeling of the spine cytoskeleton, also potently block LTD (Morishita, Marie et al. 2005). Injection of inhibitory peptides for calcineurin, which act upstream of cofilin, also block NMDA receptor dependent LTD, as did injection of actin stabilizing drug jasplakinolide (Wang, Yang et al. 2007). Further evidence that this necessary reorganization is mediated by cofilin comes from the observation that knockdown or inhibition of slingshot reduces AMPA receptor-mediated excitatory postsynaptic current (EPSC) amplitude and prevented the induction of synaptic plasticity (Yuen, Liu et al. 2010). Thus, cofilin mediates active remodeling of the actin cytoskeleton that is necessary for synaptic plasticity. It is clear that remodeling of the entire spine network is

not necessary, as LTD changes in spine size are dissociable from LTD induction itself (Sdrulla and Linden 2007; Yuen, Liu et al. 2010). However, the nature and location of the specific networks involved in AMPAR insertion or removal from the membrane remains unclear.

f. "A network of networks: cytoskeletal control of compartmentalized function within dendritic spines." Adapted from Frost et Blanpied, 2010.

Actin roles specifically at the PSD

At excitatory synapses, a collection of multi-domain scaffold proteins comprises the core of the postsynaptic density (PSD). The PSD positions glutamate receptors in close apposition to the presynaptic active zone and provides a scaffold for synaptic signaling molecules. Larger PSDs are generally more morphologically complex, include more glutamate receptors, and are closely correlated with larger spine heads. Thus, the size and shape of the PSD not only directly control synapse function, but may also seed organization of the remaining areas of the spine.

Actin filaments are closely associated with the PSD, apparently contacting it directly (Fifkova and Delay 1982; Capani, Martone et al. 2001). These filaments are involved in several distinct mechanisms of PSD regulation. Inhibition of polymerization with latrunculin destabilizes synapses in an age-dependent fashion (Zhang and Benson 2001), and prompts the dissociation of AMPA receptors (Allison, Gelfand et al. 1998; Kim and Lisman 1999; Zhou, Xiao et al. 2001) and PSD proteins (Allison, Chervin et al.

2000). Within minutes of latrunculin treatment, enough time for one or a few complete cycles of treadmilling on spine actin filaments, approximately half of the PSD-bound Shank, GKAP, and homer 1c (PSD-Zip45) is lost (Kuriu, Inoue et al. 2006). Surprisingly, this occurs without affecting the molecular exchange rate of the remaining 50% (Kuriu, Inoue et al. 2006), and with only partial loss of AMPA receptors (Allison, Gelfand et al. 1998; Kim and Lisman 1999; Zhou, Xiao et al. 2001).

Whereas the loss of AMPA receptors could involve actin-dependent processes outside the synapse, the immediate influence of depolymerization on PSD protein copy number is strong evidence that actin filaments act directly at the PSD. However, the latrunculin-insensitive subset of PSD molecules is poorly understood. Interestingly, latrunculin does not affect the stability of PSD-95 (Kuriu, Inoue et al. 2006; Blanpied, Kerr et al. 2008), presumably because of the protein's direct association with the plasma membrane or transmembrane proteins. Thus, the intermolecular binding of scaffold molecules that is the foundation of PSD architecture is apparently not sufficient to maintain GKAP, Shank, and Homer1C in the absence of polymerizing actin. So, while interconnected, the PSD is not entirely cohesive. Instead, it may be organized into functional subsets that are partially autonomous, allowing dispersal of molecules from PSD subcompartments. Alternatively, it may comprise interlinked lamina, with interfaces that require constant support from actin-driven processes. Measuring PSD internal organization and determining the role of cytoskeleton in establishing this organization are important goals for understanding synapse architecture.

An important, additional mechanism for cytoskeletal regulation of the PSD is clear from high-resolution time-lapse imaging of PSD morphology. Surprisingly, even at synapses in mature neurons (i.e., synapses that on average persist days or weeks (Minerbi, Kahana et al. 2009)), the morphology of the PSD undergoes continuous change on a time-scale of seconds to minutes (Blanpied, Kerr et al. 2008) (Fig 1.1A). Nevertheless, depolymerization of actin filaments rapidly halts ongoing morphology changes (Fig 1.1B), as does stabilization of filaments with jasplakinolide. Notably, these changes do not tightly correlate with changes in spine morphology, but are regulated by changes in synapse activity (Fig. 1.1C). Thus, the PSD behaves not as a rigid body but as a flexible matrix, the shape of which is continuously adjusted by dynamics or treadmilling of the actin cytoskeleton. Importantly, these actin-driven changes in the overall size of the synapse occur much more rapidly than fluctuations in scaffold protein copy number (Kuriu, Inoue et al. 2006; Blanpied, Kerr et al. 2008). Accordingly, it is likely that morphological distortion acutely regulates the density of PSD scaffold molecules, potentially within subdomains (Blanpied, Kerr et al. 2008). Because the local density of PSD molecules at the nanometer-scale plays an important role in receptor confinement and mobility in the synapse (Ehlers, Heine et al. 2007; Triller and Choquet 2008), actin-driven change in the shape of the PSD may influence the alignment of presynaptic and postsynaptic elements.

Figure 1.1: Actin regulates the PSD scaffold, and acts at other distinct locations throughout spines.

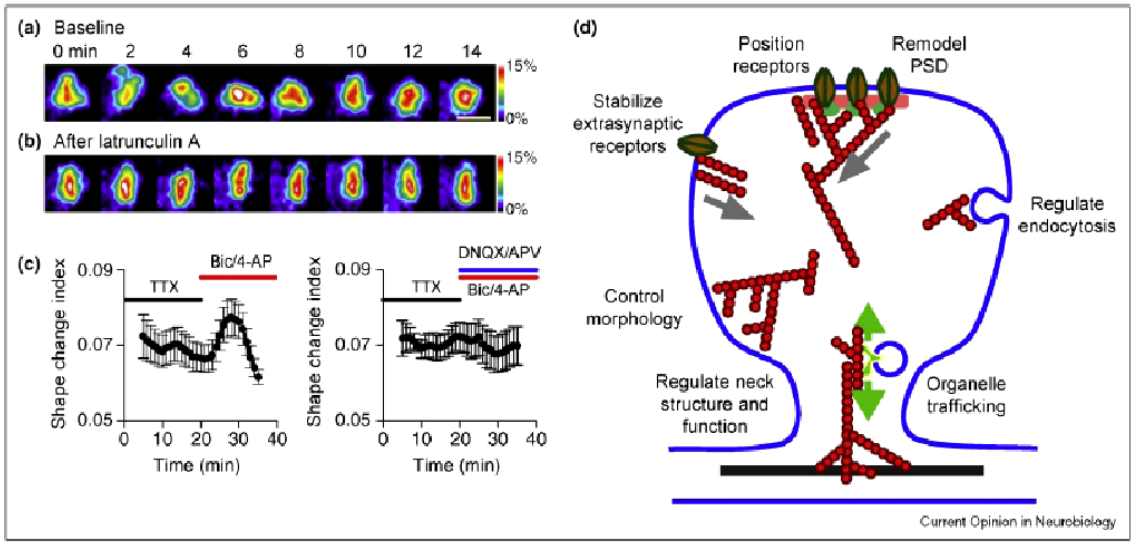

(a) Individual PSDs undergo morphological changes accompanied by internal changes in scaffold protein density. Hippocampal neuron four weeks in culture, transfected with PSD-95-GFP, and imaged by confocal microscopy. Color scale shows the proportion of total PSD-95 molecules per 1000 nm^2 in the image (spatial scale bar: 1 μm). Panels (a)–(c) adapted from Blanpied *et al.*, copyright 2008 National Academy of Sciences, USA. **(b)** Actin drives changes in shape and spatial fluctuations of PSD-95 molecular density of individual PSDs. Same PSD as in (a), after application of latrunculin A to prompt depolymerization of actin filaments. **(c)** Increasing neuronal activity increases the rate of actin-driven PSD morphological change, as measured with a shape change index based on the variance of PSD shape over time. This increase is blocked by glutamate receptor antagonists. **(d)** Summary of several known sites of actin regulation throughout individual spines, illustrating that the spine cytoskeleton is a network of networks that coordinately control synapse function via numerous distributed mechanisms. Gray arrows indicate direction of actin flow; green arrows indicate potential for cargo transport along filaments oriented in either direction.

Though NMDA receptors can attach to actin via single intermediate actin-binding proteins, such as alpha-actinin (Wyszynski, Lin et al. 1997), AMPARs in the synapse generally contact the cytoskeleton through PSD scaffold proteins (via PSD-95 to citron or SPAR (Pak, Yang et al. 2001), or via GKAP and Shank to cortactin (Naisbitt, Kim et al. 1999), βpix, or oligophrenin (Tada and Sheng 2006). Given that actin both

regulates PSD scaffold composition and drives changes in overall PSD size and shape, how might these aspects of actin function control synaptic AMPA receptor number? One possibility is that this control stems from regulation of PSD composition and molecular positioning. Importantly, AMPARs reach the postsynaptic membrane through free diffusion from extrasynaptic sites (Triller and Choquet 2008), but once they reach the PSD, their motion is considerably slowed. Receptors are likely retained within the PSD both by direct interaction between binding partners such as PSD-95 and stargazin (Bats, Groc et al. 2007), and by steric hindrance to free diffusion due to crowding within the molecularly dense postsynaptic membrane. In fact, the motion of even exogenous proteins linked to the external leaflet of the plasma membrane is hindered by steric obstruction when these molecules enter the synapse (Renner, Choquet et al. 2009). However, this obstruction is reduced by latrunculin A (Renner, Choquet et al. 2009), suggesting that actin-mediated changes in scaffold density control behavior of membrane proteins like receptors even in the absence of high affinity binding interactions. Thus, actin-mediated control of PSD scaffold density by component release (Allison, Chervin et al. 2000; Kuriu, Inoue et al. 2006) or by flexing (Blanpied, Kerr et al. 2008) may tune the ability of the synapse to retain AMPARs (Allison, Gelfand et al. 1998; Kim and Lisman 1999; Zhou, Xiao et al. 2001). .

Segregation of actin function in spine membrane subdomains

Perisynaptic membrane

Single-particle tracking has made clear that receptors outside the synapse, even those very near it, for the most part diffuse nearly freely within the plasma membrane

(Tardin, Cognet et al. 2003; Triller and Choquet 2008). However, under specific circumstances, actin polymerization may directly restrict the motion of extrasynaptic AMPARs. The regulation of spine or spine neck morphology by actin may help to trap membrane proteins passively within the extrasynaptic spine membrane (Bloodgood and Sabatini 2005; Ashby, Maier et al. 2006). However, the cytoskeleton may more directly influence the distribution of AMPAR in the extrasynaptic membrane. For instance, the increase of receptors in the synapse during induction of long-term potentiation depends on delivery of AMPA receptors to a unique "pool" near but outside the synapse (Yang, Wang et al. 2008). Remarkably, whereas delivery of receptors to the pool was insensitive to latrunculin, latrunculin application after the induction stimulus disperses the receptors and prevents synaptic potentiation. While the precise molecular mechanisms by which actin anchors this receptor pool near the synapse are unclear, it is not likely to be merely through control of spine morphology. This is clear because treatment with latrunculin two minutes following LTP induction resulted in a loss of these perisynaptic receptors and a decrease in potentiation, but did not block the LTP-associated increase in spine size (Yang, Wang et al. 2008). The site of this actin-dependent accumulation is unclear, as is the role of receptors themselves in establishing the accumulation. One interesting possibility is that GluA1 receptors themselves, through protein interactions with their C-termini that are triggered by LTP induction, may help stabilize actin filaments (Kopec, Real et al. 2007).

Non-synaptic spine membrane

The details of potential spine membrane specialization outside the PSD are largely uncharacterized. However, one clearly defined spine subregion is the endocytic zone (EZ), a point of persistent accumulation of clathrin several hundred nanometers outside the synapse, where AMPAR endocytosis takes place (Blanpied, Scott et al. 2002; Racz, Blanpied et al. 2004; Lu, Helton et al. 2007). Molecular perturbations that displace EZs from their normal close association with the PSD result in synapses that contain fewer receptors, are smaller, and undergo less robust LTP (Lu, Helton et al. 2007). Though strong roles of actin in endocytosis (Kaksonen, Toret et al. 2006) might suggest that the cytoskeleton anchors or seeds the location of the EZ, latrunculin does not alter the perisynaptic positioning of the endocytic machinery within spines (Blanpied, Scott et al. 2002). In fact, dynamin 3, an endocytic large GTPase, is required for PSD-EZ positioning, but its binding to the actin regulatory protein cortactin is dispensable for this function. Thus, this resistance to latrunculin may indicate that AMPAR endocytosis in spines requires actin polymerization only in sporadic bursts during internalization, contrast to the need for ongoing polymerization to maintain the PSD.

If synaptic AMPA receptor stabilization and endocytosis are each regulated by actin polymerization, are there common molecules that coordinate these two processes? Recent evidence supports this idea. Rocca et al. [36] found that the BAR-domain protein PICK1, previously known to regulate AMPAR trafficking, binds to actin and inhibits the Arp2/3 complex, and that this negative regulation is important for AMPA receptor endocytosis. Importantly, the efficacy of PICK1 inhibition is strongly enhanced by

concurrent binding of PICK1 to the C-terminus of GluA2. This causes a local inhibition of actin branching, and, potentially with contribution from the PICK1 BAR domain, facilitates progression of clathrin-mediated endocytosis. Consistent with this model, shRNA targeted against PICK1 blocked endocytosis of GluA2 in response to a chemical LTD stimulus (Rocca, Martin et al. 2008). Thus, it may be that following LTD induction, PICK1 can facilitate rapid and efficient synaptic removal and subsequent endocytosis of AMPA receptors.

An important question is where inhibition of Arp2/3 by the GluA2-PICK1 complex takes place. One intriguing possibility is at the PSD directly, where inhibition of ongoing Arp2/3-mediated branching could transiently destabilize PSD components and help free receptors for migration to the endocytic zone during LTD. However, it is not clear whether mobilization of receptors between the synapse and the endocytic zone during LTD is influenced by non-synaptic actin. Thus, alternatively, transient inhibition of Arp2/3 may facilitate extrasynaptic receptor mobility. A third possibility is that actin branching may act as a constitutive negative regulator of endocytosis via establishment of a cortical actin barrier; transient disassembly of this barrier by inhibition of Arp2/3 at the endocytic zone could facilitate the maturation of coated pits that contain GluA2. Testing these hypotheses will require discrimination of actin molecular dynamics in spine subregions.

Spine-localized endocytosis is well established, but the role of AMPAR exocytosis into the spine plasma membrane is under intense consideration (Park, Salgado

et al. 2006; Yudowski, Puthenveedu et al. 2007; Wang, Edwards et al. 2008; Lin, Makino et al. 2009; Makino and Malinow 2009). However, AMPAR and transferrin receptors undergo activity-triggered exocytosis from large organelles directly in spines of cultured neurons at zones of clustered syntaxin 4 lateral to the PSD (Kennedy, Davidson et al. 2010). Actin directly binds syntaxin 4 (Jewell, Luo et al. 2008) and regulates its plasma membrane clustering (Low, Vasanji et al. 2006). Syntaxin 4 is also found in Rab11-positive endosomes (Band, Ali et al. 2002), though whether this facilitates or retards exocytosis of these organelles is not known. Thus, whether actin plays a role at sites of exocytosis near synapses in neurons remains to be determined, and it will be important to distinguish whether actin independently or coordinately regulates both exocytosis and endocytosis at distinct zones of the spine membrane.

Distributed sites of actin function during receptor trafficking

Intracellular mobilization of organelles and vesicles to, from, and within the spine requires myosin-based motors that move cargo along actin filaments. Myosin transport is directionally specific along the filament, and so the distribution within spines, the length, and the orientation of filaments dictate the molecular requirements of transport. Myosin VI is required for efficient endocytosis in many cells (Hasson 2003), and for clathrin-mediated AMPAR endocytosis in neurons (Osterweil, Wells et al. 2005). Because it walks towards the pointed end of actin filaments, myosin VI could draw vesicles inward from the membrane on filaments with barbed ends polymerizing at the membrane, a likely orientation. Because latrunculin does not obviate AMPAR endocytosis, it may be that filaments required by myosin VI are more stable than those involved in securing

receptors at the synapse (Cingolani and Goda 2008). In fact, generation of shorter, branched filaments may compete with long filaments ideal for myosin-based transport (Cingolani and Goda 2008). If so, then the localized inhibition of Arp2/3 that facilitates endocytosis (Rocca, Martin et al. 2008) may do so by permitting the assembly of longer filaments that more easily transport myosin VI-driven endocytic vesicles away from the membrane.

A number of potential myosins have been proposed to mediate the trafficking of endosomes in the spine (Correia, Bassani et al. 2008), including myosin Vb (Wang, Edwards et al. 2008) which walks toward the barbed end of actin filaments. Thus, a potential regulator of endosome traffic in spines is not merely the density but the orientation of polymerizing actin filaments within the spine head. In addition to myosin-dependent traffic, exocytosis may be regulated by other actin-dependent steps. Exocytosis of GluA1 AMPARs requires the actin-binding protein 4.1N, which binds to GluA1 at phosphorylated, membrane-proximal residues (Lin, Makino et al. 2009). Because 4.1N is member of the large FERM domain actin/spectrin-binding family, this suggests a further role of cytoskeleton in exocytic AMPAR trafficking. It will be important to determine whether this regulation occurs at the membrane or during prior organelle mobilization.

Other organelles important for spine function, including mitochondria (MacAskill and Kittler 2010) and mRNA granules (Bramham and Wells 2007), are also mobilized within spines, often via myosin-dependent transport. Regulation of actin filament

assembly, branching, and length at distributed locations within the spine can thus actively control spine organelle trafficking.

Actin in other regions of the spine

Ongoing actin polymerization has been implicated in the maintenance of spine function at other locations, including the spine neck and spine apparatus. Spine necks have traditionally been thought to contain linear bundles of actin filaments, and actin-bundling proteins such as neurabin/spinophilin affect filopodia outgrowth and spine morphological maturation (Terry-Lorenzo, Roadcap et al. 2005). However, recent work has highlighted the presence of anti-parallel (Hotulainen, Llano et al. 2009) or even branching (Korobova and Svitkina 2009) networks in the spine neck, suggesting a more complex neck cytoskeleton. This actin network within the spine neck is likely to play several roles. First, because the orientation of actin filaments determines the direction of travel of specific molecular motors carrying cargo during plasticity (Correia, Bassani et al. 2008; Wang, Edwards et al. 2008), heterogeneous filament orientation may facilitate motion through the neck based on diverse myosins. However, locations in the neck where pointed ends of antiparallel filaments abut one another may serve as filters, since only organelles carrying more than one kind of motor could transit through. Second, neck morphology, presumably actin-dependent (Meng, Zhang et al. 2002), controls the diffusion of both receptors (Ashby, Maier et al. 2006) and cytosolic molecules or Ca^{2+} ions (Majewska, Tashiro et al. 2000; Bloodgood and Sabatini 2005).

The spine apparatus, a specialization of smooth endoplasmic reticulum found in a subset of mushroom spines (Spacek 1985; Deller, Korte et al. 2003), is associated with dense, filamentous actin (Capani, Martone et al. 2001) and the actin/α-actinin binding protein synaptopodin (Kremerskothen, Plaas et al. 2005). Deletion of synaptopodin eliminates the spine apparatus and reduces hippocampal LTP (Deller, Korte et al. 2003), though the precise role of the spine apparatus remains a mystery. Actin filaments at the spine apparatus are a candidate for what may constitute the small fraction of rather stable spine actin that is regulated during LTP (Honkura, Matsuzaki et al. 2008), and it will be important to determine whether the bulky spine apparatus and associated actin filaments may regulate transit of organelles through the spine neck.

g. Summary and Hypothesis

The myriad of actin binding proteins present in the spine provide a wealth of molecular tools whereby actin dynamics may be regulated in response to different sets of stimuli. The convergence of multiple signaling pathways onto multiple regulatory proteins of the actin cytoskeleton permits the regulation of filaments which sub-serve a variety of functions within the spine.

One possible model is a single network of filaments encompassing the entire spine, which is regulated as a whole, thus affecting its functional roles at various locations within the spine. However, the actin-dependent processes within dendritic spines are temporally and spatially heterogeneous. Furthermore, whereas LTP induction depends on rearrangement of parts of the actin cytoskeleton, it is clear that widespread alterations in

the spine actin network are not required, as LTP induction is dissociable from spine enlargement. Alternatively, actin structures within spines as in other systems (Galbraith, Yamada et al. 2007), may be regulated on nanometer spatial scales to perform specific, localized functions.

I propose a model in which actin networks within individual dendritic spines have multiple points of control at distributed locations, allowing regulation of parts of the network within specific spine subdomains. In particular, actin filaments may be regulated independently at the PSD, allowing localized cytoskeletal structures which may be involved in stabilization of synaptic AMPA receptors or PSD morphology and composition. I hypothesize that actin at the synapse is dynamic, and that filament assembly is regulated at this location by mechanisms existing within the postsynaptic density. This provides a mechanism for direct modulation of synaptic form and function by actin. By extension, I propose that regulated assembly at other sites within the spine may be responsible for actin-dependent processes that do not directly involve the synapse proper.

A number of predictions can be drawn from this hypothesis. First, I predicted that polymerization will take place at the PSD. Previous studies have measured actin dynamics (Star, Kwiatkowski et al. 2002) or structural features of polymerized actin (Okamoto, Nagai et al. 2004), but have lacked sufficient resolution to distinguish actin dynamics at subregions within the spine. To overcome the obstacle of spatial resolution, I have developed a collection of high resolution optical assays for mapping the motion of

actin and other molecules within spines. Specifically, I have utilized Photoactivated Localization Microscopy (PALM) to define the sites and rates of actin polymerization within spines at high resolution. PALM is a single molecule imaging technique that uses photoconvertible probes converted at low density so that individual molecules can be discriminated and localized in each frame **(Figure 1.2)**. Each single molecule can be localized with a high degree of accuracy (tens of nanometers). Through the acquisition of many hundreds or thousands of frames and molecules, images can be rendered at resolution far surpassing conventional optical techniques(Betzig, Patterson et al. 2006). I have used PALM both to image the distribution of actin molecules with regards to the postsynaptic density and to measure polymerization rates at the PSD and elsewhere using single molecule tracking PALM.

Second, I predicted that localized regulation of actin networks occurs via mechanisms that influence nucleation and polymerization, rather than through regulation of depolymerization at the pointed end. This would be reflected in measurable differences in actin retrograde flow rates at different subdomains of the spine. For instance, the postsynaptic density, which requires ongoing actin polymerization, would be predicted to have actin polymerization rates that differ from those at the endocytic zone, where polymerization is needed only sporadically. I tested these predictions by measuring actin flow at high resolution within individual spines and compare polymerization rates at the PSD and the endocytic zone.

A third prediction of the hypothesis is that specific actin binding molecules would be localized to the PSD and responsible for regulating actin polymerization at this specific location. I examined the role of cortactin, which through its -SH3 domain and its role in activating the Arp2/3 complex, is a strong candidate mechanism whereby the nucleation of branching actin filaments may be specifically regulated at the PSD. I tested this first by measuring the effect of well-characterized cortactin mutants on the polymerization rates of actin within spines. I also tested the prediction that cortactin would bind sites within the spine in the absence of polymerized actin.

Finally, actin polymerization is expected to have unique roles at specific spine subdomains. I sought to test the prediction that actin in the spine neck may act as a barrier to the diffusion of membrane molecules into and out of the spine. To accomplish this, I developed a method of rapid acquisition PALM to simultaneously measure the location and motion of freely diffusing membrane-bound probes, allowing both precise definition of membrane morphology and molecular motion within the membrane. Further development of this technique will allow determination of spine neck morphology before and after the application of inhibition of actin polymerization, combined with simultaneous measurement of diffusion rates of molecules as they move through the spine neck. Although not completed, these studies will allow me to determine the role of actin in regulating spine neck diameter as well as its ability to influence the motion of diffusing molecules in the spine membrane.

Figure 1.2: Photoactivated localization microscopy is a sequential process

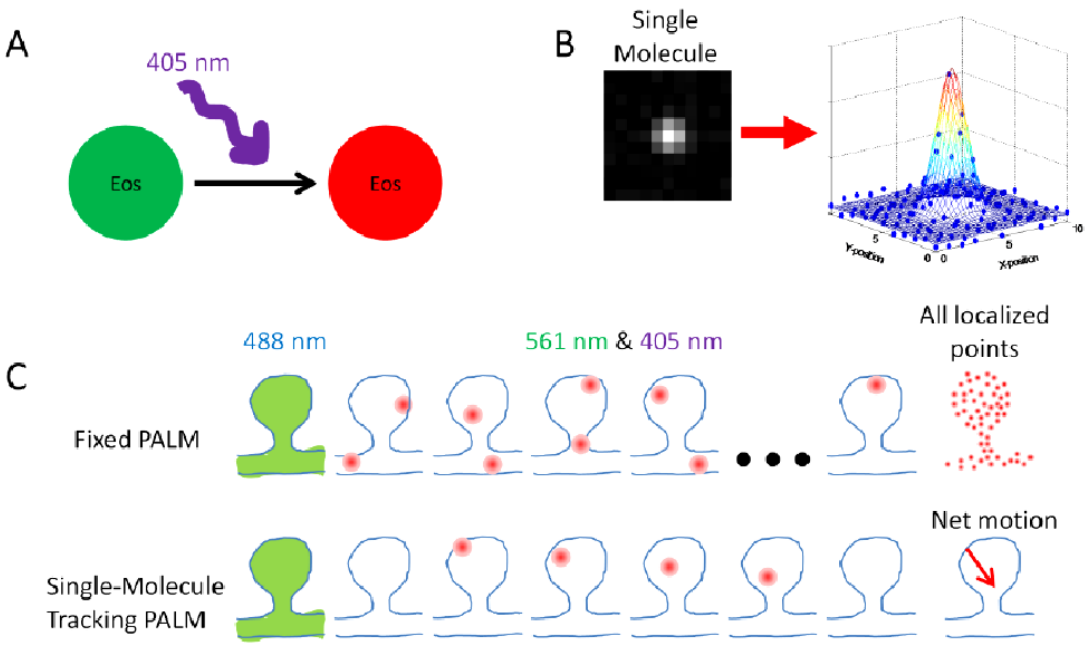

(A) Photoconvertible probes such as Eos are key to PALM. Eos is a fluorescent green molecule, which photoconverts under UV (405 nm) excitation to become a red fluorecent molecule. **(B)** Emitted photons from single molecules form a predictable pattern which can be fitted with a one or two-dimensional gaussian function, allowing precise localization of the molecule in two-dimensional space **(C)** Using low intensity photoconversion, single molecules can be stochastically photoconverted at very low density **(top)**. Individual single molecules can be easily resolved from neighboring molecules and localized using a gaussian fit of the distribution of emitted photons. Following acquisition of many frames and molecules, a high-resolution image can be rendered from the positions of all localized points. In living cells **(bottom)**, single molecules can be photoactivated and followed over multiple frames, providing information regarding velocity, diffusion coefficient, and vectorial motion **(pictured)**.

2. Development of PALM for imaging neuronal morphology

The development of fluorescence microscopy, and especially the cloning and improvement of intrinsically fluorescent proteins such as GFP, have allowed researchers to visualize neuronal morphology and protein distribution at high resolution. Advancements in confocal and multiphoton excitation allow the visualization of fluorescent proteins deep within tissue or even in the brain of behaving animals. Optical microscopy thus provides researcher with a powerful set of tools to investigate protein dynamics and distributions within living cells. Using the example of actin, microscopy has allowed the visualization of changes in actin density in response to external stimuli, the minute-to-minute reshaping of the actin cytoskeleton, and the measurement of overall turnover and net motion of polymerized actin within spines.

However, the diffraction of light passing through optical elements limits the resolving power of optical instruments. Rather than being recorded as a single point, the emitted photons from an infinitely small point source are blurred predictably into a finitely-sized distribution known as the point spread function (PSF). The PSF of a circular optical system with rotational symmetry forms particular distribution referred to as the airy disk, which consists of a sharp peak surrounded by alternating minima and maxima radiating outward. If two light-emitting points are farther apart than a minimum distance dependent on the width of the optical system's PSF, they can be effectively resolved. But if they are separated by less than this diffraction-defined distance, they cannot be differentiated from a single point or object. The size of the PSF is directly dependent on wavelength; Abbe defined the resolution limit in 1874 as the Full Width at

Half Maximum of the central peak of the PSF, corresponding roughly to λ/2. Rayleigh defined the resolution limit as the distance between the peak of the PSF and the first minima; this distance is 0.61λ/NA. Thus, using emitted light from most practical available fluorophores the resolution limit of conventional optical systems is approximately 225-300 nm. While this is more than sufficient for many applications, the small scale of many biological structures and organelles, dendritic spines, has made it difficult to differentiate features within them using conventional optical approaches.

Thus, testing the predictions of my hypothesis required utilization of methods that allow discrimination of spatial and kinetic properties of molecules within spines at higher precision than that possible by confocal microscopy. In particular, I reasoned that I would require the ability to resolve molecular motion within regions of the spine with spatial scales on the order of 100 nm in living neurons. Thus, I focused on techniques that were amenable to live cell experiments, allowed the visualization of intracellular proteins, and had the ability to resolve biological features with sub-100 nm precision.

A number of techniques exist that possess one or more of these features. PALM was attractive because it provides high precision localization of individual molecules, allows the visualization of molecular motion over time, and in contrast to other methods of single particle tracking which rely on labeling of extracellular proteins with quantum dots or other tags, I reasoned could be easily applied to the visualization of intracellular proteins.

With PALM (Photoactivated Localization Microscopy (Betzig, Patterson et al. 2006) and FPALM (Fluorescence Photoactivated Localization Microscopy (Hess, Girirajan et al. 2006), endogenously expressed photoconvertible proteins fused to targets of interest can be imaged in living (Hess, Gould et al. 2007; Manley, Gillette et al. 2008; Shroff, Galbraith et al. 2008; Frost, Shroff et al. 2010), one molecule at a time. Importantly, the use of endogenously expressed proteins, rather than antibody or dye-labeling makes PALM an attractive option for studying intracellular protein dynamics.

Localization microscopy relies on the principle that although light passing through an optical system from a single point is blurred by diffraction, the point spread is a predictable function. Thus, by fitting the distribution of collected photons emitted from a solitary point source, one can localize the position of a fluorescent molecule with a high degree of accuracy. In PALM, a protein of interest such as actin can be tagged with a photoconvertible probe which does not fluoresce until it is activated. By photoconverting only a sparse population of molecules at a given time one can visualize molecules as they appear, localize their positions over multiple frames until they irreversibly photobleach, and then photoconvert a new population of molecules. Over many sequential steps of photoactivation, localization and photobleaching, thousands of molecular positions can be accrued, allowing the distribution of tagged molecules to be displayed as a single high resolution image.

Photoactivated Localized Microscopy has been employed to investigate the structure and dynamics of adhesion complexes (Shroff, Galbraith et al. 2007; Shroff,

Galbraith et al. 2008; Shtengel, Galbraith et al. 2009), Bacterial membrane protein distributions (Greenfield, McEvoy et al. 2009), and the mobility of integral membrane proteins (Hess, Gould et al. 2007; Manley, Gillette et al. 2008). I have employed modified approaches to investigate the function of neuronal proteins and structures at high resolution in living neurons. I expected that specific applications of PALM imaging would provide a method for collecting structural and biophysical information not accessible by other imaging modalities within the living cell. The precise localization of individual molecules provides a means to create highly resolved images. This level of resolution is also accessible by other methods such as Stimulated Emission Depletion Microscopy (STED) (Nagerl, Willig et al. 2008; Ding, Takasaki et al. 2009), which possess clear advantages relating to speed of image acquisition. However, combining PALM with single particle tracking provides a means for simultaneously acquiring biophysical data on the movement of individual molecules and defining highly resolved maps of averaged molecular behavior. It is this author's opinion that photobleaching from the high intensity excitation and depletion lasers required for STED make biophysical measurements of protein mobility using fluorescence recovery or other methods technically challenging from a quantitative standpoint. On the other hand it would be feasible to acquire high resolution STED images and subsequently perform a standard FRAP or photoactivation experiment to measure turnover within a bounded region such as a spine. While this would provide high resolution morphology, and permit the correlation of protein mobility within the spine as a whole to morphological features of the spine such as neck width or diameter, we wished to measure protein dynamics at subdomains within the spine head. Similarly, although quantum dot tracking of surface

receptors is a powerful tool for measuring the mobility of membrane bound proteins and receptors within the cellular membrane, it is not applicable to intracellular proteins.

I thus have developed separate assays to utilizing PALM for:

1. Tracking mobility of intracellular proteins, including polymerization-driven retrograde flow of intracellular actin
2. High resolution imaging of neuronal morphology
3. High resolution mapping of surface protein mobility

The specific properties of the imaged molecules in each assay required tuning of both acquisition and analysis parameters. Localization error in various single molecule techniques has been defined both experimentally and quantitatively. Precision of localization of individual single molecules is easily calculated for experiments utilizing quantum dots, or other slowly bleaching fluorophores, as frame to frame changes in position of non-moving particles can be statistically analyzed. Alternately, for techniques with more rapid bleach rates, such as PALM, the half-width of diffraction-limited structures or the average distance traveled by individual fixed molecules have been utilized to provide a measure of precision. Alternately, mathematical approaches to the estimation of precision have been defined by (Thompson, Larson et al. 2002), wherein the precision of fitted molecules can be calculated by the equation:

$$<(\Delta x)^2> = (s^2+a^2/12)/N + 8\pi s^4 b^2/a^2 N^2 \qquad \text{Equation 2.1}$$

Where Δx represents the error in localization precision, N is the number of photons within the spot, b represents the background noise, s represents the width of the PSF, and

a is the pixel size of the image acquisition system in nm. Thus, precision increases with photons and decreases with background noise. It should be noted that this equation underestimates the error of fit by approximately 30%. However, although single molecule localization and tracking is widely used to chart the motion of diffusing molecules in living cells, none of these techniques account for possible effects imposed by the motion of diffusing molecules during acquisition.

I reasoned that the primary factors limiting our ability to accurately track the motion of rapidly diffusing molecules would be the rate of flux of photons from the molecule coupled with the short imaging time necessary to prevent individual molecules from blurring over xy-space within a single frame. In contrast, for anchored or slowly moving molecules such as actin, the limiting factor would be whether individual molecules would move far enough that net motion could be distinguished from noise caused by the imprecision of single molecular localization.

In both cases, the number of emitted photons collected in each frame influences the precision achieved in fitting molecular positions. Localization of molecules tagged with dyes or quantum dots can be extremely precise due to the high flux of photons emitted from these dyes and molecules can be tracked over many frames due to the stability and high photon emission of these agents. In contrast, the fluorophores used in PALM bleach rapidly; the lower photon yield introduces an inherent and finite error to the localization precision while simultaneously placing a substantial constraint on our ability to track particles over many frames.

The fitting error and the track length thus set the lower limits of detection using particle tracking PALM. Although theoretical descriptions have been derived of the localization precision with respect to photon number, the characteristics of the optical and detection system, and background noise, these descriptions are confined to nonmoving sources. I therefore asked how motion of molecules affects our ability to localize them, how the magnitude of the localization precision affects our ability to track molecules over multiple points in time, and how this motion would affect our ability to render a high resolution map of neuronal structures. Because preliminary experiments and published data indicated that many fluorescent proteins used for PALM will be bleached after imaging for only two frames, I was particularly concerned what could be deduced from two measurements of the same molecule's location.

How does localization precision affect our measurement of molecular motion?

Though an analytical solution to these problems may be possible to derive, my approach was a numerical one. I began by considering the 2-dimensional distribution of potential localizations of a single point representing a stationary molecule. This distribution was defined with a standard deviation σ_{loc} corresponding to the inaccuracy of localizing molecules with a finite number of photons (Fig 2.1A). By definition, a molecule located at the origin represented perfect localization, with the degree of error corresponding to the distance from the origin. By measuring the distance from the origin for each of 10,000 generated points (**Figure 2.1A, black bars**), I found that approximately 95% of the localizations were accurate to within $2*\sigma_{loc}$, and 68% of the

points were within σ_{loc} of the true location, as expected for a normal distribution. The mean of this distribution was approximately $0.8*\sigma_{loc}$.

To extend this consideration to the realm of tracking, I first simulated two successive measurements in the location of this immobile molecule by measuring the distance between 10,000 randomly sampled pairs of points within this distribution. The histogram of distances peaked at $1.2*\sigma_{loc}$ and had a mean of $1.19*\sigma_{loc}$ (**Figure 2.1A, red bars**). Only 46% of localized pairs were less than $1*\sigma_{loc}$ apart, whereas 89% were within $2*\sigma_{loc}$, and 97.5% were within $3*\sigma_{loc}$. Thus, even for an immobile molecule, repeated imprecise measurements give a non-zero estimate of its motion, and the error in localization inherent in each fit is substantially magnified.

Figure 2.1: Masking of true motion by localization error

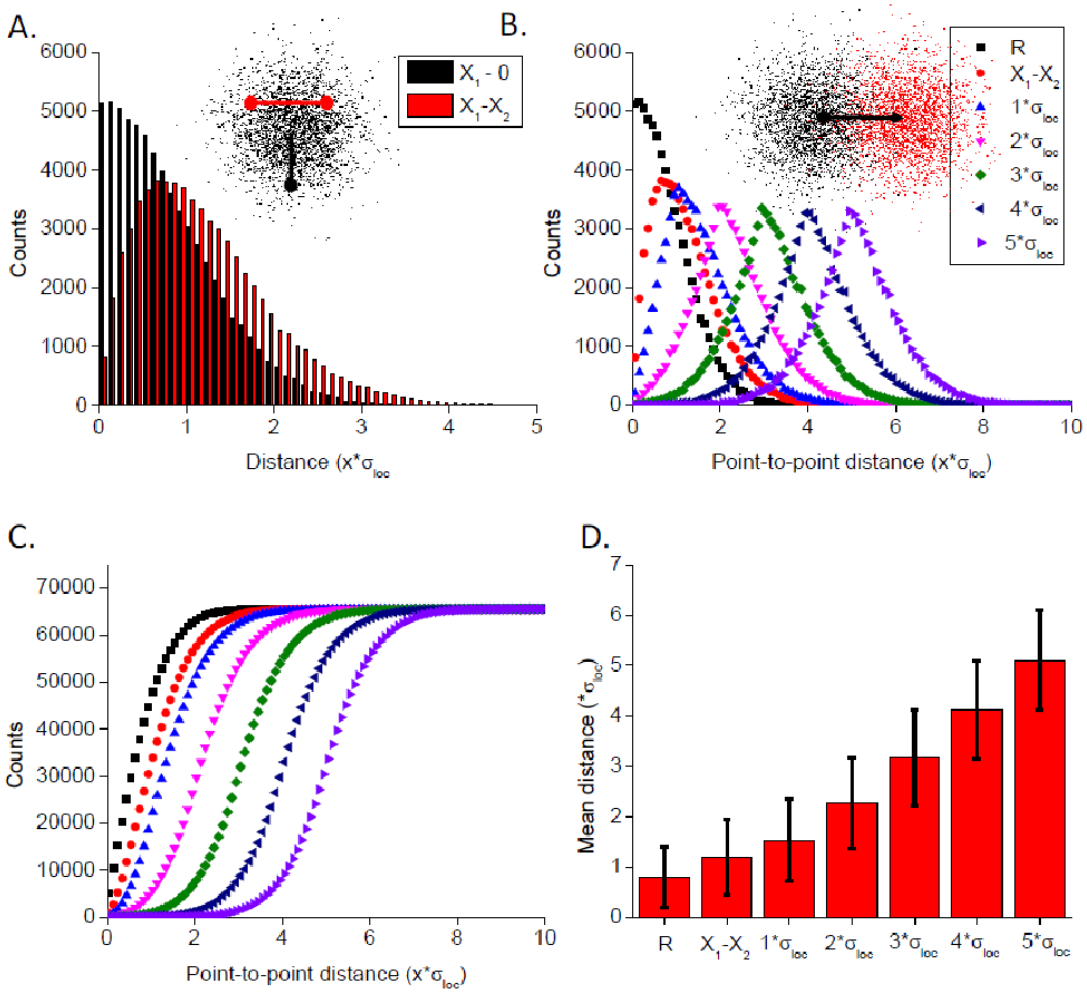

(A) 10,000 points representing localized positions of a molecule were randomly generated with 1 dimensional precision σ_{loc} surrounding the true location of the light-generating molecule. **(B)** The distance of individual individual localized positions from the true position of the molecule is plotted as a histogram. The histogram peaks at distances slightly greater than the one dimensional localization precision (σ_{loc}). Localized positions were randomly generated **(C)** for pairs of molecules with true locations spaced at increasing multiples of σ_{loc} apart. The distance between random pairs of localized positions is plotted as a histogram for each true intermolecular spacing. **(D)** Cumulative plots of intermolecular distances plotted in C. **(E)** Mean point-to-point distance for molecules with increasing intermolecular distances as in C and D. **(F)** Histogram of point-to-point distances for a series of 10,000 localizations of molecules spaced a random distance apart.

This error makes it difficult to discern motion over distance scales close to σ_{loc}, and so I sought to determine the distance a particle had to move to be accurately tracked. To accomplish this, I again created two normally distributed series of points, each with a standard deviation of σ_{loc}, with the second centered at increasing distances from the initial peak. For convenience I spaced the second distribution at multiples of σ_{loc} along the x axis. I then plotted the measured point to point distances as a histogram (**Figure 2.1B**) or cumulative distribution (**Figure 2.1C**). When the peaks were spaced $1*\sigma_{loc}$ apart the distribution of distances between points were remarkably similar to the distribution of measured distances between pairs centered at the same location, with a small increase in mean from $1.19*\sigma_{loc}$ to $1.52*\sigma_{loc}$. Increasing the separation between the peaks to $2*\sigma_{loc}$ created a distribution of point to point distances with a mean of $2.26*\sigma_{loc}$. Greater degrees of separation resulted in further rightward shifts of distribution of measured distances, which became increasingly evenly spaced on the cumulative distribution plot (**Figure 2.1C,D**).

This has clear implications on the measurement of particle motion. The distribution of measured distances between peaks spaced $1*\sigma_{loc}$ apart largely overlaps with the measured distance of a nonmoving peak. However, the mean distance between points increases in a manner approaching linearity as the separation between the two peaks increases (**Figure 2.1D**). Whereas 95% of the measured distances between randomly chosen points from a single peak were within $2*\sigma_{loc}$, 50% of points from peaks separated by $2*\sigma_{loc}$ were greater than $2*\sigma_{loc}$. 90% of points chosen from peaks separated by $3*\sigma_{loc}$ were more than $2*\sigma_{loc}$.

Taken together, these results suggest that as a population, it should be possible to differentiate particles moving as little as $2*\sigma_{loc}$ from non-moving particles, with increasing confidence in individual tracks as molecular motion increases past $3*\sigma_{loc}$. It should be noted that the true motion of a population of molecules with a range of distances traveled will be overestimated by an amount up to $\sim 1.2*\sigma_{loc,}$ depending on the proportion of molecules that move only a short distance.

How does localization precision affect our measurement of directionality?

One of my primary goals was to measure the direction of molecular motion within dendritic spines. Actin filaments are polarized, with preferential incorporation of monomers at one end driving polymerized actin along the filament away from the site of polymerization. I reasoned that measurement of the direction molecules moved would provide insights to the locations where polymerization take place within spines. Since polymerized actin molecules move relatively slowly photobleaching and depolymerization limit our ability to follow the motion of single molecules along filaments for long periods of time, it was important to understand the lower limit of movement required to accurately define the orientation of polymerizing filaments.

As the direction assigned to a tracked particle moving between two points sequentially localized could be dramatically altered by poor fitting of one or both of the points, I investigated the effect of localization error on the angle assigned to pairs of points generated along normal distributions with peaks centered at varying distances

apart (**Figure 2.2A**). The xy positions of each pair of points was then adjusted so that the first point was at (0,0), facilitating visualization of the angle of the vectors drawn from the first point to the second point. Vectors connecting points chosen from peaks centered at the same location emanated in an apparently random pattern, but as the separation between the two peaks increased, the vectors became increasingly aligned with the true angle between the center of each peak. To quantify the precision at which angles could be determined, I quantified the percentage of pairs separated by 0 to $10*\sigma_{loc}$ at $0.1*\ \sigma_{loc}$ intervals (100,000 intervals at each point) in which the angle of the vector (theta) connecting the two points was accurate to within 45 degrees (**Figure 2.2B**).

When points were selected from peaks located at the same position, 25% of the vectors pointed within the correct quadrant, as expected for a random distribution. As the separation between the peaks' centers increased, the percentage of pairs in which the direction was accurately identified to within 45 degrees increased rapidly, reaching 100% when the peaks were separated by $3*\sigma_{loc}$. In addition, the standard deviation of theta decreased rapidly as distance between the peaks increased until the true separation reached $2*\sigma_{loc}$ distance apart, at which point the curve continued to approach zero at a much slower rate (**Figure 2.2C**). Thus directionality of molecules that move 2 σ_{loc} or more can be assigned with greater than 85% accuracy, and with spatial averaging direction can be accurately assigned for even slower-moving molecules.

Figure 2.2: Effect of localization precision on ability to discern directionality of motion

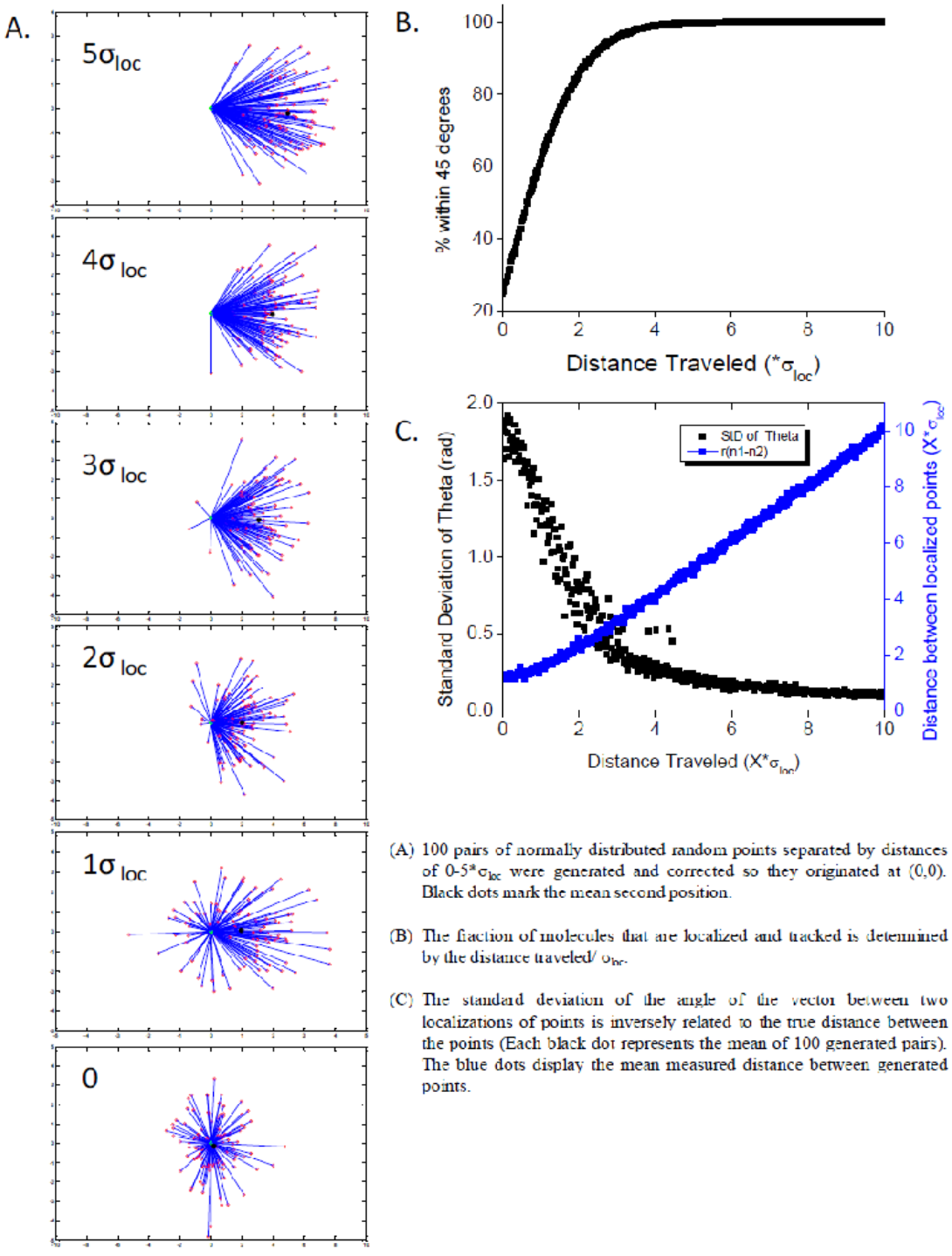

(A) 100 pairs of normally distributed random points separated by distances of 0-5*σ_{loc} were generated and corrected so they originated at (0,0). Black dots mark the mean second position.

(B) The fraction of molecules that are localized and tracked is determined by the distance traveled/ σ_{loc}.

(C) The standard deviation of the angle of the vector between two localizations of points is inversely related to the true distance between the points (Each black dot represents the mean of 100 generated pairs). The blue dots display the mean measured distance between generated points.

I applied this analysis to data collected from actin-mEos2 in Hippocampal neurons (see figure 3.5). In fixed cells I measured an average track distance of 81.7 +/-

7.5 nm, which would correspond to a σ_{loc} of 68 nm. In live cells at acquisition rates of 3.3 Hz, actin-mEos2 tracks measured 104.9 +/- 6.9 nm ($1.52*\sigma_{loc}$). If all molecules moved at the same rate within the cell (likely not the case), this would be very close to the limit of detection. To overcome the slow rate of actin motion, I collected frames at 0.5 Hz, giving molecules 2 seconds to move between frames. This resulted in a mean measured motion of 144.01 +/- 9.4 nm, or $2.11*\sigma_{loc}$, ensuring that real motion of individual tracks were readily discernible, particularly as this is likely to represent molecules with a range of movement rates. Jasplakinolide reduced the mean distance that particles moved to 91.1 +/- 6.9 nm ($1.33* \sigma_{loc}$), nearly to the level of fixed molecules.

Thus, accurately tracking the motion of a molecule moving with an arbitrary velocity can be accomplished in one of two ways: by increasing the localization precision, or by increasing the time between measurements to allow molecules to move a sufficient distance that their motion may be accurately measured.

How does molecular motion affect our ability to define the position of molecules?

In contrast to polymerized actin which moves relatively slowly, many molecules diffuse rapidly within the cytosol or the plasma membrane. Thus, in the span of one image acquisition, they may cover hundreds of nanometers or even microns. This results in ‘blurring’ of the molecule as photons are emitted and collected throughout the image acquisition. This has two primary effects on the detected image of the molecule. As the photons are emitted from multiple locations as the molecule moves, it can no longer be considered a point source, and the detected photon distribution may now depend on both

the PSF of the optical system as well as the molecules behavior. Photons from moving molecules are thus spread across a wider distribution, with shorter peaks.

I reasoned that the blurring is dependent on both the speed of the molecule and the integration time of image acquisition. To understand how this might affect our ability to correctly localize a diffusing molecule, I modeled molecular diffusion as a random walk in two dimensions. Molecules were forced to take a number of steps, based on the diffusion coefficient of the molecule and the desired integration time (representing exposure time) **(Figure 2.3)**. Using this approach, I found that molecules covered a wide area in exposure times as little as 25 ms (**figure 2.4**). Both the area covered and the distance between the initial and final positions increased with time of exposure (**Figure 2.5**).

Figure 2.3: Molecules move large distances on the time frame of image acquisition

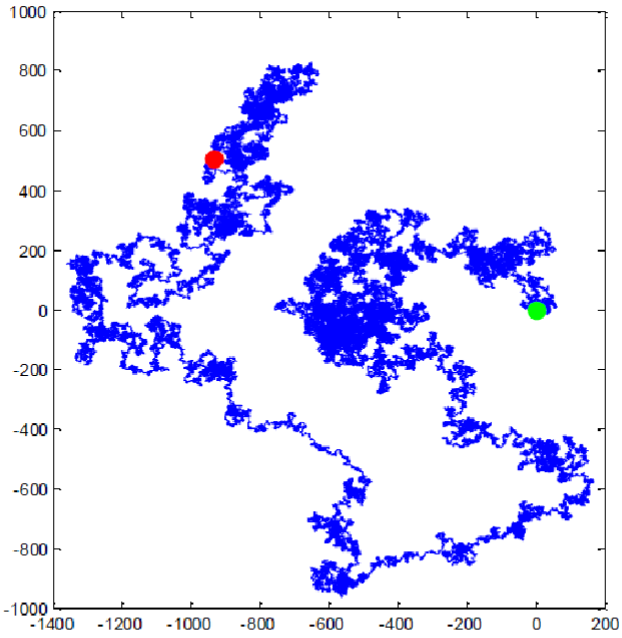

Path taken by a molecule with diffusion coefficient of 1 um^2/s in 25 ms; 1 nm steps.

A random walk was generated for a molecule with a diffusion coefficient of 1 um^2/s over 25 ms. Randomly generated steps with an average size r of 1 nm in any direction were generated using the equation Steps = round(4*(DC*1000000)*time/r^2), where DC is the diffusion coefficient in um^2/s, and time represents the amount of time over which the molecule is imaged. The initial position of the molecule is noted by a green dot. The final position is noted by the red dot.

Figure 2.4: Calibrating the random walk

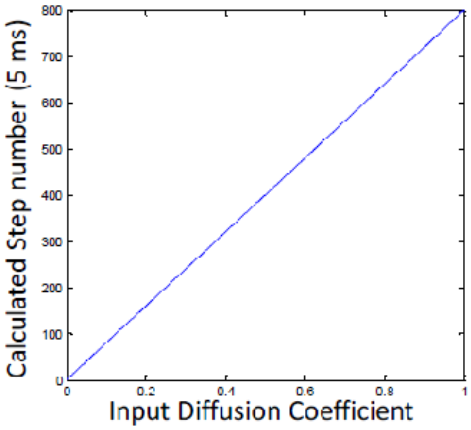

Appropriate numbers of 5 nm steps were calculated for molecules with diffusion coefficients ranging from 0 – 1 um^2/s using the formula:

Steps = round(4*(DC*1000000)*exposure_sec/r^2)

With exposure_sec = 5 ms.

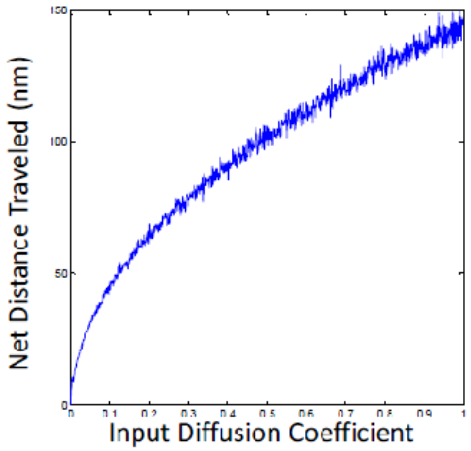

Molecules were allowed to take the appropriate number of steps calculated from their diffusion coefficient. Steps are random in both length and direction, with an average length of r = 5 nm. The mean distance traveled is plotted as a function of the input diffusion coefficient.

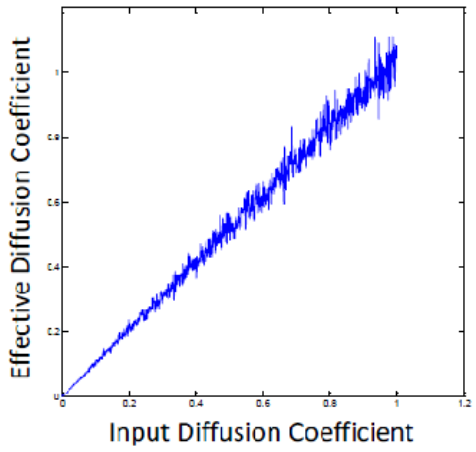

The effective diffusion coefficient of molecules taking the calculated number of steps is plotted.

Figure 2.5: Paths taken by molecules during random walks of varying timescales

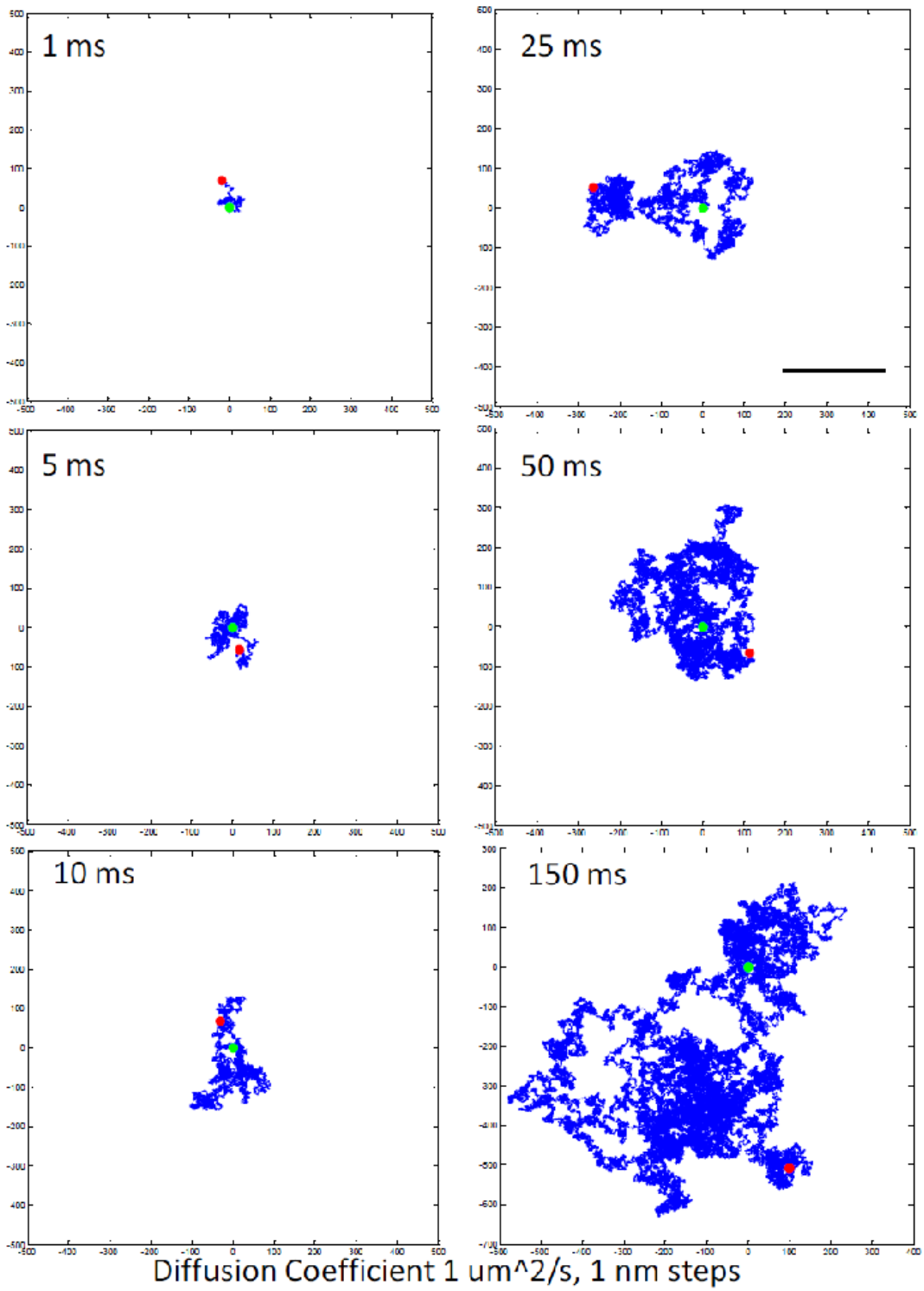

Paths taken by molecules of varying diffusion coefficients. Scale bar = 250 nm.

To examine quantitatively the effect of this motion on the acquired image of a molecule, 1000 simulated photons were generated at a fixed rate during the course of the random walk. Each photon was given a randomly generated location in a normal Gaussian distribution centered at the current position of the moving molecule and with a standard deviation σ_{psf} = 250 nm to represent the diffraction-limited PSF of the optical system. The photons were then assigned to 100 nm bins representing camera pixels. (The molecule starting position was the center of one of these camera pixels.) With no motion, the photon distribution formed a sharp peak which rapidly fell off in intensity. The intensity of the center pixel was clearly decreased in as little as 1 ms when the molecule was modeled with D = 1 $\mu m^2/s$, with the shape of the distribution becoming visibly blurred in as little as 5 ms and clearly unusable with integration times of 50 ms (**Figure 2.6**). In contrast, the slower motion of molecules modeled with D = 0.1 $\mu m^2/s$ clearly increased the range of exposure times over which the molecule could be imaged. However, there was clear degradation on the quality of the imaged photon distribution even at 10 ms.

Figure 2.6: Motion of single molecules during image acquisition affects photon distribution

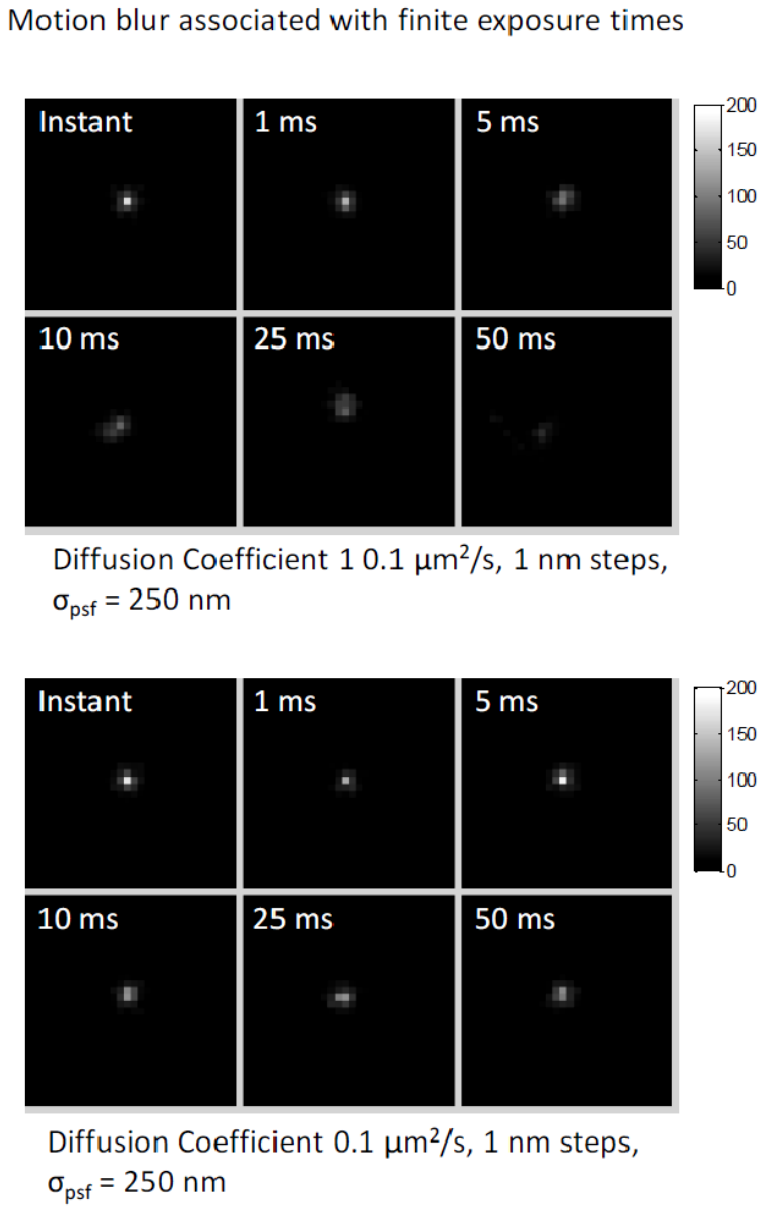

To examine the effect that motion blur would have on imaged single molecules, random walks were generated for molecules with the described diffusion coefficients and exposure times. At equally spaced steps along the walk, "photons" were randomly generated with a 1 dimensional σ_{psf} of 250 nm. The distribution of photons was then plotted in 100 nm bins representing camera pixels.

To determine how this affected the precision of our fit-derived localization, 1000 molecules with diffusion coefficients of 1 $\mu m^2/s$ were allowed to travel for exposure times ranging from 1 to 50 ms and localized by fitting simulated images with an elliptical Gaussian function. The precision of individually generated molecules was estimated as in Thompson et Webb (**Equation 2.1**) and was compared to that of unmoving molecules (**Figure 2.7A,C,E**). For ease of comparison and generalizability, precision was normalized to that obtained in the nonmoving condition without noise. The peak of the distribution of localization precisions of unmoving molecules was sharp, with a notable right shift in as little as 1 ms of motion, with increasingly rightward shifted, shortened and broadened distributions with increasing exposure. Notably, at 25 and 50 ms a significant number of generated molecules could not be localized. To simulate real data, noise was added to the background of each molecule, with a resulting signal-to noise ratio of 16.6 for nonmoving molecules. This resulted in a broadening of the nonmoving distribution (**Figure 2.7B, D-E**), and increased right-shift and broadening of molecules at increasing exposures. Furthermore, a number of molecules were not identified to be fit. Similar effects were seen on the ellipticity of the fit of these molecules, with increasing ellipticity at higher noise or exposure lengths (**Figure 2.8**). Thus, in practical terms it is important to minimize exposure time to maximize localization precision of rapidly moving molecules.

Figure 2.7: Motion blur affects localization precision

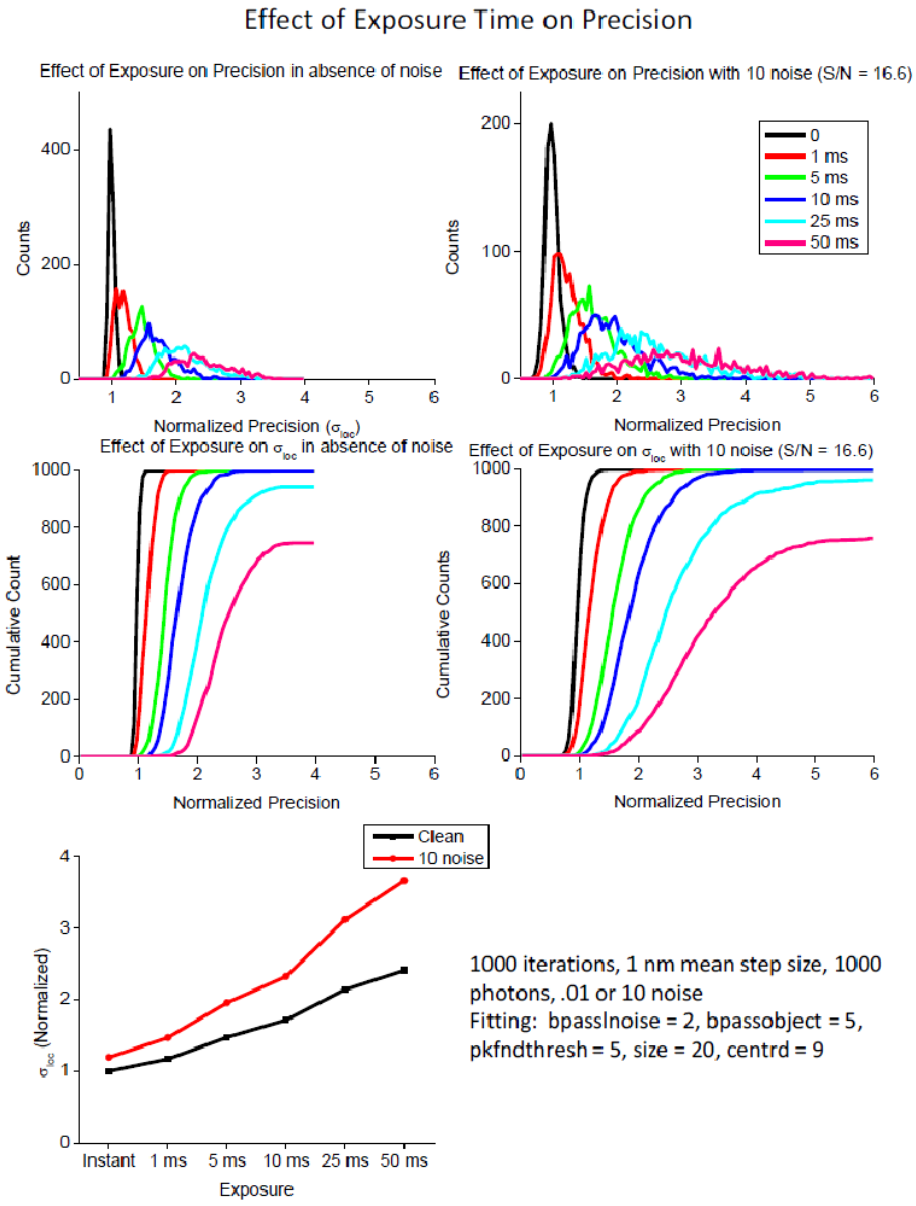

Photon distributions were generated as in figure 2.6. Molecules were fit using a 2 dimensional Gaussian. The precision was normalized to that measured for nonmoving particles and plotted as a histogram in the upper panels. The panel on the right is the same as upper left, but with the addition of noise (SNR of ~16). Middle panels are cumulative plots of normalized precision. The mean σ_{loc} (normalized in this case to nonmoving, noiseless condition) of molecules imaged for up to 50 ms is plotted in the bottom panel. Note that ~25% of molecules were not identified for fitting in the 50 ms exposure.

Figure 2.8: Motion affects ellipticity of fit

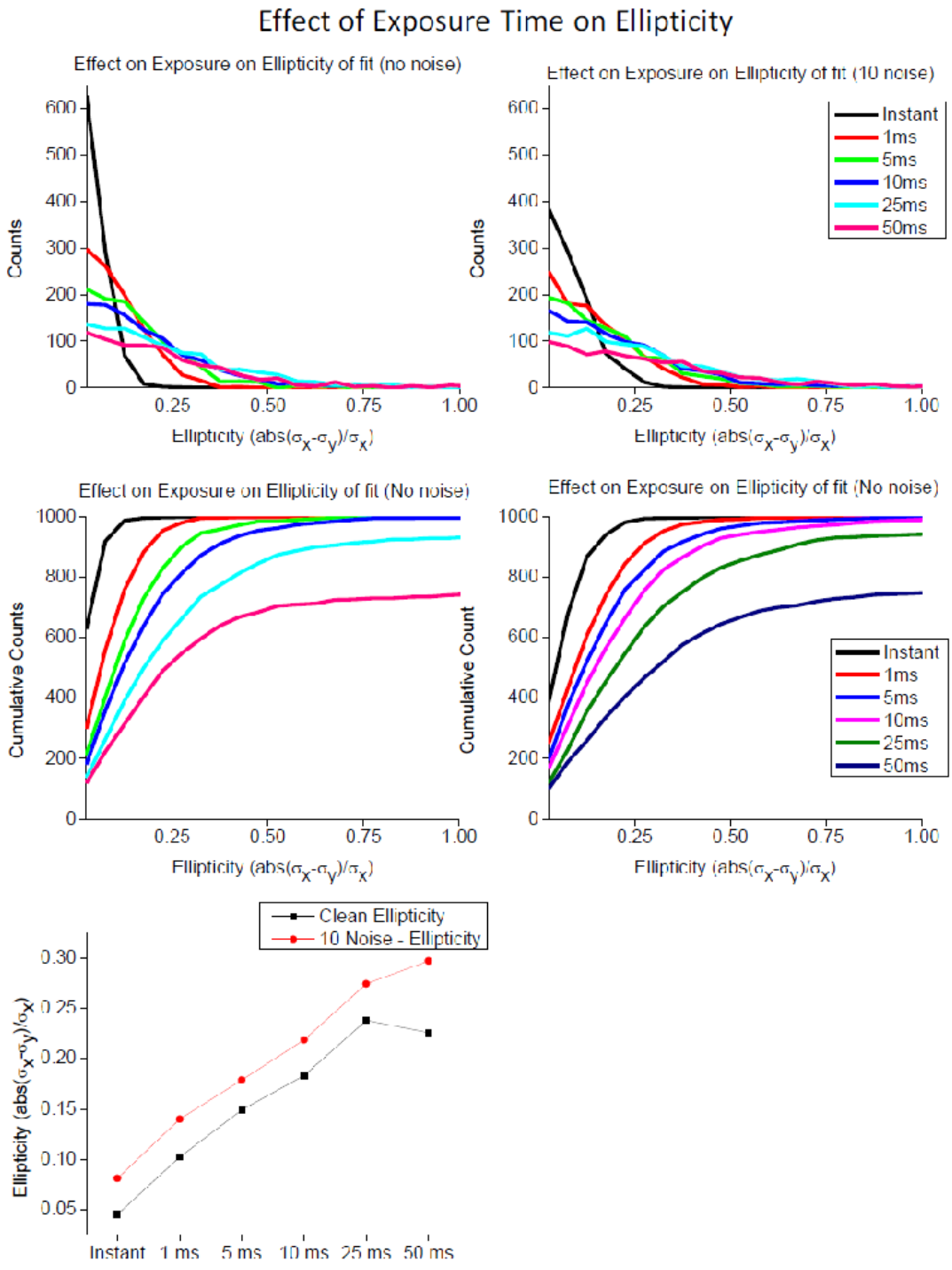

The effect of motion on Ellipticity ($abs(\sigma_x-\sigma_y)/\sigma_x$)) is generated as in figure 2.7 and plotted.

How does molecular motion affect our ability to define structural morphology?

The motion of moving molecules influences the localization precision of individual molecules, as well as our ability to accurately track their motion. It will also affect our ability to define neuronal morphology using large numbers of localized molecules acquired in living cells. There are at least two adverse effects that molecular motion is expected to have on the final distribution of localized points. First, broadening of the distribution of photons (refer to above figures) will decrease the localization precision, directly decreasing our ability to resolve fine-scale details of the final image. Secondly, the actual motion of the molecules is biased away from the edges of bounded regions, so that while the molecule may be located at the edge of a cell at the beginning of the acquisition, it will move away from the edge over the course of the acquisition. Thus, the average position of a localized molecule will never be located at the boundary of a region; it will trend inward over time. Given sufficient time, the average position of any freely moving molecule exploring a bounded region by a random walk will be the center of the region.

Importantly, using an elliptical Gaussian fitting routine, the localized position is very close to the average position of a moving molecule (**Figure 2.9**). In the absence of noise, the location determined from the centroid of the molecule image performed similarly, but the introduction of background noise degraded the centroid substantially compared to the elliptical Gaussian method.

Figure 2.9: Distance to center of mass

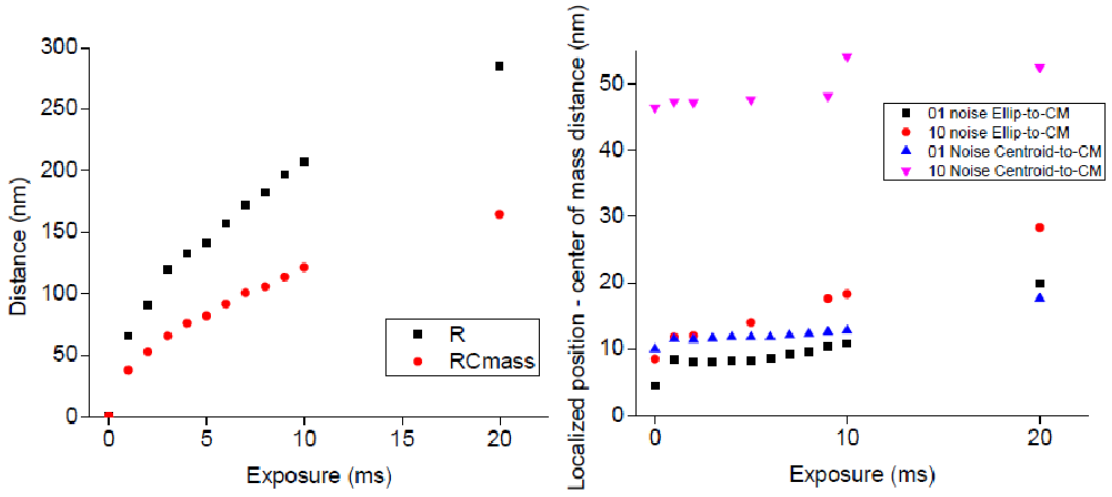

The center of mass for a molecule in motion moves away from the starting position with time. 100 molecules with diffusion coefficients of 1 $\mu m^2/s$ were generated and allowed to diffuse for the indicated amount of time (Left Panel). The net distance traveled is shown in black. The center of mass (shown in red) was defined as the average position of the molecule over the course of the walk.

The distance between the localized position and the center of mass was calculated for each iteration. The average of 100 iterations is shown (Right Panel). Using the Elliptical Gaussian fitting algorithm, the distance between the localized position and the center of mass was 5 nm in the absence of noise and motion (Black squares). This distance increased to around 10 nm with the addition of noise (Red dots). Interestingly, the localized position tracked the center of mass relatively well. In the absence of noise, the centroid algorithm performed similarly (blue triangles), but degraded significantly with the addition of noise (pink triangles).

Thus, the bias toward localization of moving molecules toward the interior of cellular structures might be a primary limiting factor governing the ability of PALM to accurately define the boundaries of a region or cell. To quantify this effect, I constructed a model in which molecules were generated at random positions within a bounded

rectangular region 100 nm wide and 1000 nm long, approximating a long spine neck. Molecules were allowed to move freely within the boundaries of this region according to their diffusion coefficient and a specified amount of time corresponding to camera exposure times (**Figure 2.10a**). Molecules with a diffusion coefficient of 1 $\mu m^2/s$ moved freely within the boundaries of the region and as expected, over longer exposure times occupied a larger region within the boundaries.

Figure 2.10: Effect of molecular diffusion on distribution of localized positions

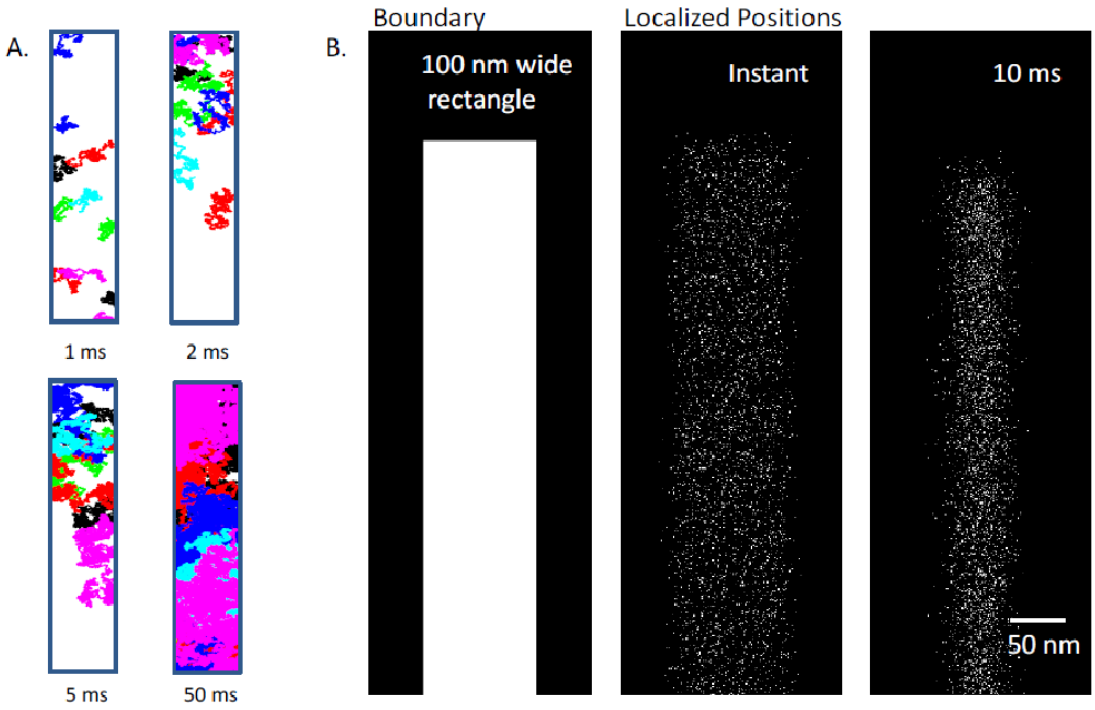

With increasing exposure time, individual randomly generated molecules with diffusion coefficient of 1 um^2/s traveled across an increasing fraction of a bounded region (A). To examine the effect of this motion on our ability to define the morphology of the bounded region, the localized positions of molecules randomly generated inside a 100 nm wide rectangle are plotted in B. In the absence of motion, molecules are evenly distributed across the width of the rectangle. In contrast, the distribution of localized positions of

molecules diffusing for 10 ms appeared narrower and was densest at the center of the bounded region.

Each molecule was then localized using an elliptical Gaussian fitting algorithm and the position of each molecule was mapped. In the absence of motion the edges of the rectangle were well defined and the density of molecules was relatively even across the bounded region (**Figure 2.10b**). Following 10 ms exposures however, the localized positions were clearly further from the edge of the bounded region, resulting in increased apparent molecular density at the center of the rectangle, and a much thinner-appearing region.

I quantified the decrease in width at timescales from 1 to 150 ms by drawing histograms with the integrated molecular density across the width of the rectangles ranging in width from 50 to 150 nm. For each simulation 0.067 molecules/nm^2 (~6700 molecules in a 100 nm wide rectangle) were generated and allowed to move freely within the confines of the rectangle. Individual molecules were localized using a fit of their Gaussian distribution and the halfwidth of each density histogram was measured (**Figure 2.11**). In each case, the histogram appeared wider and shorter in the fixed condition with a gradual decrease in width and increase in height as the exposure time was increased (n = 5 simulations for each condition). Thus, when imaging was modeled using 2 ms exposures of molecules with a diffusion coefficient of 1 μm^2/s, the measured halfwidth of regions 150 nm in width was diminished by approximately 25 nm; The measured halfwidth decreased by more than 80 nm when molecules were allowed to travel for as little as 10 ms. Modeling image acquisition using probes with slower diffusion coefficients resulted in more accurate measurement of the dimensions of the region. This

emphasizes the need for rapid imaging in applications in which one wishes to define the boundaries of free diffusion.

Figure 2.11: Quantification of width underestimation with increasing exposure lengths

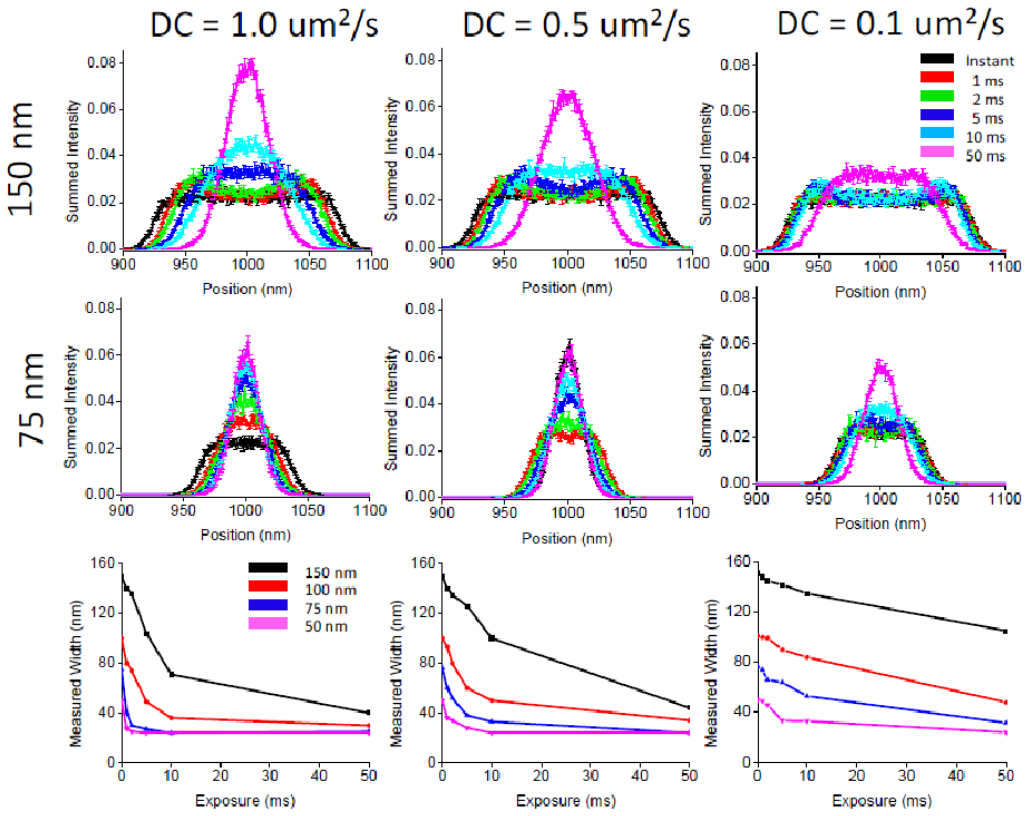

Molecules with diffusion coefficients of 1 $\mu m^2/s$ (Left column), 0.5 $\mu m^2/s$ (Middle), or 0.1 $\mu m^2/s$ (Right) were generated within the bounded rectangle as in Figure 2.8. The density of localized molecules across rectangles 150 nm in width (Top row) or 75 nm (Middle row) plotted as histograms for exposures ranging from 0 to 50 ms are shown. The halfwidth of the bounded regions is quantified in the bottom row, using a diffusion coefficient of 1.0 $\mu m^2/s$ (Left), 0.5 $\mu m^2/s$ (Middle), or 0.1 $\mu m^2/s$ (Right). With increasing exposures there is a clear decrease in the apparent width of the bounded region.

To illustrate these effects on imaging spine morphology, I again modeled the diffusion of molecules within a 2 dimensional bounded region, this time defined as a 500 nm square spine head connected to a dendrite of 500 nm diameter via a spine neck 100 nm wide and 1 μm long (**Figure 2.12**). Molecules with a diffusion coefficient of 1 $\mu m^2/s$ were generated and allowed to diffuse within this spine, and were subsequently localized. After even 5 ms exposure, the spine neck and spine head appeared thinner, with dramatic thinning of the spine head observed following 50 nm exposures. This again emphasizes the need for either extremely rapid acquisition parameters, or slower moving molecules for imaging neuronal morphology.

Figure 2.12: Modeling the effect of diffusing molecules on measurements of a 2 dimensional spine

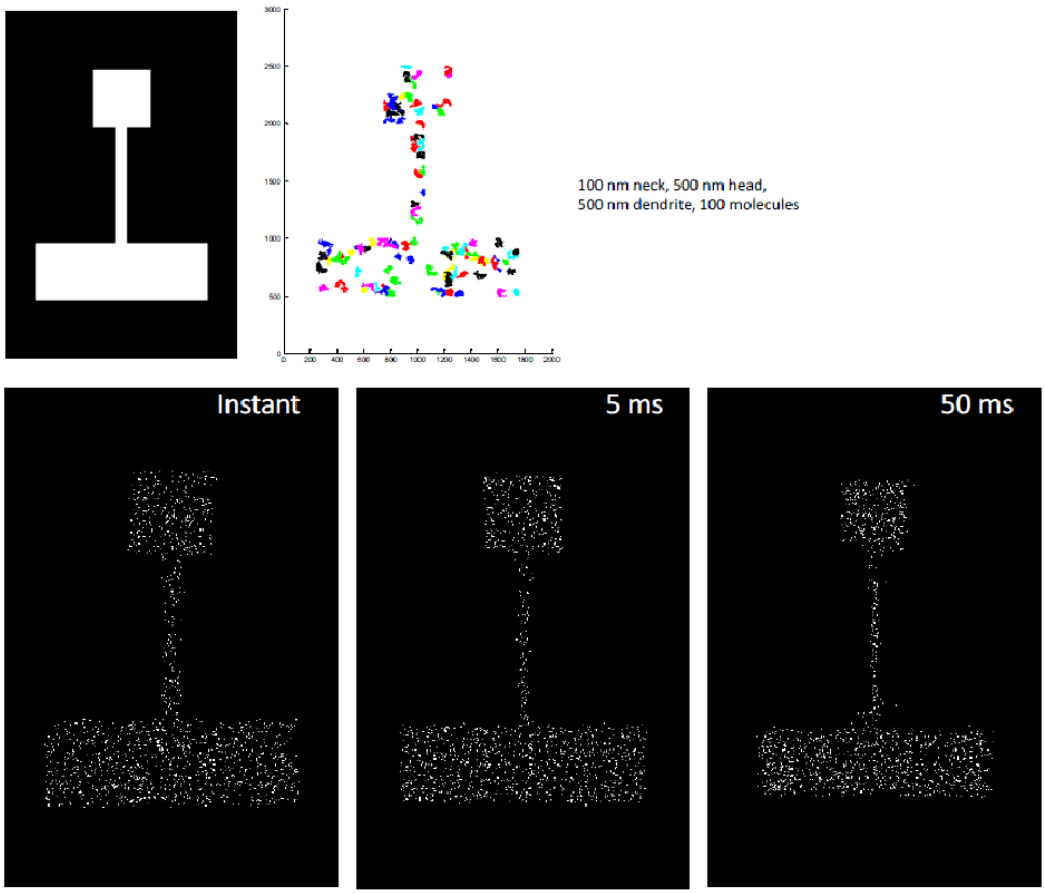

The effect of motion on distribution of localized molecules within a spine was modeled using a bounded region consisting of a 500 nm square spine head, a neck that was 1000 nm long and 100 nm wide connected to a dendrite that was 500 nm wide and 1500 nm long (Top Left). Plots of the paths taken by individual molecules with a diffusion coefficient of 1 um^2/s and an exposure duration of 1 ms are shown in top right. Localized positions of molecules following exposure durations of 0, 5, and 50 ms are shown in bottom panels. As with the simple rectangle, the distribution of localized molecules within the spine neck and head was clearly thinner with increased exposure durations.

This clearly applies to the imaging of dendritic spines. Imaging membrane-bound photoconvertible proteins would allow simultaneous resolution of neuronal morphology and the measurement of diffusive properties of proteins within various membrane

locations. However, it is clear that the drawback of using mobile particles is the apparent decrease in width of bounded structures, as discussed above.

Imaging neuronal morphology using PALM

I reasoned based on the above information that using very rapid acquisition parameters, imaging of a membrane tagged photoconvertible probe would allow the measurement of spine neck width at high resolution while simultaneously allowing the measurement of the effective diffusion coefficients of molecules moving through this confined space. To overcome motion blur caused by the rapid motion of freely diffusing membrane molecules (with diffusion coefficients ~ 1 $\mu m^2/s$), I designed and built a PALM scope in the lab optimized for rapid acquisition with short excitation pulses. To accomplish this, I utilized TTL gating of the AOTF controlling the excitation laser to initiate the excitation pulse. Gating was triggered by the start of the camera frame. This allowed the length of the excitation pulse, the delay with respect to frame initiation, and the frame length to be independently controlled. Millisecond excitation required high excitation intensity, which was achieved by expanding the incident collimated laser to only ~2.2 µm before focusing on the back plane of the objective for oblique (near total internal reflection) sample illumination. With the length of excitation pulses uncoupled from theacquisition frame duration we could achieve high acquisition frame rate (routinely 100 Hz of 15 x 50 µm with 100 nm per pixel) and short excitation pulses of 0.5 to 10 ms.

I transfected hippocampal cultures with either membrane bound mCherry or mEos2 and imaged neurons aged 10 to 18 days. 15,000 images were acquired of each neuron at 50 or 100 Hz using 4 ms excitation pulses. Molecules were localized by fitting the distribution of photons to a 2 dimensional Gaussian and images were rendered based on the distribution of localized molecules within 50 nm pixels (**Figure 2.13**). Neuronal dendrites were clearly visualized, with spine-like protrusions consisting of thin necks and bulbous heads protruding from the neuronal dendrite. Images were exported to ImageJ, and morphological characteristics were measured using the halfwidth of hand drawn linescans 250 nm in width. Spines averaged approximately 1 µm in length (**Figure 2.14, blue**) Nearly all spine necks were less than 250 nm in diameter (**Figure 2.14, red**), demonstrating the advantage of this method over diffraction-limited approaches in determination of spine morphology.

Figure 2.13: Imaging neuronal morphology at nanometer resolution using smtPALM

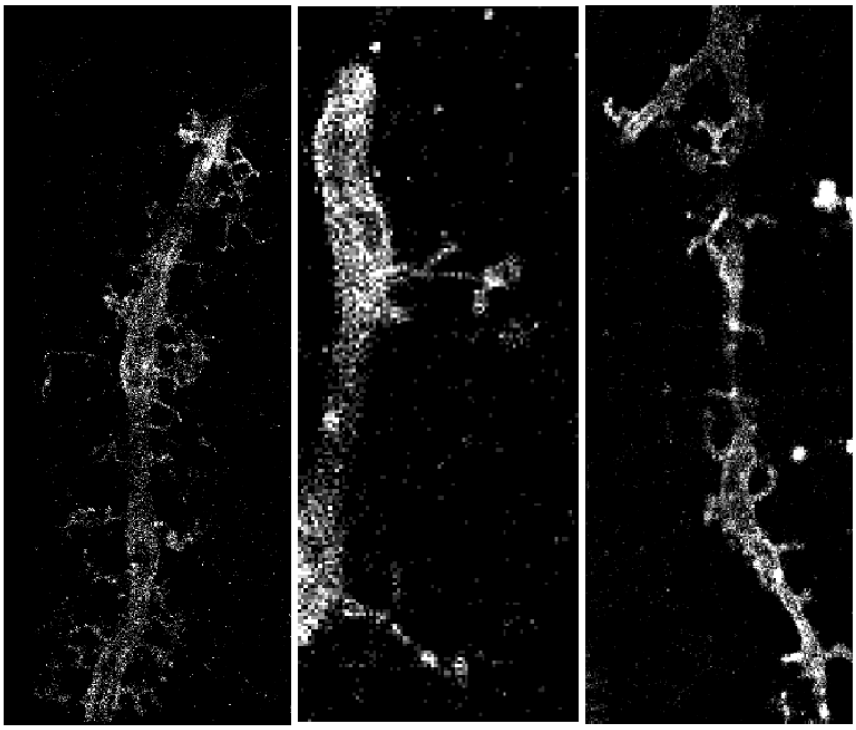

15,000 images were acquired of cultured hippocampal neurons expressing membrane-bound PA-mCherry at 100 Hz using 4 ms excitation pulses.

Figure 2.14: Measurement of spine neck geometry using rapid acquisition and short excitation pulses

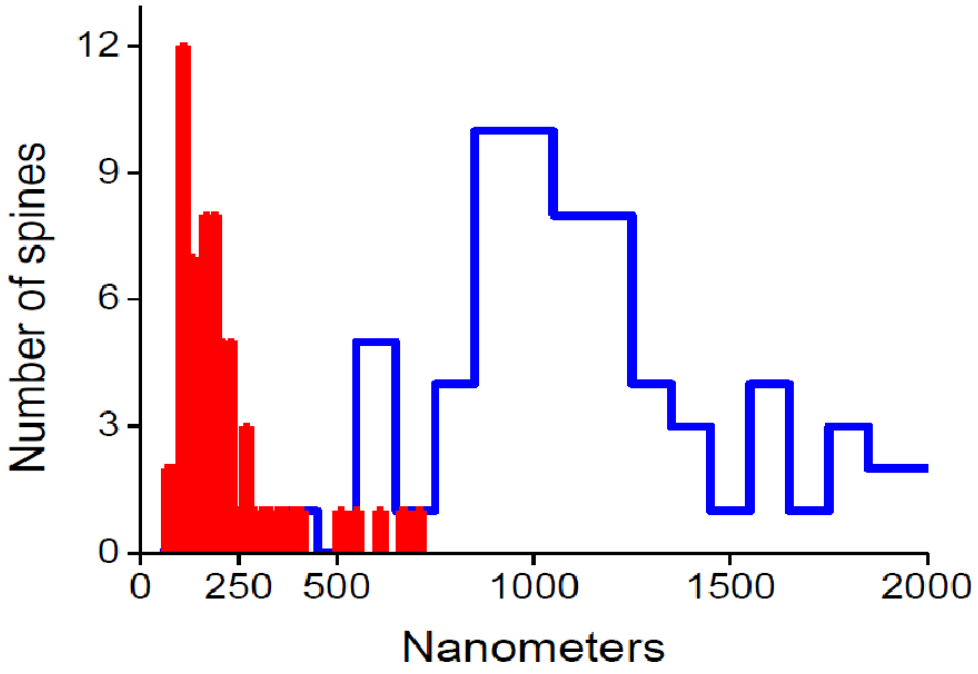

Spine length (blue) and neckwidth (red) were measured using line profiles of localized molecule distributions in ImageJ. Nearly all measured spine necks were less than 250 nm.

Discussion

Single molecule localization allows the position of individual molecules to be pinpointed with accuracy far in excess of the resolution of the optics through which the molecules are being viewed. This has permitted detailed study of the behavior of single molecule motion in living cells. PALM and STORM expand this basic method to allow the localization of thousands and thousands of molecules within minutes, permitting super-resolved images to be rendered from the distribution of localized molecules. I will

disregard STORM for the purposes of this discussion, as the required conditions are prohibitive to live-cell imaging. PALM, on the other hand is amenable to live cell imaging, allowing both single molecule tracking and super resolution of endogenously expressed protein in living cells.

I sought to define characteristics of suitable probes for PALM imaging within living neurons. I reasoned that the optimal imaging conditions would be determined by the goal of a particular experiment. In my experience, there have been two primary goals when imaging single molecules using PALM. The first is the definition of structures or protein distribution at high resolution. Several requirements must be met to fulfill this goal. First, a sufficient number of molecules must be imaged to accurately define structures at a given level of detail; essentially Nyquist sampling criteria must be met. Second, the localization precision of individual molecules must be finer than the desired resolution of the final image. This requires that a high number of photons be collected from individual molecules with minimal background. Background can be limited using thin samples, TIRF or oblique illumination, or photobleaching of background fluorescence. High numbers of photons can be generated through use of bright, photostable fluorophores and either long exposures or high intensity excitation. Finally, imaging should be optimized to limit morphological changes occurring within living, moving cells. Thus, the optimal imaging strategy may be to image as rapidly as possible to achieve imaging times on the order of seconds.

Conversely, if the goal is to accurately track the motion of individual molecules, then one must carefully consider the expected behavior of the molecules. The minimum distance that can be accurately determined depends on the localization precision achieved in a given experiment, as repeated imprecise measurements will resemble true molecular motion. Thus, it is critical to collect many photons in each frame, while at the same time it must be realized that each molecule will emit a finite number of photons before bleaching and these photons must be budgeted across multiple frames so that the molecule may be tracked. Anchored or slowly moving molecules require more time to move beyond the limit imposed by imprecision in molecular localization, whereas rapidly moving molecules will diffuse beyond an arbitrarily defined tracking radius between frames, causing them to appear as multiple separate, untracked molecules. Thus, interframe delays must be optimized so that molecules move far enough that their motion is detected, but not so far that it becomes difficult to identify and track molecules which are present over multiple frames.

Molecules at either end of this spectrum provide unique challenges. Slowly mobile molecules approach immobility and are difficult to distinguish from molecules in fixed samples. Thus, imaging will be primarily restricted by time. Whereas the collection of sufficient frames and molecules to render high resolution images is fairly simple in this condition, the long interframe delays necessary to allow molecules to move a perceptible distance may be prohibitive to collecting sufficient numbers of frames and molecules in tracking experiments. On the other hand, the rapid motion of freely diffusing molecules appears to allow both the accumulation of large numbers of individual points and the

measurement of molecular behavior with frame rates as high as 100 Hz. However, although the factors influencing protein localization of slowly moving and fixed molecules is well-described, it was not known how motion-blur induced by rapidly moving molecules during image acquisition would influence our ability to accurately localize individual molecules. Additionally, as my data sets often included a preponderance of molecules tracked over two to three frames before photobleaching, I wanted to determine the minimum factors needed to determine with accuracy the direction and velocity of individual molecules using single molecule localization.

My data demonstrate that our ability to localize molecules is critical in our ability to track them; poor localization precision results in exponential increases in time required for a molecule to move the minimum detectable distance. The increase in distance measured distance traveled with increasing true distance traveled is initially slow, largely due to the initial error derived from random sampling of points generated around a Gaussian distribution. In some ways, this underestimates our ability to measure protein motion, as the initial error is in all directions. This is apparent from my analysis of the ability to correctly determine angle of motion from two randomly generated points centered at increasing distances apart. Antiparallel vectors were virtually eliminated with just $2*\sigma$ of true separation. This indicates that while significant error exists from repeated sampling, both the angle and velocity of vectors drawn from two points can be drawn with confidence when molecules are given sufficient time to move $2\text{-}3*\sigma$ between frames.

Once again however, the precision with which we can determine not only the position of molecules, but the angle and velocity of their motion, is determined by our ability to properly localize them. I demonstrate in this work the deleterious effect of motion during image acquisition on localization precision. The rapid loss of sharply centered photon distributions leads to a rapid loss of pointing accuracy, even in the absence of noise. Noise is unavoidable in biological imaging due to autofluorescence, the imperfect contrast ratio of photoconvertible molecules, and shot-noise. A large fraction of rapidly moving molecules fail to be detected at 50 ms exposures, even in the absence of noise. With the addition of noise the peak of individual molecule photon distributions would likely diminish quickly to become undetectable. This is striking as a great deal of single molecule tracking of membrane bound molecules and receptors is performed with 50 ms exposures. While quantum dots and other dye-based probes are bright enough that they are easily detected despite their motion, they could certainly be localized more accurately using shorter exposure times.

Perhaps more surprising is the effect that motion of diffusing molecules during image acquisition has on determination of morphology. This effect is created from the tendency for molecules located at the very edge of a bounded region at the initiation of tracking to move inward. Molecules located within the boundaries of the region have an equal chance of moving in any direction. As molecules are localized near their center of mass, ie the center of their occupied territory during imaging, molecules that start at the very edge will be on average localized at a position a certain distance away from the edge, based on their diffusion coefficient and the time elapsed. Molecules initially located at

the center of the region will on average be localized at their starting location, as they have equal chances of moving in all directions. The net effect of this bias is that objects rendered from the localized positions of moving molecules will appear smaller than they actually are. This effect is minimized by use of slowly moving molecules or very short exposure times.

These were the factors that I considered when designing a microscope to image neuronal morphology in living cells using freely diffusing membrane bound probes. In doing so, we accomplished a number of objectives. First, we were able to maximize the delivery of high intensity excitation over a minimum area. Besides increasing the intensity of incident excitation light, this has the added benefit of not illuminating nearby regions of the cell; this limits phototoxic effects while simultaneously ensuring that a supply of unphotobleached membrane proteins is located in a nearby portion of the cell, waiting to diffuse freely into the region being imaged and replenish photobleached molecules. Although I have not quantitatively measured the effect, my impression is that this significantly increases the number of frames that I can collect before depletion of photoconvertible molecules.

Second, using very rapid excitation pulses that are controlled independently from frame acquisition length, I am able to image and accurately localize freely diffusing membrane molecules with excitation pulses as short as 0.5 ms. These extremely short pulses do not allow localization of all but the brightest of mEos2 molecules. In general

using our set up 4-5 ms pulses provide large number of localizable peaks with good precision.

Using this set up I was able to image dendritic spines from 10-18 day old neuronal cultures. Importantly, the vast majority of spine necks were less than 250 nm in width, highlighting the importance of super-resolution techniques in accurately defining spine morphology. My early experiments have also suggested that I will be able to accurately measure effective protein diffusion coefficients as molecules diffuse through spine necks.

3. Independent Regulation of actin polymerization at discrete sites within the spine.

INTRODUCTION

Synapses are inherently plastic, and undergo persistent changes in both strength and postsynaptic composition which are thought to underlie many forms of experience-driven learning. Remarkably, plasticity at individual synapses is not coupled to changes at nearby synapses (Malenka and Bear 2004). Such autonomy apparently is possible because dendritic spines, the micron-sized dendritic protrusions that are the site of most synaptic contacts in the brain, contain molecular machinery to permit modification independent of neighboring spines (Newpher and Ehlers 2009).

A critical component of this machinery is actin, the major cytoskeletal element of dendritic spines known to play a variety of roles regulating the synapse. Most prominently, actin has long been recognized as the principle determinant of spine morphology (Caceres, Payne et al. 1983; Penzes, Cahill et al. 2008), and it is clear that regulation of actin drives spine structural plasticity over time scales of minutes to hours (Matus 2000). Rapid morphological change is possible because actin within spines undergoes continuous turnover, driven by the broadly conserved mechanism of new monomer addition at the barbed end of existing filaments, and removal from the pointed end (Star, Kwiatkowski et al. 2002; Honkura, Matsuzaki et al. 2008; Hotulainen and Hoogenraad 2010). Except in the cases of synaptogenesis or synapse disassembly, the physiological role of actin-driven changes in spine morphology is surprisingly unclear. In fact, it is probable that control of spine morphology *per se* is not the most important

function of ongoing actin polymerization within spines. This is clear from observations that spine morphology is in many cases dissociable from plasticity of synaptic strength (Zhou, Homma et al. 2004; Bagal, Kao et al. 2005; Sdrulla and Linden 2007; Wang, Yang et al. 2007), whereas ongoing actin polymerization is critical for the induction and maintenance of long-term potentiation (Krucker, Siggins et al. 2000; Fukazawa, Saitoh et al. 2003; Rex, Chen et al. 2009).

On the other hand, accumulating evidence suggests that actin plays a variety of other, specific roles in spines, most notably at the postsynaptic density (PSD). A number of actin binding proteins interact with neurotransmitter receptors or PSD scaffold molecules (Cingolani and Goda 2008; Penzes, Cahill et al. 2008), supporting the notion that actin serves to "anchor" receptors in the synapse. However, disruption of actin polymerization with latrunculin results in a reduction of AMPA receptors in synapses (Zhou, Xiao et al. 2001), suggesting that this role of actin may involve dynamic filaments instead of static anchorage. Consistent with this, ongoing polymerization exerts direct control over the structure and composition of the PSD itself, both by driving ongoing structural rearrangement (Blanpied, Kerr et al. 2008) and maintaining a defined subset of scaffolding proteins within the PSD (Allison, Chervin et al. 2000; Kuriu, Inoue et al. 2006). Actin filaments have in addition been suggested to regulate both AMPA receptor exocytic mobilization and internalization (Osterweil, Wells et al. 2005; Correia, Bassani et al. 2008; Wang, Edwards et al. 2008), actions which are likely distinct from effects at the PSD. Thus, actin polymerization serves multiple roles in spines to regulate synaptic function, in particular by regulating components of the synapse directly.

Despite the importance of actin polymerization in controlling synaptic function, the nature of perisynaptic actin remains undetermined. Electron microscopy has provided a static picture of branching actin filaments, which reach throughout the spine and appear to interact with the PSD (Landis and Reese 1983), but has not revealed any potential dynamic nature of these structures. Conversely, numerous studies have investigated the regulation of actin in spines of living neurons (Star, Kwiatkowski et al. 2002; Okamoto, Nagai et al. 2004; Honkura, Matsuzaki et al. 2008; Hotulainen, Llano et al. 2009), but generally lacked the resolution for measurement of actin dynamics at spine subregions. Further, though actin regulates AMPAR internalization, and endocytosis in many systems is actin-dependent (Merrifield, Feldman et al. 2002; Kaksonen, Toret et al. 2006), whether actin is directly associated with the endocytic zone is not clear. Thus, it is not known whether actin at the PSD or endocytic zone is static or dynamic, and more generally whether actin polymerization in single spines is regulated globally throughout the spine or more precisely within functional spine subdomains.

A major obstacle to discerning the spatial organization of actin polymerization within spines is their small size. Here, I reasoned that tracking single molecules of intracellular proteins within the small confines of living neurons could resolve spine organizational substructure by surpassing the limits imposed by diffraction. Using single molecule tracking PALM to track single actin molecules in the spines of living neurons, I find that spines contain highly localized but spatially diverse foci of polymerization, frequently but not exclusively at the PSD.

EXPERIMENTAL PROCEDURES

Hippocampal neuronal cultures were prepared from E18 rats (Blanpied et al., 2002). Transfections were performed using Lipofectamine 2000 after 13-21 days in culture and imaging was performed 48 hours later. Multiphoton photoactivation was conducted on an LSM510 Meta (Zeiss), using 820 nm excitation from a MaiTai Ti:Sapphire laser (SpectraPhysics) and a 60x, 1.4NA objective. PALM imaging of fixed neurons expressing actin-tdEos and GKAP-Dronpa was conducted essentially as described (Shroff, Galbraith et al. 2007). sptPALM was carried out by modifying the approach of (Manley, Gillette et al. 2008). For tracking single actin molecules (Tatavarty, Kim et al. 2009), images were acquired using 150 ms exposures every 300 ms or 2 s as noted.

Following acquisition of sptPALM images, widefield images of PSD95- or clathrin-cerulean were acquired using a Xenon lamp and appropriate filters at multiple Z positions surrounding the sptPALM focal position, deconvolved in ImageJ, and summed. Molecules were localized by fitting a 2D elliptical Gaussian function to a 9x9 pixel array surrounding the peak, and locations were assembled into tracks using freely available algorithms (Manley, Gillette et al. 2008). All subsequent analysis was written in Matlab. Molecules were segregated into those which were tracked over multiple frames, and those which appeared in a single frame only. The distribution of tracked molecules representing polymerized actin was calculated based on the density of molecules within a search radius of 1 camera pixel (111 nm). Local mean velocities and local flow rates were

calculated using the first and last points of tracks originating within this radius. Velocities and vectors were mapped only in pixels with 3 or more tracks originating within the search radius.

Transfections and cell culture

Hippocampal neuronal cultures were prepared at embryonic day 18 essentially as described(Blanpied et al., 2002). Glass coverslips (Warner Instruments) were coated overnight with poly-D-Lysine (Sigma) and incubated in Neurobasal medium (Gibco) supplemented with B27 (Gibco), glutaMAX1 (Gibco), 5% FBS (Hyclone), and gentamycin (Cambrex). Neurons were transfected with Lipofectamine 2000 after 13-21 days in culture, and used for experiments 48 hrs thereafter.

Plasmid constructs

Actin-GFP was obtained from Beat Imhof, and the GFP sequence was replaced with PA-GFP(Patterson and Lippincott-Schwartz 2002). tdEos-paxillin was a gift from Jennifer Lippincott-Schwartz. The tdEos sequence was removed and inserted in place of the GFP sequence to make actin-GFP. mEos2 (McKinney, Murphy et al. 2009) was a kind gift from Sean McKinney. The coding sequence of mEos2 was inserted in place of EGFP in EGFP-C1, and then inserted in place of GFP to make actin-mEos2. GKAP-dronpa was created by inserting dronpa (a gift from Michael Davidson) into GKAP-GFP (SAPAP2-GFP, a gift from Guoping Feng). The GFP sequence of PSD-95-GFP (a gift from David Bredt) was replaced with cerulean (a gift from Mark Rizzo) to make PSD95-

cerulean (Rizzo, Springer et al. 2004). All constructs were confirmed by sequencing. tdTomato was a gift from R. Y. Tsien.

Confocal photoactivation experiments

Actin turnover kinetics in individual spines were measured on a Zeiss LSM510 Meta imaging system (Zeiss) using a 60X/1.40 Plan Apo oil immersion objective. Coverslips were held near 37 degrees using a Tempcontrol Mini objective warmer (Zeiss). Live cell imaging medium contained 120 mM NaCl, 3 mM KCl, 10 mM HEPES, 2 mM $CaCl_2$, 2 mM $MgCl_2$, and 10 mM glucose with pH adjusted to 7.35. Jasplakinolide (Invitrogen) or latrunculin A (Invitrogen) were added from 5 mM stocks in DMSO to this media to a final concentration of 5 µM for specified experiments. GFP was imaged with excitation from a 488 nm Ar ion laser, and mCherry and tdTomato excited with a 543 nm HeNe laser. Activation was achieved with a SpectraPhysics MaiTai Titanium Sapphire laser tuned to 820 nm. Laser power and scan speed for activation were adjusted to achieve > 90% activation in fixed cells expressing actin-PA-GFP with one scan of the region (Fig. S1a-c**;** 17.5 mW; 6.4 µsec/pixel scan). Regions were drawn to fully encompass individual spines but exclude the dendritic shaft. Images were collected at 1 Hz when only the green channel was being imaged, except for latrunculin or PA-GFP experiments, which were imaged at ~ 3 and 10 Hz, respectively. Experiments in which both the green and red channels were imaged were acquired at approximately 4 second intervals. As a control in whole spine activation protocols, a second photoactivation step was placed at the end of experiments to ensure that photoactivation occurred to a similar

level. Spines which did not photoactivate to similar intensity (within 30%) were assumed to have drifted out of focus and were excluded.

Monomer incorporation assay

Actin flow has been measured most accurately using total internal reflection fluorescence speckle microscopy (TIR-FSM), but dendritic spines have a small volume incompatible with the analysis required. Our alternative approach is optical mapping of monomer incorporation using photoactivation, which I termed the "phreckle" assay. In these experiments, regions encompassing entire spines were sequentially activated as above at 820 nm, and then bleached rapidly under 488 nm excitation. Imaging and photoactivation scan settings were identical to those used in previously described photoactivation experiments. I calibrated our laser power and scan settings to achieve nearly complete bleaching (11 iterations, 5.1 µsec pixel dwell time, 90% laser power). A second photoactivation of the same region was employed after 19 s to activate these new monomers. This delay was necessary for changing dichroics and allowed ample time for ongoing treadmilling of actin filaments to result in the loss of existing monomers within the spine and incorporation of new unbleached monomers. Simultaneous acquisition of green (PA-actin) and red (tdTomato cell fill) images allowed us to track the movement of these newly incorporated actin monomers, while simultaneously allowing us to monitor changes in spine morphology. A third activation pass was added at 42 s to test the full recovery of intensity and measure fluorescence decay rates. Images were analyzed offline using Metamorph (Molecular Devices, California).

PALM acquisition

For PALM experiments, 25 mm coverslips were washed for 3 hours in a 1:1:5 ratio of ammonium hydroxide:hydrogen peroxide:water and briefly flamed with methanol. To provide fiducial markers to monitor drift during image acquisition, 50 nm gold beads (Microspheres-Nanospheres, 790116-010) were diluted 1:20 in EtOH and dried onto the coverslips prior to overnight Poly-D-Lysine coating. Imaging was performed on an Olympus IX81 inverted microscope with a 60X/1.49 PLAN Apo oil immersion objective. Coverslips were held near 37 degrees with a warmed air stream and the imaging well was covered to prevent evaporation. Fluorescence emission was detected with an iXon DV887ECS-BV backthinned EM-CCD camera (Andor Technology) placed after a 2X magnification optic and a 1.2X relay lens. The 16.0 µm pixels of the camera thus covered 111 nm in the imaging plane.

Transfected cells were located in TIRF by exciting using 488 nm excitation and monitoring green fluorescence from the unconverted state of mEos2. To increase the depth of penetration of 561 nm excitation while still maintaining low background fluorescence, I adjusted the incident angle of excitation to achieve oblique illumination (Sako, Minoghchi et al. 2000). It was often helpful to bleach background red fluorescence before beginning acquisition of PALM or single-molecule tracking images.

For two-color fixed-cell PALM (Shroff, Galbraith et al. 2007), I first acquired a series of images of actin-Eos, employing continuous 150 ms exposures. 561 nm excitation was 12 mW entering the objective. 405 nm activation power was initially set at

~50 µW, and gradually increased over the course of imaging to maintain a low density of activated molecules. When the rate of Eos molecule appearance fell to unproductive levels despite strong 405 nm illumination, GKAP-dronpa was imaged following a sustained exposure to 488 nm light to convert photoactivated dronpa molecules to their dark state. Green fluorescence of sparsely activated Dronpa was imaged using continuous 400 ms exposures and 488 nm excitation of 4 mW.

Fixed-cell PALM images were analyzed to measure the position of each molecule and the uncertainty in its position based on the number of photons collected from it (Thompson, Larson et al. 2002). The resulting images (**Fig. 3.7**) show a probability density map of the likelihood of finding a molecule in each 5 nm output pixel by using color to encode both uncertainty and the density of molecules. The maximum localization error of molecules included for display was 30 nm (actin-tdEos) or 100 nm (GKAP-Dronpa).

Image acquisition for single-molecule tracking

In our adaptation of single-particle tracking PALM (sptPALM), I acquired a series of images of the red fluorescence from converted actin-Eos during periodic brief exposures to 405 nm laser light. The 405 nm light was kept extremely dim (generally ~5 to 50 µW) so that it photoconverted actin-mEos2 molecules in such small numbers that individual molecules were well separated (<<1 molecule per spine per frame). I used a long frame exposure time of 150 ms, reasoning as have others (Watanabe and Mitchison 2002), that molecules bound into actin filaments are expected to be relatively immobile

and be present at similar locations in repeated frames until they bleach or leave the filament, as compared to G-actin monomers which are known to be nearly freely diffusing (Pollard and Borisy 2003). Freely diffusing actin tagged with fluorescent proteins has a diffusion coefficient D of between 10-30 $\mu m^2/s$ (Pollard and Borisy 2003) and photoactivated PA-actin exits the spine in less than 1 second following treatment with latrunculin (Fig. S3C,D). Over the course of a 150 ms exposure, molecules with a diffusion coefficient of 10 $\mu m^2/s$ would move an average of ~2.4 µm ($\langle r^2 \rangle = 4D\Delta t$). The probability that a molecule with a diffusion coefficient of D has diffused a distance of L or more in time Δt is $P(L, \Delta t) = \exp(-L^2/(4D\Delta t)$ (Saxton 1993). Over the 150 ms exposure, 94.4% of free actin monomers would have diffused over a path of >1 µm and therefore would not form a localizable spot.

To further ensure that freely diffusing molecules were not tracked, I inserted a 2-sec gap between frames, during which time, freely diffusing molecules will on average travel 8.9 µm ($\langle r^2 \rangle = 4D\Delta t$). In addition, when assembling tracks followed by single molecules from positions localized in consecutive frames (see below), I limited to 444 nm (4 pixels) the radius over which a molecule could move over consecutive frames and be assigned to a single track. The probability of a molecule of D = 10 μm^2/sec moving beyond a 444 nm radius in 2 seconds is 99.4%. Thus, our acquisition settings effectively prevent the localization and tracking of freely diffusing monomers. Moreover, coupling our tracking radius with a frame rate of 0.5 Hz provides enough time for polymerized molecules to travel beyond our localization error, and allows tracking of polymerized actin with flow rates as high as 13.3 µm/minute.

To visualize the postsynaptic scaffold following single-molecule tracking acquisition, I acquired widefield, diffraction-limited images of PSD95-cerulean. Because not all synapses were assured to lie within the zone of oblique illumination, the widefield images were acquired at 3 focal planes near the coverslip to capture all PSD-95 puncta. Two dimensional deconvolution of each plane was performed in ImageJ (http://rsb.info.nih.gov/ij), and the maximum intensity projection of each stack was used to provide a 2-dimensional view of PSD location.

These imaging parameters appeared to protect cell health. One advantage of TIR and oblique illumination is that the low incident angle of light reduces the overall photon dose experienced by the cell. Furthermore, using 561 nm excitation as appropriate for Eos and other red molecules further reduces cell auto-fluorescence. After PALM imaging, cells were visualized using the green fluorescence of unconverted Eos molecules to ensure viability. No cellular blebbing was observed in the imaged or surrounding cells. Moreover, I did not observe changes in molecule behavior over the course of imaging (**Figure 3.6**) and molecule dynamics were altered in all cells by jasplakinolide.

Analysis of single-molecule dynamics

Single-molecule localization and analysis was carried out in MATLAB (The Mathworks, Inc., Natwick, MA). To identify potential molecules, the raw data was bandpass filtered, and thresholded to select high-intensity peaks. To ensure that neighboring molecules did not cause errors in localization or tracking accuracy, care was

taken to keep the density of photoconverted molecules low, and peaks were excluded if other peaks existed within a 9 pixel radius in the same frame. The location of molecules was deduced by fitting a 9x9 pixel array of the raw image data surrounding the peak with a 2D elliptical Gaussian function:

$$PSF(x,y,A,w_x,w_y,B) = A\exp(-[(x-x_o)^2/2w_x^2+(y-y_o)^2/2w_y^2])+B \qquad \textbf{Equation 3.1}$$

where x_o and y_o are the coordinates of the molecule, A the amplitude of the intensity distribution, w_x *and* w_y are the width of the ellipse in the respective axes, and B the background signal intensity. All variables were treated as free fitting parameters. The low density of photoconverted molecules made it very unlikely that two would exist simultaneously within the same diffraction-limited spot (i.e., at a distance below our ability to resolve them as two individual peaks). Peaks were discarded which were poorly fitted (w_x *or* w_y > 5 pixels) or eccentric (x/y *or* y/x > 1.3).

Tracking software was written in MATLAB, based on available algorithms (Manley, Gillette et al. 2008). To minimize the inclusion of molecules not bound within filaments, a maximal frame-to-frame displacement of 444 nm was permitted within a track, and frames without tracked positions terminated a track (i.e. no fluorophore "blinking" was included via interpolation). Net distance and velocity were calculated from the first and last localized point in each track. Net distance increased with the amount of frames in which molecules were tracked. I noted that rapidly moving polymerized monomers could be tracked at 3.3 Hz, but not at 0.5 Hz if the tracking radius

was less than 444 nm (data not shown). Thus, the 444 nm tracking radius appeared to allow the tracking of all polymerized molecules, while still preventing the tracking of freely diffusing monomers. Fiducials, which were distinguished from localized Eos molecules as having track lengths greater than 30 frames, demonstrated that stage drift was insignificant over the time courses for which individual molecules were tracked.

Maps of polymerized actin density and velocity were constructed using rescaled pixels of the indicated size. At each pixel, I calculated both the density and mean velocity of molecules whose tracks initiated within a 111 nm search radius (1 camera pixel). To ensure that mapped pixels represented an average, I calculated and mapped averaged velocity only in pixels with a local density of three or more tracked molecules. Local net flow was calculated as the vector average of molecules within the search radius.

Pharmacology

Latrunculin A was applied from 5 mM stocks in DMSO to cells in live-cell imaging medium at a concentration of 5 µM, and photoactivation experiments were conducted between 2 and 15 minutes following application. To test the effect of jasplakinolide on whole-spine actin turnover rate, images were recorded at 1 Hz following photoactivation, imaging medium was replaced with medium containing 5 µM jasplakinolide, allowed to incubate for 5 minutes, refocused, and photoactivated once again. Actin turnover measured in spines allowed to incubate for 5-15 minutes in jasplakinolide showed a similar rate of decay following photoactivation (data not shown). For single-molecule tracking experiments, jasplakinolide was diluted to 1:2 working concentration, and

pipetted into the imaging well on the microscope. Image acquisition was resumed after 5 minutes.

Distributed Sites of Actin Polymerization Within Single Spines

To identify regions of actin polymerization within dendritic spines, I transfected cultured hippocampal neurons with actin tagged with photoactivatable-GFP (PA-actin). Actin molecules in single spines were labeled selectively by two-photon photoactivation. Photoactivation within the targeted region was complete with a single activation (**Figure 3.1A-C**). Photoactivated PA-actin exited the spine rapidly, following a time course described well by a single exponential decay (τ = 17.94 ± 0.70 s; r2 = 0.991 ± 0.001, n = 32) with 4.1 ± 0.6 % remaining after 96 seconds. We, like others (Honkura et al., 2008; Star et al., 2002) find that this rate is far slower than the diffusion of monomeric PA-actin (**Figure 3.1D-F**) or PA-GFP (**Figure 3.1G**), and instead reflects treadmilling cycles of actin polymerization (elongating filaments through addition of actin monomers to their free, barbed ends) and depolymerization (**Figure. 3.1H,I**).

Figure 3.1: Measurement of actin dynamics in individual dendritic spines reveals a net polarized organization of spine actin cytoskeleton with behavior consistent with retrograde flow.

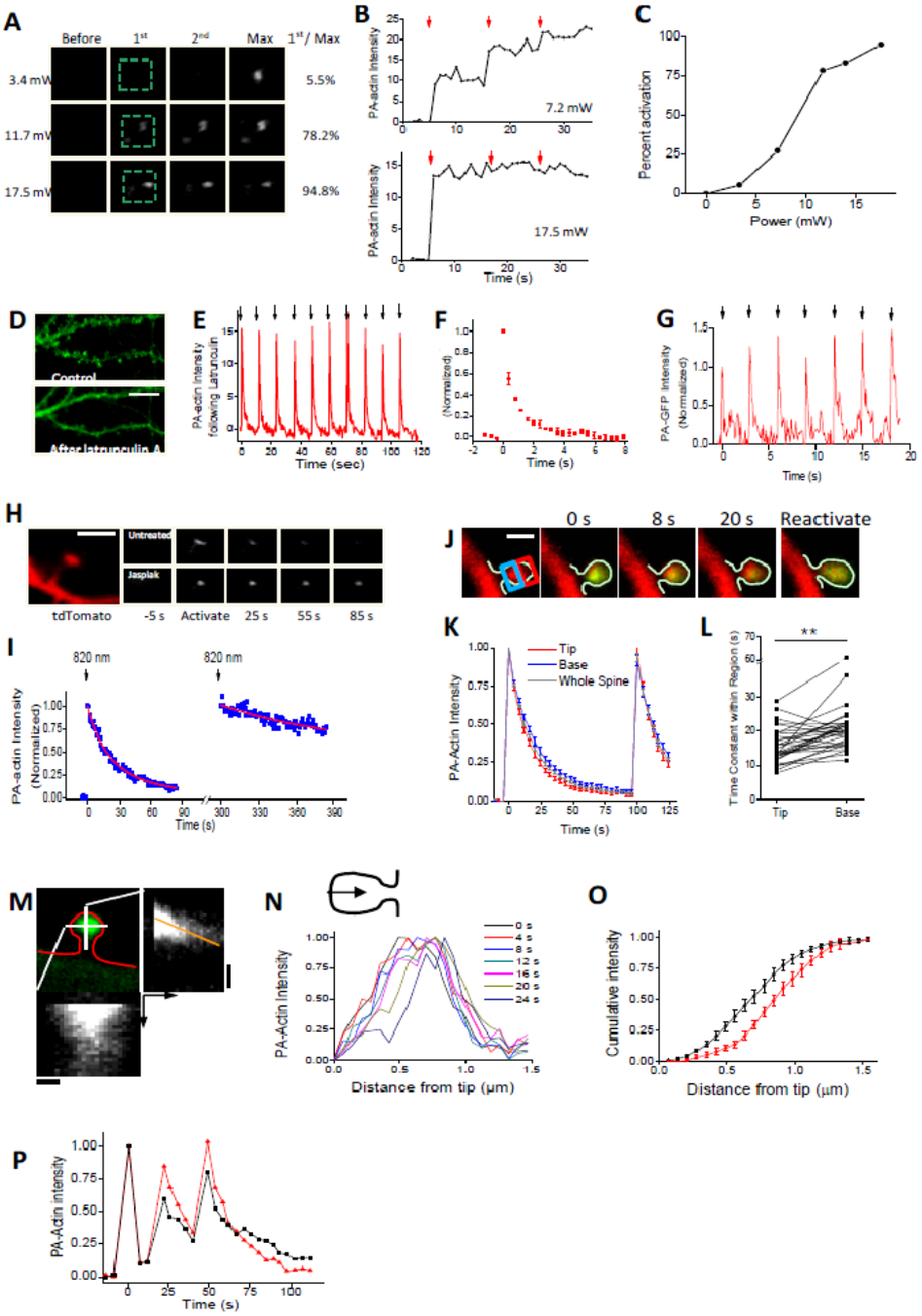

(A) Photoactivation was proportional to laser power. The laser was tuned to 820 nm and laser power was measured at the objective. Submaximal activation within the targeted regions was achieved using 3.4 mW or 11.7 mW. Subsequent photoactivation steps resulted in increased fluorescence intensity. A 17.5 mW photoactivation achieved

essentially complete photoactivation, as indicated by failure of subsequent photoactivation steps to increases fluorescence intensity further. A 17.5 mW photoactivation step was added after a series of three activation steps to achieve a saturating level of photoactivation (4^{th} column, labeled Max). **(B)** Intensity within targeted region as in A. At submaximal laser power, subsequent photoactivation steps (arrows) resulted in further increases in intensity (top). Maximum photoactivation was achieved with 17.5 mW (bottom). At this setting, photobleaching was also minimal, as revealed by the lack of decrease in fluorescence following several activation steps. **(C)** The mean intensity in the region following the first photoactivation step normalized to the mean intensity following the final saturating photoactivation step. **(D)** Treatment of neuron expressing actin-GFP with latrunculin A (5 µM), which inhibits polymerization, resulted in loss of actin-GFP from dendritic spines within 5 minutes. **(E)** Repeated photoactivation steps (arrows) in a cultured hippocampal neuron expressing PA-actin treated with latrunculin as in D revealed rapid turnover of freely diffusing, depolymerized actin. **(F)** Plot showing mean intensity of PA-actin following each photoactivation step from three neurons as in B. For the best single-exponential fit, τ = 0.72 +/- 0.13 s. **(G)** Freely diffusing PA-GFP rapidly exited the spine following photoactivation with τ = 264 ± 38 ms, n=5. **(H)** Photoactivation was targeted to an individual dendritic spine of a neuron expressing PA-actin and tdTomato as a cell fill. The actin filament-stabilizing drug jasplakinolide was added (5 µM) for five minutes before photoactivation was again targeted to the spine. Bottom panels show time course of intensity loss following jasplakinolide was slowed by when depolymerization was reduced with jasplakinolide (top right panel series). Scale bar, 1 µm. **(I)** Plot of the time course of actin loss from the photoactivated spine in D, before and after jasplakinolide. Representative of 5 cells. Red lines show single exponential fits to the data, with τ = 23.5 s and τ = 96.6 s. **(J)** Fluorescence time-series in a single spine from a neuron expressing tdTomato (red) and PA-actin (green). Activation with 820 nm light at time 0 s was directed over the entire spine head but not the dendrite shaft. Equal sized regions encompassing the entire spine head drawn at the tip and base (red and blue boxes, respectively) were analyzed in E. Scale bar, 1 µm. **(K)** PA-actin intensity following photoactivation of entire spines, measured within the spine tip (red), the spine base (blue) or the whole spine head (gray). Mean ± sem of n=32 spines. **(L)** Decay time constants in all spines measured in tip and base regions. In 26 of 32 spines, the decay was faster in the tip. **, $p<0.01$ (paired sample t-test). **(M)** Velocity calculation from kymographs of PA-actin distribution over time following targeted photoactivation at the spine tip. Upper left image shows PA-actin in a single spine following photoactivation at its tip. The fluorescence intensity profile in the spine along a line from tip to base (vertical line) is shown over time in the upper right kymograph. Fluorescence along a line perpendicular to this (horizontal line) is shown on the bottom. Note that the vertical kymograph clearly shows the time-dependent translocation of the actin distribution. A line estimating the peak (orange line) had a slope of 1.1 µm ± 0.04 µm/min. No lateral shift was apparent in the horizontal kymograph. Scale bars, 0.5 µm. Time scale arrows, 30 s. **(N)** Fluorescence intensity profile along vertical line in A, measured over time, revealing a shift of intensity in the direction of the spine base. Intensity was normalized to the peak at each time point. Net velocity was measured from the distance from the tip at which the intensity was 50% of its maximum. Representative example shown; mean of n = 8 was 0.7 ± 0.3 µm/min. **(O)** Cumulative

intensity along vertical lines as in A, displayed at 4 s (black) and 24 s (red) after photoactivation. Net rightward shift at 50% between 4 and 24 seconds occurred at a rate of 0.5 ± 0.1 μm/min. **(P)** Additional data accompanying Figure 1E-G. Jasplakinolide (5 μM) substantially prevented incorporation into spine filaments following initial photoactivation and bleaching steps.

The rate of decay was faster at the spine tip than in the center (**Figure 3.1J,K**; τtip = 17.55 ± 1.42 s, τcenter = 20.50 ± 1.09 s; two sample t test $p<<0.01$), and nearly all spines (26 of 32) exhibited faster fractional loss of PA-actin at the tip (**Figure 3.1L**). To determine whether this difference in kinetics was due to constitutively slower treadmilling of filaments in the spine center, I sequentially targeted the tip and center of individual spines. Following tip activation, I observed a delayed peak of intensity at the center which occurred 9.3 ± 1.6 s following the peak at the tip (**Figure 3.2A,B**). Overall, fluorescence at the center diminished dramatically more slowly than at the tip (time to 50% intensity: 37.20 ± 5.70 s vs. 10.55 ± 0.91 s; N=9, $p<<0.01$). In contrast, following targeting of the center (**Figure 3.2C,D**) of the same spines, I observed neither a delayed peak at the tip, nor a tendency for tip kinetics to be slowed (τcenter = 19.55 ± 2.73 s; τtip = 18.66 ± 2.51 s). Following spine tip activation, I measured PA-actin fluorescence intensity move toward the center at speeds between 0.5 ± 0.1 μm/min and 1.1 ± .04 μm/min (**Figure 3.1M,O**), consistent with the speed of polymerization-driven actin flow (Schaefer, Kabir et al. 2002; Danuser and Waterman-Storer 2006), and suggesting (Honkura, Matsuzaki et al. 2008) that actin dynamics at the spine tip drive flow toward the center.

Sites of actin polymerization are important points of regulatory control over the cytoskeleton, so measuring these sites is necessary for clarifying spine organization. To test whether overall flow is driven by addition of monomers preferentially at the tip, I designed an experiment to measure relative rates of monomer incorporation throughout the spine without the spatial bias of targeted photoactivation (**Figure 3.2E-G**). Whole spines were first photoactivated but then immediately photobleached. A delay of roughly the time constant of actin turnover (19 s) then permitted the spine to refill with new monomers which can become polymerized, and the spine was again photoactivated. Because non-polymerized monomers diffuse rapidly out of the spine (**Figure 3.1FD-G**), the pattern of fluorescence intensity following the second activation reveals sites at which new monomers were incorporated into filaments during the pause. I measured intensity at the tip and the center in each spine through this assay, and plotted these values normalized to the region intensity following initial photoactivation (**Figure 3.2F,G**). In each spine, relative incorporation was greater at the spine tip than at the center. Overall, incorporation was 71.7 ±6.4% complete within 19 sec at the tip but only 58.2 ± 2.5% at the center (n=9, p=0.014, paired sample t test). However, reincorporation was not restricted to the spine tip (**Figure 3.2E**) but broadly distributed within the spine head, apparent in some cases along its circumference. Reincorporation was blocked by addition of jasplakinolide (**Figure 3.1P**). Thus, this assay directly confirms that the spine tip is a site of ongoing actin polymerization, but clearly suggests that actin dynamics within spines are more spatially heterogeneous than can be resolved using confocal microscopy.

Figure 3.2: Heterogeneous actin polymerization rates within single spines

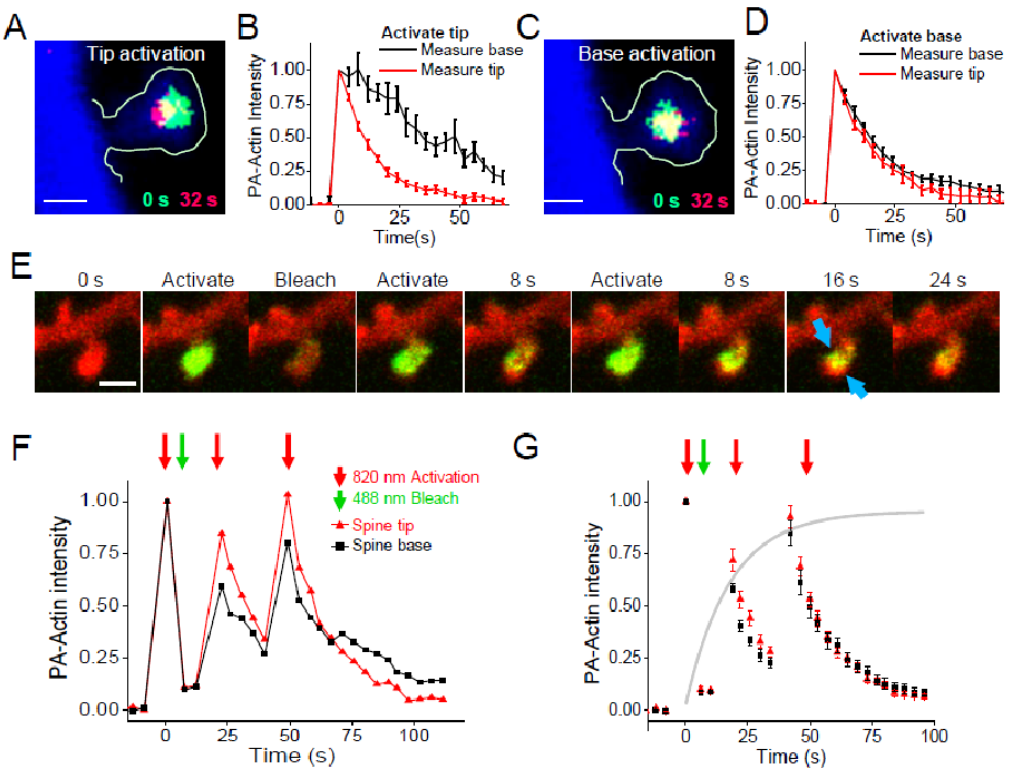

Intensity was thresholded to reveal the peak 25% of the fluorescence at each time point. PA-actin distribution is shown superimposed on cell morphology obtained from tdTomato image (blue). Scale bar, 0.5 µm in A and C. **(B)** PA-actin intensity measured within tip (red) or base (black) regions, following photoactivation in spine tip. Intensities are normalized within-region. n = 8 spines, separate neurons. **(C)** As in A, except photoactivation was targeted at the spine base. **(D)** As in B, except photoactivation was targeted at the spine base. **(E)** Optical monomer incorporation assay to identify sites of ongoing polymerization. Actin in single dendritic spines was entirely photoactivated and then photobleached. After a pause to allow additional, unactivated monomers to enter the spine, spines were photoactivated again. Newly incorporated actin moved inward from the spine membrane, with restricted regions of high and low flow along the membrane (arrows). **(F)** Analysis of example shown in E. Fractional PA-Actin intensity was normalized to the intensity after the first activation step within ROIs at the spine tip (red) and base (black). **(G)** Group data from monomer incorporation assay (n = 9 spines, separate neurons), showing higher fractional intensity in the spine tip following subsequent photoactivation steps. The grey line represents the expected time course of new monomer incorporation within whole spines, estimated from the time course (measured in Fig. 1b) of actin loss from whole spines following photoactivation. *, p=0.014.

Tracking the Behavior of Single Actin Molecules within Living Neurons

To obtain higher resolution than achievable through traditional light microscopy, I turned to photoactivated localization microscopy (PALM), which uses the sequential localization of activatable probes at very low spatial density to provide nanometer resolution of macromolecular structures (Betzig, Patterson et al. 2006; Hess, Girirajan et al. 2006). I reasoned that tracking polymerized actin molecules would allow measurement of orientation and dynamics of filaments within the small confines of dendritic spines. Importantly, whereas the image of any individual molecule is diffracted to a broad peak as expected by the PSF of the microscope objective, the error in our estimate of the location of the molecule is expected to be much smaller (~10x smaller) than the width of this blurred image (Thompson, Larson et al. 2002). Tracking individual molecules over time in a living cell provides not only nm-scale localization but also direct observation of molecular motion within the cell. I therefore acquired single-molecule images of actin in the spines of cultured neurons by adapting a previous approach (Manley, Gillette et al. 2008).

Cells were transfected with actin fused to mEos2, which fluoresces green until exposed to UV light that irreversibly converts its emission to red. As expected, transfection with actin-mEos2 did not affect spine number or head size (**Figure 3.3A-D**).

Figure 3.3: Actin-mEos2 expression does not alter spine morphology.

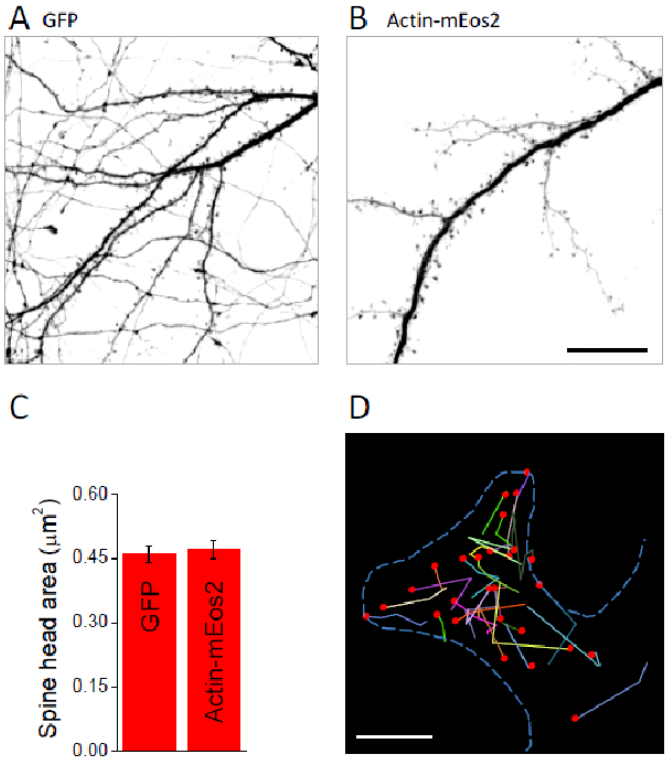

(A-B) Cultured neurons 13DIV were co-transfected with tdTomato and the indicated constructs. After 48 hrs, the cells were fixed and the tdTomato was imaged. Plentiful, mature spines were observed in neurons expressing each construct. Scalebar, 25 µm. (C) Spine head area did not differ in neurons expressing tdTomato along with either GFP or Actin-mEos2. Regions from projected confocal stacks including the spine head but not the neck or dendrite shaft were drawn and the area was calculated after thresholding at 50% of the maximum pixel intensity value within each spine. n = 769 spines, 12 neurons (gfp) and 875 spines, 15 neurons (actin-mEos2), from sister coverslips in 2 cultures. (D) Replotted data from Fig. 2G. Tracks are displayed in unique colors, and the starting position from each track is shown in red. Scale bar, 250 nm.

Molecules were activated with very low intensity 405 nm excitation, providing roughly 0.010 to 0.025 molecules per µm2 in a given frame. Using oblique excitation illumination, molecules could frequently be followed by eye over consecutive frames

before their stepwise disappearance (**Figure 3.4A,B**). I adopted several strategies for preferentially measuring the dynamics of polymerized actin (see Supplementary Methods), most notably a long frame exposure time (Watanabe and Mitchison 2002) with gaps between frames. By acquiring time-lapse datasets that included 100s or 1000s of images, I were able to compile trajectories for tens of thousands of localized molecules within transfected cells (**Figure 3.4C-G**), many of which were tracked over multiple frames. Consistent with the distribution of phalloidin staining of F-actin in neurons (Allison, Gelfand et al. 1998), tracked molecules were primarily found in spines and spine-like protrusions from the dendritic shaft.

Figure 3.4: Single actin molecules tracked with PALM have systematically polarized trajectories within dendritic spines

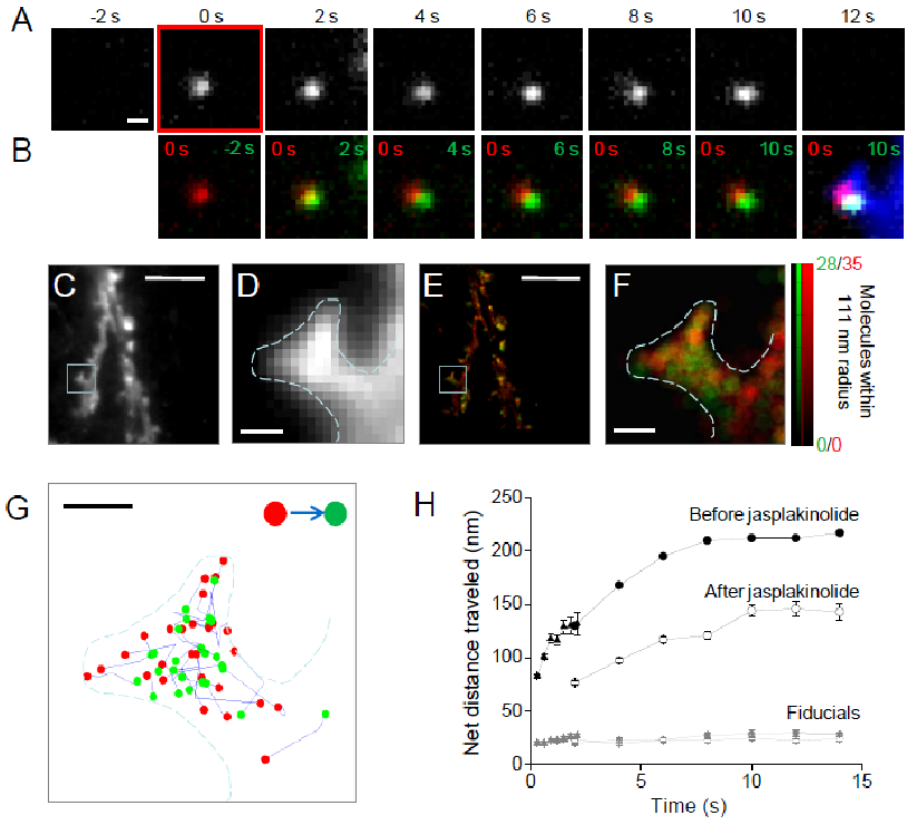

(A) Time series from sequential images, showing a molecule which appears at time = 0 s and persists for 6 frames before disappearing. Scale bar, 200 nm. **(B)** Overlays showing the molecule when it first appeared (red) and in each of the ensuing frames (green) before its disappearance. The final image shows the position of the molecule at time = 0 s (red) and 10 s (green) superimposed over the mean intensity image of all 1531 frames (blue). **(C)** Mean intensity projection of all 1531 frames provides a diffraction-limited image of the neuronal dendrite. Scale bar, C&E, 5 µm. **(D)** High magnification of boxed region in D. Dashed line represents the border of the image in E. Scale bar, D&F, 250 nm. **(E)** The local density of polymerized actin calculated as the total number of molecules which appeared within a radius of 111 nm (1 camera pixel) and that were tracked over two or more frames (green) or localized in only a single frame (red). Output plotted in 27.8 nm bins (1/4 the search radius). **(F)** High magnification view of the highlighted region in E. The dashed line in D, F, and G represents the outline of this image. **(G)** The first localized position (red) and last localized position (green) of molecules tracked over a distance greater than 111 nm are displayed. Tracks are concentrated in the spine head, and point predominantly away from the spine membrane. Scale bar, 250 nm. **(H)** Net distance traveled by molecules in a representative cell plotted as a function of the time since their appearance. 150 ms exposures were collected at 0.5 Hz (triangles) or 3.3 Hz (circles). 1978 frames were collected at 3.3 Hz, in which 7608 molecules were localized in only a single frame, and 3278 were tracked over 2 frames or more. 1025 frames were collected at 0.5 Hz, in which 12708 molecules were localized for a single frame and 3662

were tracked for at least 2 frames. Of these, 54.9% were tracked for 2 frames, and only 3.1% persisted >5 frames. Following jasplakinolide (open circles), 704 frames were collected at 0.5 Hz, in which 2599 molecules were localized in a single frame and 1921 were tracked for at least 2 frames. Of these tracked molecules, 44.0% persisted at least 2 frames, and 12.8% persisted >5 frames. Fiducial beads showed little motion (gray symbols).

To quantify the distribution of localized molecules, I mapped their density within subresolution spatial bins (111 nm bins, 1 camera pixel). The molecular density of tracked molecules provided a map of the polymerized actin distribution within unperturbed, living neurons (**Figure 3.4E,F, green**). Importantly, the distribution of untracked molecules (those appearing in only one frame) in addition revealed the extent of the cell cytosol, providing a map of cell morphology derived from super-resolved molecular localization information (**Figure 3.4E,F, red**). Within spines identified from these maps, the trajectories of tracked molecules showed a propensity for inward polarization often readily discernible without further analysis (**Figure 3.4G**).

To quantify molecular dynamics, I plotted the mean distance traveled by each molecule as a function of its time since appearance (**Figure 3.4H**). Because photobleaching limits the number of frames for which molecules can be imaged, I tracked populations of molecules over short and longer periods by acquiring images with first a rapid (3.3 Hz) then a slow (0.5 Hz) frame rate. The distance traveled by molecules tracked at 3.3 Hz over 2.1 s was essentially the same as molecules tracked at 0.5 Hz over 2 s (3 Hz at 2.1 s: 137.5 ± 12.6 nm; 0.5 Hz at 2.0 s: 137.0 ± 6.9 nm, n = 11), verifying our tracking criteria. Molecules tracked over longer periods of time moved greater distances,

as expected. The initial slope of this relationship is expected to reflect the average velocity of molecular motion along filaments.

Figure 3.5: Single molecule motion describes the behavior of polymerized actin monomers

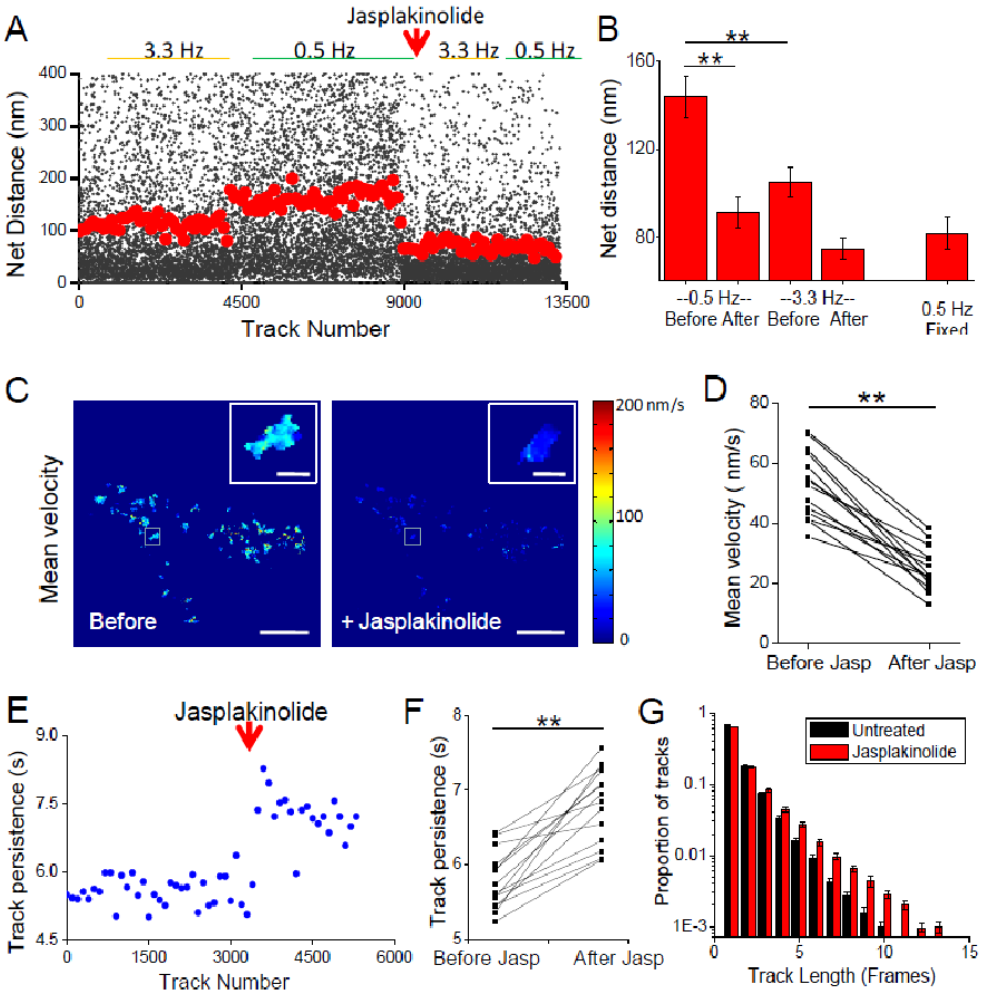

(A) A neuron expressing actin-mEos2 was imaged sequentially at 3.3 Hz and 0.5 Hz. Following the addition of jasplakinolide, the neuron was again imaged at 3.3 Hz and 0.5 Hz. Each black point represents the distance traveled by a tracked molecule. Red circles represent the mean distance traveled of 100 consecutive tracked molecules. Note that the time-dependent increase in molecule motion is abrogated by the addition of jasplakinolide. (B) Local mean net distance traveled by localized molecules within cells which were consecutively imaged at 3.3 Hz and 0.5 Hz before and after jasplakinolide (n

= 7) as in A, and separate cells which were fixed in 4% paraformaldehyde before imaging at 0.5 Hz (n = 7). Two-way ANOVA; ** P < 0.001. (C) Molecule velocity map of the same neuron before (left) and after (right) jasplakinolide. Molecule velocity decreased in all spines following treatment. Inset: High magnification of a representative spine from indicated region. Scale bar: 5 µm, inset 1 µm. (D) Local mean velocity was calculated by averaging the velocity of each track originating within a 111 nm radius of each 55.5 nm output pixel (as in A). Local mean velocity was decreased in 14/14 cells (8 cultures) following jasplakinolide (averaged per pixel). **, p < 0.001. (E) Representative example showing average time over which molecules were tracked (in seconds; tracked at 0.5 Hz; same cell as S6a,b) before and after addition of jasplakinolide. Each point represents the average track length of 100 tracked molecules. (F) The mean time over which molecules were tracked increased after the addition of jasplakinolide in 14/14 cells (8 cultures). Paired t-test; ** p < .0001. (G) Analysis of all tracked molecules before and after the addition of jasplakinolide (14 neurons, 8 cultures). Total molecules tracked before jasplakinolide was 172,879. Total molecules tracked after the addition of jasplakinolide was 96,240. The fraction of tracks persisting over the designated number of frames is plotted.

Tracks in images acquired at 3.3 Hz revealed that molecules moved on average 38.8 nm/s (2.3 µm/min). This value is considerably higher than the measured bulk flow velocity (**Figure 3.1M-O**), suggesting that bulk flow obscures faster flow rates along individual fibers of different orientations. However, the slope decreased in longer tracks (13.5 nm/s between 2 and 8 s), and approached 0 for the longest tracks between 8 and 14 sec long (0.9 nm/s). The asymptote of 205.4 ± 11.7 (mean length of tracks 5 to 8 frames in length at 0.5 Hz, n = 14 neurons) is potentially explained if filaments within spines rarely extend beyond this length, similar to a confinement radius describing a limited area over which an otherwise freely diffusing molecule can roam, as derived from single-molecule mean squared displacement over time (Saxton and Jacobson 1997). Alternatively, these data may reflect that flow velocity on spine filaments is heterogeneous, such that slower moving molecules remain on filaments for longer periods of time.

I tested whether our analysis selectively tracked the motion of polymerized actin molecules by examining the effects of jasplakinolide, an actin filament stabilizer. Jasplakinolide greatly restricted the motion of tracked molecules (**Figure 3.4H**), reducing the distance traveled during the initial 2 s (130 nm to 76.6 nm) as well as the slope of the relationship between 2 and 8 s (13.5 nm/s before; 8.7 nm/s after jasplakinolide). Jasplakinolide reduced the mean distance traveled by tracked molecules to a level indistinguishable from that seen in fixed cells (i.e. from the value arising from instrumentation noise) at both rapid and slow frame rates (**Figure 3.5A,B; Figure 3.6A-C**). The fraction of molecules that traveled beyond 100 nm was also decreased following jasplakinolide to a level similar to that seen in fixed cells (**Figure 3.6D**), and the mean net distance for tracks 5 to 8 frames in length was reduced to 110.1 ± 8.2 nm (from 205.4 ± 11.7 prior to treatment, $p << 0.01$; paired t test, $n = 14$). Maps of mean local molecular velocity were created by averaging the velocity (net distance/track duration in sec) of all molecules which originated within 111 nm (1 camera pixel) of each 55.5 nm output pixel (**Figure 3C**). Mean local molecular velocity was reduced by jasplakinolide throughout each of 14 neurons (**Figure 3.5C,D; Figure 3.6E-F**; 53.2 ± 11.2 nm/s before, 24.8 ± 7.3 nm/s after, $n=14$, $p <<.01$). The value after jasplakinolide was essentially indistinguishable from that in fixed cells (24.6 ± 2.3 nm/s, $n=7$; **Figure 3.6G**), indicating that any remaining motion was within the limit of our detection.

If continuous polymerization is responsible for driving most actin flow along spine filaments, depolymerization and subsequent free diffusion of molecules would be

expected to terminate tracks. Indeed, the mean persistence of tracked molecules (in seconds) increased after jasplakinolide treatment in 14/14 cells (**Figure 3.5E-G, Figure 3.6H**).

Figure 3.6: Movement of single actin-mEos2 molecules derives from polymerization-driven flow

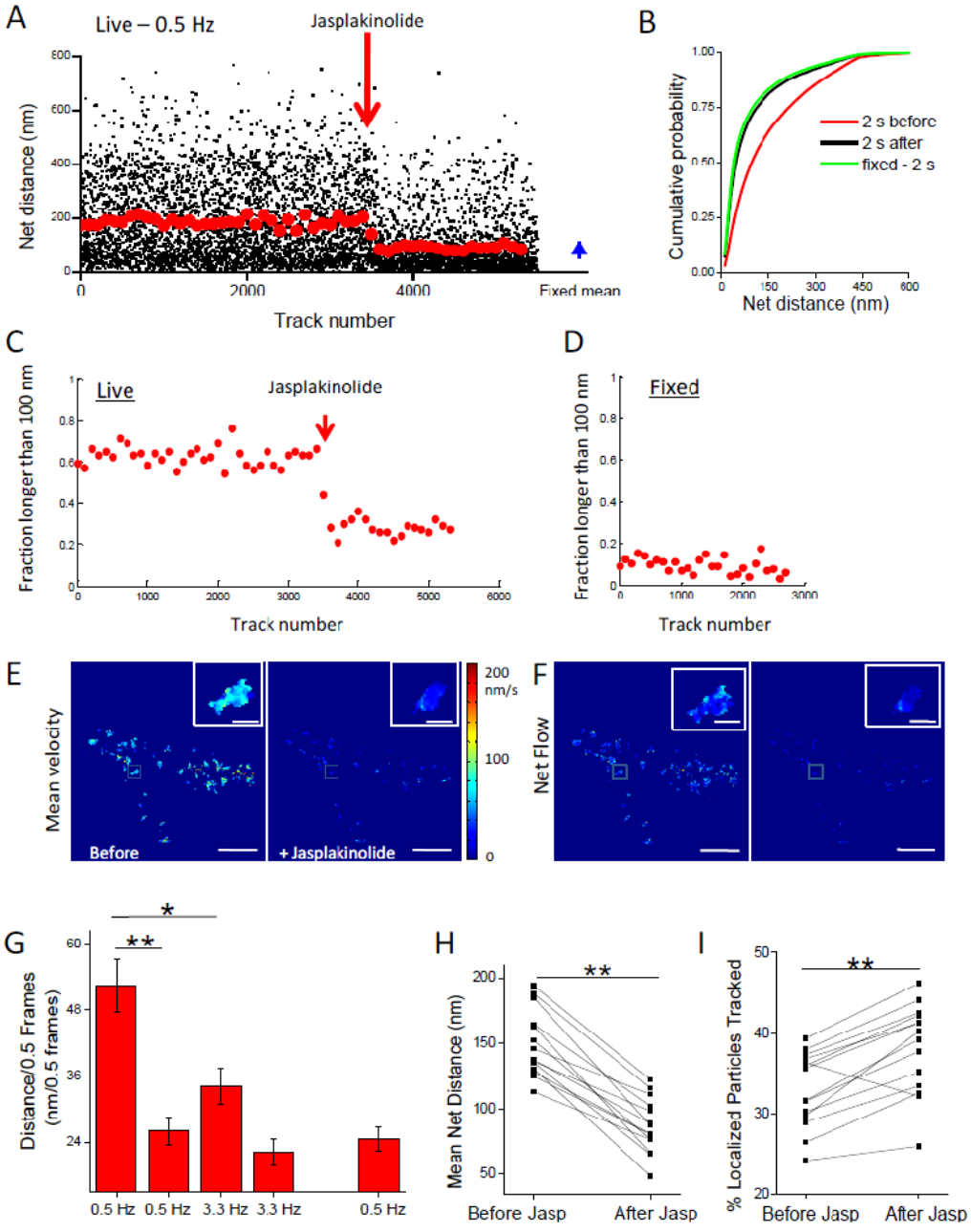

(A) Net distance traveled by each molecule tracked at 0.5 Hz, plotted in chronological order before and after addition of jasplakinolide (red arrow). Red circles represent the mean distance traveled by consecutive groups of 100 tracked molecules. Blue triangle represents mean net distance traveled for 7 cells fixed in 4% paraformaldehyde (81.8 ± 7.5 nm). **(B)** Cumulative probability plot of molecule net distance traveled. Tracked molecules were binned into 10 nm groups based on net distance traveled for each cell, and averaged. Data represents the mean distribution for 52704 tracked molecules in 14 cells before and 34272 tracked molecules following jasplakinolide, and 26392 tracked

molecules in 7 cells fixed in 4% paraformaldehyde. The 50% probability for fixed cells was 38.5 nm, presumably stemming from the imprecision of single-molecule localization. For molecules in live cells tracked at 0.5 Hz, the 50% probability was 95.9 nm, which was reduced to 46.0 nm following jasplakinolide. **(C)** Red dots represent the percent of groups of 100 tracks which traveled more than 100 nm before and after the addition of jasplakinolide (individual points shown in A). **(D)** Percent of groups of 100 tracks which extended more than 100 nm in a representative fixed cell. **(E)** Molecule velocity map of the same neuron before (left) and after (right) jasplakinolide. Molecule velocity decreased in all spines following treatment. Inset: High magnification of a representative spine from indicated region. Scale bar: 5 µm, inset 1 µm. **(F)** Maps of net flow, calculated as the net motion of all molecules originating within a 111 nm radius. Like mean molecule velocity, net flow was higher in all spines before jasplakinolide (left) than after (right). Inset: High magnification of same representative spine from indicated region shows that restricted regions of high velocity flow within individual spines disappear following treatment. Scale bar: 5 µm, inset 1 µm. **(G)** Local mean particle velocity within cells which were consecutively imaged at 3.3 Hz and 0.5 Hz before and after jasplakinolide (n = 7) as in Figure 3A, and separate cells which were fixed in 4% paraformaldehyde before imaging at 0.5 Hz (n = 7). 2 Way ANOVA; ** $p < 0.001$. **(H)** Local net distance was calculated by averaging the net distance traveled for all tracks originating within a 111 nm radius of each 55 nm output pixel. Local net distance decreased in each of 14 cells measured before and after application of jasplakinolide. **, $p < 0.001$. **(I)** The probability that a localized molecule would be tracked in subsequent frames increased following jasplakinolide. Paired t-test; ** $p < 0.001$.

Together with the rapid time constant for turnover of photoactivated PA-actin (**Figure 3.2**), these data indicate that many tracked molecules reach the end of filaments and are depolymerized before photobleaching, consistent with a population of short filaments within spines. The strong effects of jasplakinolide on molecular velocity suggest that polymerization drives the large majority of actin flow in spines. It is likely that the remaining motion (above the error-derived values in fixed cells) reflects the role of myosin-based contractility.

Resolution of Perisynaptic Polymerized Actin

To measure the distribution of actin near synapses, I used two-color PALM (Shroff, Galbraith et al. 2007) of fixed neurons co-transfected with actin-tdEos and the postsynaptic density protein GKAP (Welch, Wang et al. 2004) tagged with the photoswitchable green protein dronpa (**Figure 3.7A-C**). Molecules of each were photoactivated, and the locations and localization uncertainty were plotted to encode the probability of finding a molecule at any position (Betzig, Patterson et al. 2006). The resulting images showed areas of high actin density abutting the PSD of synapses both in spines and on the dendritic shaft (**Figure 3.7B**). Line profiles through areas of interest confirmed the low probability of finding actin molecules within the PSD itself (**Figure 3.7C**).

Figure 3.7: Spatially restricted distribution of polymerized actin visualized with PALM near synapses.

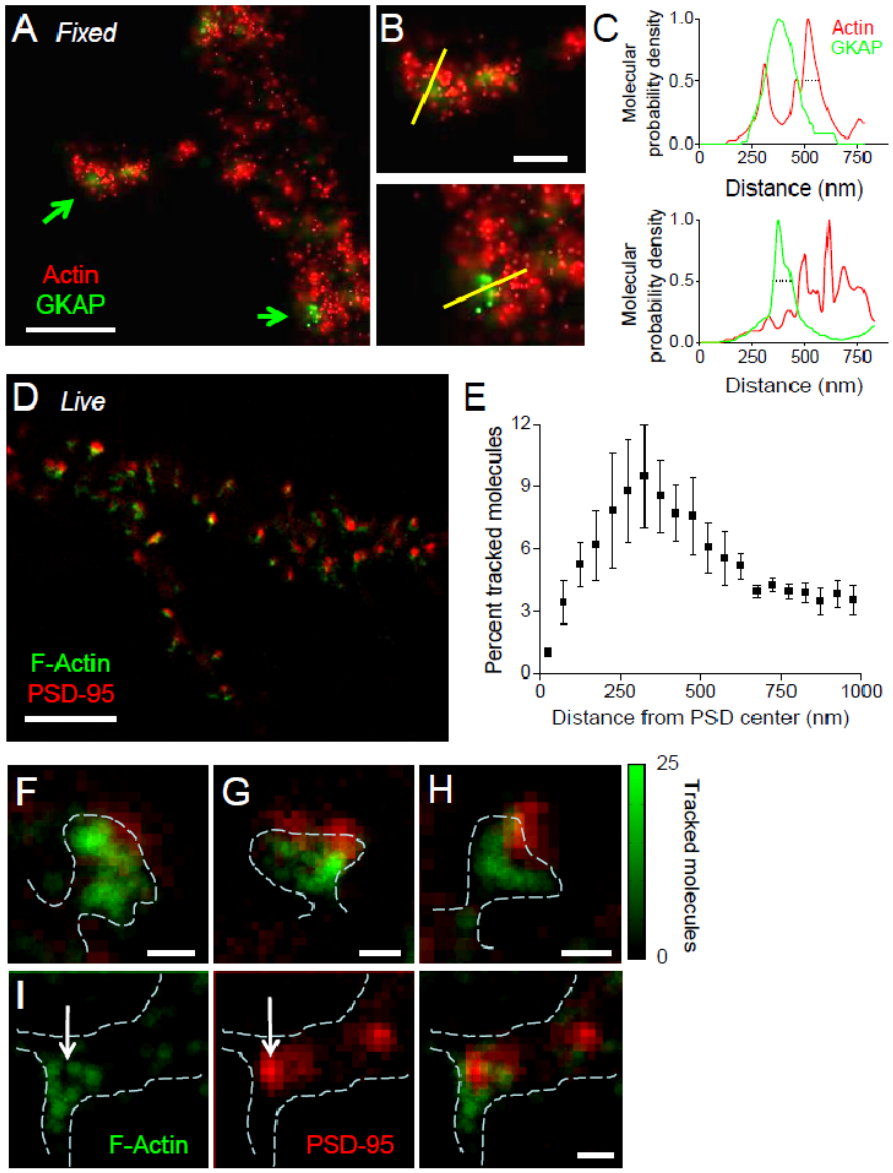

(A) Two-color PALM image of actin-tdEos and GKAP-dronpa in a fixed neuron. Molecules localized with error less than 30 nm (Actin-tdEos, red) or 100 nm (GKAP-Dronpa, green) are shown mapped with a pixel size of 5 nm. Scale bar, 1 µm. **(B)** Closer view of synapses on a spine (top) and shaft (bottom), showing lines along which measurements were made in C. Scale bar, 500 nm. **(C)** Relative molecular density probability of actin-tdEos (green) and GKAP-Dronpa (red) along 75-nm wide lines (30 pixels) shown in B. Dotted lines highlight the width of the profile at a probability of 0.5 (top, 121 nm; bottom, 87 nm). **(D)** The local density of polymerized actin calculated as the number of tracked actin-mEos2 molecules within a 111 nm radius. Local density

(green) was plotted at ¼ this scale (27.8 nm bins), and overlaid on the diffraction-limited image of PSD-95-cerulean (red). Scale bar, 5 µm. **(E)** Plot showing the distribution of tracked actin-mEos2 molecules with increasing distance from the center of PSDs identified by localization of PSD-95-cerulean puncta (n = 4 neurons, 148 PSDs). Three synapses **(F-H)** from D, revealing a characteristic cuplike subsynaptic actin structure. Scale bars, 500 nm. **(I)** Actin distribution at a shaft synapse showing a ring-like distribution (left) encircling the PSD (middle). Scale bar, 500 nm. Green color bar represents local density of polymerized actin in A-E.

To examine polymerized actin density in relation to the PSD in living cells, I acquired single-molecule time lapses of actin-mEos2 followed by diffraction-limited images of PSD95-cerulean (**Figure 3.7D**), and compared the molecular density maps created from tracked actin molecules to the position of PSD95-cerulean. This analysis revealed a striking peak density of polymerized actin near the PSD (**Figure 3.7E**). Examining individual images confirmed that polymerized actin density was notably higher near the edge of the PSD (**Figure 3.7F-H**), even in the case of morphologically complex PSDs. Some actin molecules were localized overlaying the PSD, though the finite thickness of the optical section precludes determining whether these molecules were above or truly within the PSD. These observations using PALM thus confirm EM of fixed cells showing filaments near or touching the PSD (Fifkova and Delay 1982; Capani, Martone et al. 2001). Further analysis (see below) extends these results significantly by demonstrating directly that such perisynaptic actin is highly dynamic rather than merely a stable or structural scaffold.

Heterogeneous Actin Dynamics Within Spine Subregions

Tracking single molecules permitted us to measure the spatial heterogeneity of actin dynamics across the inner extent of spines, by mapping characteristics of molecules whose tracks began within defined spatial bins. Molecular velocity was strikingly heterogeneous within spines (**Figure 3.8A**). Most notable were distinct regions of high velocity motion. Such regions were typically found along restricted portions of the spine membrane. The narrow lateral extent and the depth into the cell interior argue against the possibility that they represent an edge effect, since such an effect should be uniform along the membrane and not affect molecules farther interior than the error in molecule localization. In fixed cells and neurons treated with jasplakinolide, mean local velocities decreased to the level of localization-error-derived background noise (**Figure 3.8B**). Vector plots representing local average molecular direction and velocity were constructed to map flow at high spatial resolution. This local flow was overwhelmingly directed inward from the spine membrane (**Figure 3.8C,D**). The interior of all spines comprised dense actin of somewhat slower velocity and notably reduced local flow, most easily explained by heterogeneous filament orientation. Perhaps most strikingly, at irregular points along the membrane, regions of inwardly directed, high net velocity were observed, which I take to be sites of dramatically enhanced polymerization. These sites presumably underlie the distributed monomer incorporation observed following unbiased confocal photoactivation (**Figure 3.2E-G**).

Figure 3.8: Heterogeneous actin dynamics within individual spines.

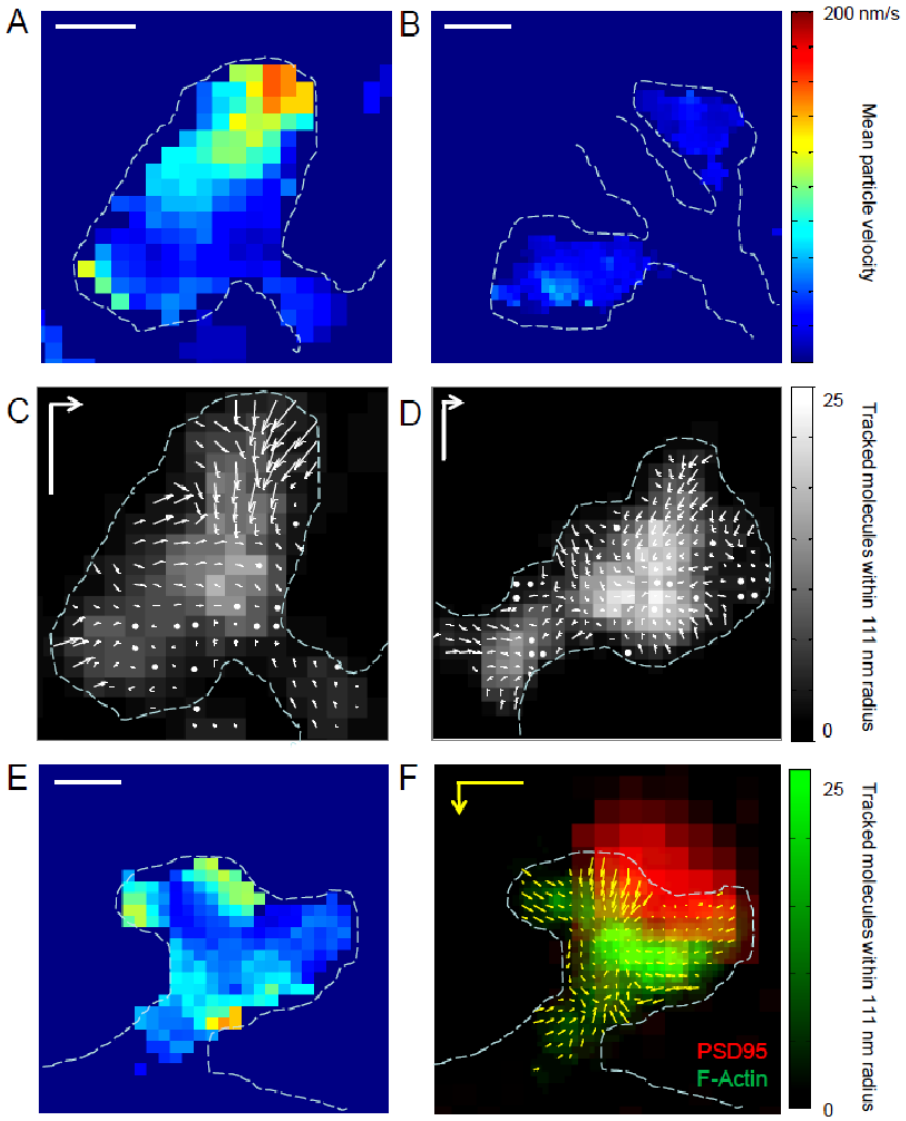

(A) Map of actin molecule velocity across the inner extent of a dendritic spine. The mean velocity of molecules within 111 nm was plotted at each 55.5 nm pixel for which there were ≥3 molecules within this radius. Restricted areas of high velocity are clearly visible. Scale bar, 250 nm **(B)** Actin velocity map of fixed spines, showing that error stemming from molecular localization precision is minimal and spatially unmodulated. Scale bar, 500 nm. **(C–D)** Representative spines showing inward orientation of actin flow. Arrow length represents relative velocity. Gray scale represents tracked molecular density. Scale bar, 200 nm; vector, 100 nm/s. **(E)** Actin velocity map and **(F)** locally averaged molecular movement vector plotted superimposed on local tracked molecule density (green) and the deconvolved widefield image of PSD-95-cerulean (red). Some but not all

foci of high velocity motion are closely associated with the synapse. Scale bar, 250 nm; vector, 200 nm/s. Color bar represents tracked molecular density for F.

Surprisingly, the inward orientation of flow was observed even at the opening of the spine neck. Actin within the spine neck has been difficult to resolve in live cells, but I found that the high sensitivity and spatial resolution of single-molecule tracking enabled measurement of molecular motion along filaments in the neck (**Figure 3.8C,D,F**). This provides direct evidence supporting the existence of dynamic actin filaments in the spine neck. Further, all spines with a clearly identified neck contained molecules with a net inward flow, though overall, roughly one-half as many actin molecules flowed outward through the neck as flowed inward (67±5% of filaments inward; n = 13 spines from 13 neurons in 4 cultures). Maps of actin molecular velocity in many cases revealed multiple foci in broadly spaced regions of the spine (**Figure 3.8E**). To examine filament orientation within these regions, I constructed vector plots of local net flow direction and magnitude (**Figure 3.8C,D,F**). This analysis indicated that foci of high velocity motion were associated with more strongly congruent directionality, i.e. a fast local flow vector. Though not all regions of relatively highly correlated motion direction were within regions of high velocity, such association was seen in nearly all of >100 foci examined. Importantly, by overlaying vector plots of net flow with widefield images of PSD-95-cerulean, it was clear that foci of high velocity motion often occurred near or overlapping with the diffraction-limited image of the PSD (**Figure 3.8F** and see below).

Distribution of focal sites of polymerization within spines

To quantitatively assess the distribution within spines of focal sites of enhanced polymerization, I identified these regions first by thresholding each cell's velocity map (**Figure 3.9A-C**; see Experimental Procedures). Spines contained on average 1.7 ± 0.6 foci (n = 68 foci in 30 spines in 5 neurons, **Figure 3.9C,D**). All foci were eliminated by application of jasplakinolide, and rescaling the threshold based on the extremely low velocity following jasplakinolide did not rescue the number of foci, confirming their dissipation in the absence of normal polymerization (**Figure 3.9D**). Foci were found distributed widely through the spine, with a preponderance in the lateral or tip regions of the spines (**Figure 3.9E**). The large majority were within 150 nm of the spine membrane (**Figure 3.9F**), (the location of which was deduced from the distribution of all localized actin molecules). Like others (Honkura et al., 2008), I found that the average velocity of actin flow was weakly correlated with the size of the spine (**Figure 3.9G**; correlation coefficient=0.43, $p<0.05$, n = 28). More notably, however, larger spines had more foci (**Figure 3.9H**; correlation coefficient=0.67, $p<0.01$, n = 28). To examine this further, I compared the number of foci in spines from neurons overexpressing clathrin-cerulean, which has no effects on spine size (Blanpied et al., 2002; Petrini et al., 2009), with those overexpressing PSD-95, which is known to increase synapse strength and spine size (Bredt and Nicoll 2003). PSD-95 overexpression increased the number of foci by 1.6-fold ($p<0.05$, n = 24 and 27 spines from 4 cells each for PSD-95 and clathrin, respectively). These data indicate that the subspine actin velocity landscape is more intricate in large

spines, and suggests that as synapses strengthen, they acquire unique organizational or functional complexity.

Figure 3.9: Widespread distribution of focal points of high velocity flow within spines.

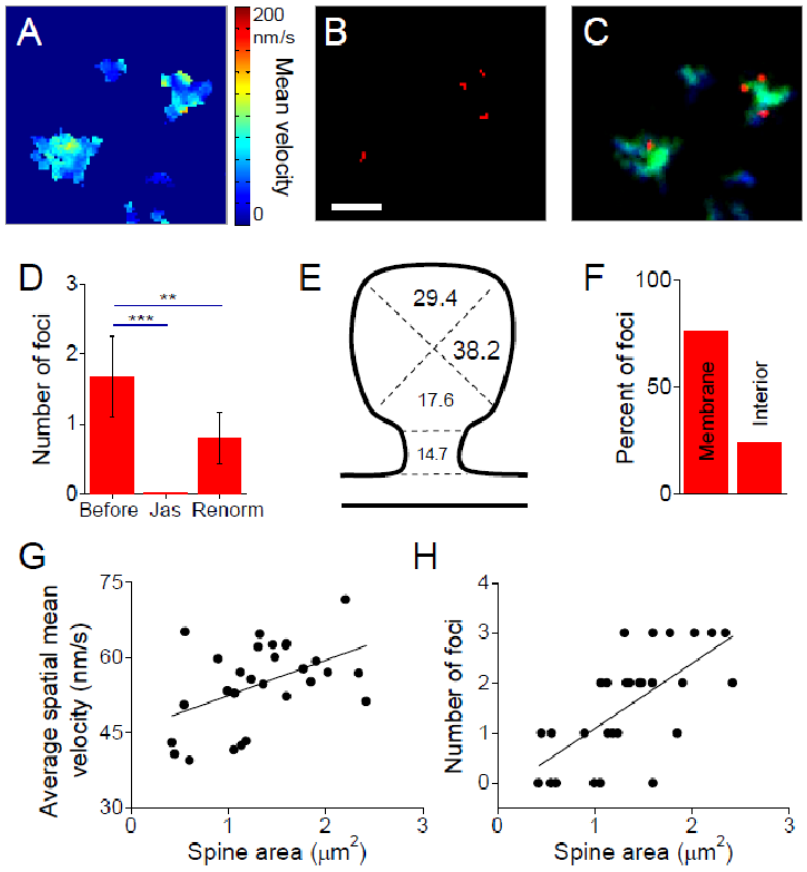

A-C. Spatially averaged velocity maps **(A)** were thresholded to their mean + 1.5 times their standard deviation. Binary thresholded maps showing the distribution of regions with high averaged particle velocity **(B)** were band pass filtered **(C)** to map the center of regions of high velocity particle motion. **(D)** Plot showing the average number of foci per spine. Foci were eliminated by jasplakinolide. Renormalizing velocity maps of neurons following jasplakinolide did not rescue the loss of foci in spines (** $p < .01$, *** $p < .0001$, repeated measures ANOVA;n = 12 spines, 5 neurons, 5 cultures). **(E)** The majority of foci were located in the tip and lateral regions of the spines of untreated neurons (n = 68 foci, 30 spines, 5 neurons, 5 cultures). **(F)** Plot showing the distribution of focal regions of high velocity particle

motion with respect to the membrane (n = 68 hot spots, 30 spines, 5 neurons, 5 cultures). **(G)** The average spatial mean velocity within individual spines increased with spine size (n = 32 spines, 6 neurons, 6 cultures). **(H)** Larger spines contained a greater number of foci (n = 32 spines, 6 neurons, 6 cultures).

Differing actin polymerization dynamics at the synapse and endocytic zone

Sites of enhanced polymerization could be randomly distributed within spines and thus presumably mediate only morphological change, or could be tied to functional domains such as the synapse or the endocytic zone (EZ). To distinguish between these possibilities, I first examined spines from neurons triply transfected with actin-mCherry, PSD-95-GFP to mark synapses, and clathrin-cerulean to mark the EZ (Blanpied, Scott et al. 2002). Intriguingly, confocal images of these spines suggested that the density of actin near PSDs was greater than near the EZ (**Figure 3.11A**), but the limited resolution prevented detailed analysis of actin dynamics in relation to each structure. I therefore measured the distribution of polymerized actin via smtPALM in relation to widefield images of clathrin-cerulean acquired after tracking. Strikingly, the distributions of thousands of tracked (polymerized) molecules surrounding the center of the EZ was quite different than that surrounding the PSD (**Figure 3.10A**). Whereas the peak density occurred only 300 nm from the imaged center of the PSD, tracked actin molecules showed no prominent peak density even within 1 μm. I therefore examined directly whether polymerization foci occurred preferentially near synapses or the EZ, by overlaying maps of foci derived from single-molecule tracking with widefield images of the PSD or EZ (**Figure 3.10B,C**). PSDs typically were found with one or more actin foci

on or almost directed opposed to them. On the other hand, actin foci appeared less frequently to abut the EZ marked with clathrin (**Figure 3.10C**). I calculated a nearest neighbor distribution by measuring the distance from the center of each PSD or clathrin punctum to the nearest actin polymerization focus. A histogram of these nearest neighbors (**Figure 3.10D**) revealed that actin foci lay significantly further from the EZ than from the PSD (median distance 565±43 nm for clathrin vs. 420±14 for PSD-95, $p<0.05$). Furthermore, the most striking difference in the distributions was in the closest bin: a significantly greater fraction of PSDs were associated with an actin polymerization focus within 250 nm ($p<0.05$, t-test). This closer relationship was apparent also in the left-shifted cumulative nearest neighbor distance (Fig. 3.10E; $p<0.005$, Man-Whitney U test). To confirm this automated analysis, I manually counted foci to score whether they overlapped 1 or more image pixels with thresholded images of PSDs or EZs. The results were very similar (**Figure 3.10F**), indicating that actin foci occurred at PSDs with roughly twice the likelihood as at EZs ($p<0.01$).

To test in an independent way whether the behavior of polymerized actin molecules in the vicinity of the PSD or EZ differed, but without relying on definition of discrete foci, I analyzed the mean molecular velocity of actin in spatial bins surrounding the functional markers. Molecules whose tracks began closest to the synapse (i.e. their tracks initiated within the borders of the PSD as determined from deconvolved, widefield images of PSD-95-cerulean) or those within a 300 nm annulus around the PSD had significantly higher mean velocities than molecules whose tracks initiated further than 300 nm away from the synapse (**Figure 3.10G**). In contrast, molecules whose tracks

initiated within the boundaries of the EZ were no faster than those lying immediately outside the EZ or more than 300 nm from it (**Figure 3.10H**). Accordingly, even though the average molecular velocity across the entire cells did not differ for neurons expressing PSD-95-cerulean or clathrin-cerulean, the velocity of molecules at the synapse was significantly greater than those at the EZ (**Figure 7I**; $p<0.01$, t-test followed by Bonferroni correction for multiple comparisons; **Figure 3.11B-D**).

Figure 3.10: The PSD and the Endocytic zone show distinct patterns of polymerization dynamics.

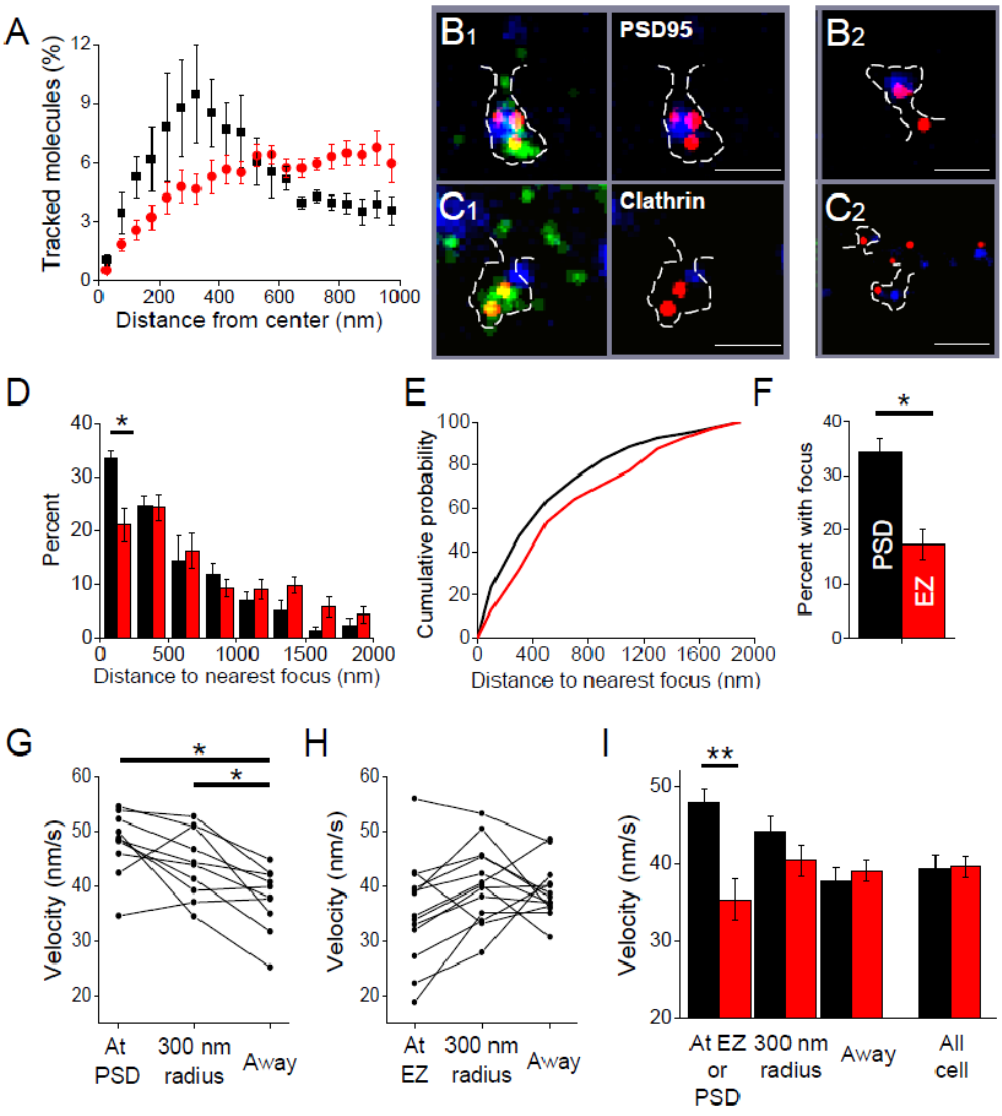

(A) The distribution of tracked actin-mEos2 molecules peaked within 300 nm of the center of localized PSDs. In contrast, the rise of the distribution curve of actin-mEos2 was less steep in the vicinity of localized endocytic zones (n = 148 PSDs, 4 neurons, 4 cultures; 354 clathrin spots, 4 neurons, 2 cultures). **(B)** PSD-95-cerulean (blue) showed a high degree of colocalization with both the distribution of tracked actin-mEos2 (green) and localized focal areas of high velocity particle motion (red). **(C)** In contrast, clathrin-cerulean3 (blue), was generally located distant from the peak of tracked actin-mEos2 distribution and did not appear to colocalize with localized focal regions of high velocity actin particle motion. **(D)** Histogram of the distribution of distances from localized

PSDs(black) or endocytic (zones) to their nearest associated focal point of high velocity actin motion. A significantly higher fraction of PSDs had associated foci within the first 250 nm ($p < .05$, t test). The average PSD was closer to a focus of high velocity particle motion than the average EZ (420.0 +- 14.4 vs 565.5 +- 42.3 nm, $p < .05$ t test). **(E)** The cumulative distribution plot showed the distribution of foci with distance from the EZ was significantly right shifted with respect to the distribution from the PSD (Mann-Whitney U test; n = 148 PSDs, n = 354 EZ, 4 cells each. **(F)** PSDs and endocytic zones were manually examined for association with localized high velocity foci. To avoid false negatives in regions where the dendrite was out of tirf, PSDs were examined only if they colocalized with tracked actin molecules. PSDs were twice as likely to be associated with a high velocity foci than EZs ($p < .05$, t test; n = 100 PSDs, 4 neurons, 4 cultures, 148 clathrin spots, 4 neurons, 2 cultures). **(G)** Plot showing the average velocity of tracked particles originating within thresholded PSDs, within 300 nm of the PSD, or elsewhere in each of 10 cells. Tracked molecules originating at and near the PSD moved significantly faster than molecules originating elsewhere in the cell ($p < .05$; paired t test with Bonferroni correction). **(H)** Plot showing the average velocity of tracked particles originating within thresholded clathrin spots (EZ), within 300 nm of the EZ, or elsewhere in each of 13 cells. Tracked molecules originating at and near the EZ did not behave significantly differently than molecules originating elsewhere in the cell ($p > .05$, t test with Bonferroni correction). **(I)** Plot comparing actin velocity at the PSD or EZ, within a 300 nm radius, or elsewhere in the cell. The velocity of tracked actin molecules originating at the PSD was significantly higher than that of tracked actin molecules originating at the EZ ($p < .01$, t test with Bonferroni correction)

Figure 3.11: The postsynaptic density is associated with regions of high velocity actin motion.

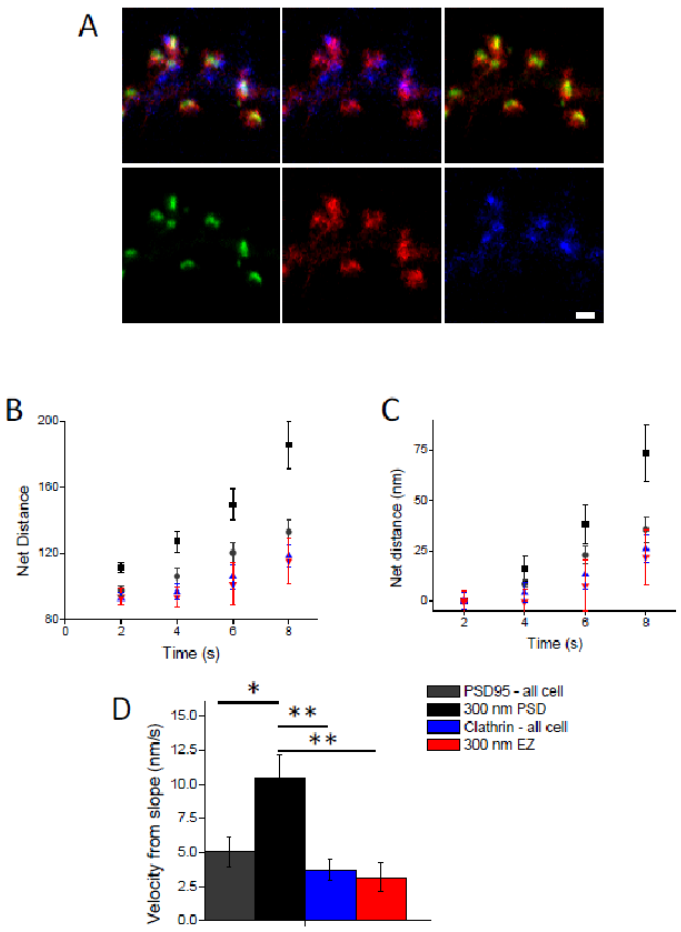

(A) Scanning Confocal images of PSD95-gfp (green), actin-mCherry (red), and clathrin-cerulean (blue) reveal that while the three molecules are distributed within the spine head, PSD95 often appears to be more closely associated with closely apposed regions of high actin density. (B) Tracked actin molecules within individual cellsin which either PSD95-cerulean or clathrin cerulean3 were divided into groups based on whether they originated from regions within 300 nm of thresholded PSD95-cerulean (black squares) or 300 nm of clathrin-cerulean3 (red triangles). Molecules originating at the PSD traveled significantly farther than molecules originating at the EZ. Comparing molecules originating at all points in individual cells revealed that expression of PSD95 or clathrin did not significantly alter actin dynamics elsewhere in the cell. (C) Renormalization of tracked molecules to their location at time = 2 s revealed that motion between 2 and 8 seconds was also enhanced at the PSD compared to elsewhere in the cell. (D) Plot of the mean of fitted curves for each cell (C) again revealed that actin motion was significantly enhanced within 300 nm of the PSD compared to elsewhere in the cell. The EZ was not

associated with high velocity actin motion (* $p < .05$, ** $p < <.01$, ANOVA, n = 26 cells expressing PSD95, 17 cells expressing clathrin-cerulean3).

DISCUSSION

I have used a variety of confocal and single-molecule tracking measurements to analyze actin dynamics within the submicron dimensions of single living dendritic spines. Our results make clear that spines contain a dense and highly dynamic perisynaptic actin network, tightly localized foci of polymerization both at and away from the synapse, a dense central core of heterogeneous filament orientation, and actin filaments in the spine neck frequently oriented with barbed ends toward the dendritic shaft.

Dynamics of perisynaptic actin

I find continuously polymerizing actin immediately apposed to the synapse, and the density of actin filaments reaches a peak within 300 nm of the PSD center. Recent indications that filament structure observed by EM is highly sensitive to fixation conditions (Urban, Jacob et al. 2010) emphasize the need for further live-cell measurement of cytoskeleton behavior and function. Nevertheless, the distribution I observed is consistent with EM localization of filaments near or abutting the PSD (Caceres, Payne et al. 1983; Capani, Martone et al. 2001). Indeed, Fifkova et al. (1982) found filaments with barbed ends oriented toward the PSD, as well as filaments of differing orientation near the PSD, even running parallel to it, which is consistent with

the highly localized and heterogeneous organization I have observed. This complex assembly pattern likely arises from the concentration of the Arp2/3 branching nucleation factor only ~200 nm from the PSD edge (Racz and Weinberg 2008), and further suggests that the perisynaptic actin network is a uniquely nimble collection of highly dynamic filaments.

The tight synaptic association of the cytoskeleton presumably underlies its role in maintaining synaptic glutamate receptors (Allison, Gelfand et al. 1998; Kim and Lisman 1999; Zhou, Xiao et al. 2001). I find that polymerization-driven flow along filaments at the synapse is faster than elsewhere in the spine, suggesting that receptor "anchoring" by the cytoskeleton may in fact involve an active process mediated by polymerizing filaments, not stable ones. Dynamic perisynaptic filaments also provide a straightforward explanation for the pronounced, actin driven morphological distortion that most PSDs undergo on a continual basis (Blanpied, Kerr et al. 2008).Direct cytoskeletal control of the morphology of the synapse proper, rather than the spine in general, may contribute to subsynaptic receptor positioning with respect to sites of neurotransmitter release important for synaptic strength (Raghavachari and Lisman 2004).

Indeed, the latrunculin sensitivity of PSD scaffold protein content (Allison, Chervin et al. 2000; Kuriu, Inoue et al. 2006) suggests that actin-dependent receptor anchoring may stem from cytoskeletal interaction with the proteins of the PSD rather than receptors directly. As actin polymerization also regulates the lateral diffusion of membrane proteins into and out of the dendritic spine (Richards, De Paola et al. 2004), it

is tempting to speculate that a dynamically regulated cytoskeleton surrounding the PSD may restrict the territory explored by freely diffusing receptors, potentially gating receptor exit or entry to synapses (Yang, Wang et al. 2008).

Roles of polymerized actin in spine subdomains

Using targeted photoactivation I observed as reported previously (Honkura, Matsuzaki et al. 2008) that spines possess a general tip-to-base orientation of actin flow. However, both an optical monomer-incorporation assay and single-molecule tracking revealed that this does not result strictly from preferential polymerization activity at the spine tip or at the synapse. Rather, sites of high polymerization activity are broadly distributed and found at spine tips, in lateral domains, and even in or near the neck. These distributed sites likely represent points of regulated control over filament density, length, and turnover. Thus, the tip-to-base flow structure that can be resolved via relatively low resolution confocal microscopy appears to be an emergent phenomenon that masks a more intricate and functionally revealing underlying organization.

Synapses but not endocytic zones were prominently associated with these foci, I take this nonrandom distribution as clear evidence in favor of the notion that actin dynamics regulate spine function through specific mechanisms aside from influencing spine morphology. Indeed, larger spines were not merely expanded versions of small spines: they were more intricate, containing more foci. Thus, I conclude that for spines,

strength is associated not merely with size but with organizational complexity that may support computational sophistication.

The high resolution of PALM allowed us to identify unexpected characteristics of actin dynamics within two clearly identified subdomains away from the synapse. The endocytic zone (EZ), a region of clathrin assembly reliably positioned 100s of nm away from the synapse (Blanpied, Scott et al. 2002; Racz, Blanpied et al. 2004; Lu, Helton et al. 2007), is an important potential site of actin polymerization within the spine. However, by a number of tests, foci of polymerization were not closely associated with clathrin puncta within the spine, and the velocity of actin monomers on filaments near the EZ was not different than the surrounding spine milieu. This is particularly surprising given that the endocytic zone contains numerous actin-binding molecules which likely regulate endocytosis (Engqvist-Goldstein and Drubin 2003; Yarar, Waterman-Storer et al. 2005; Rocca, Martin et al. 2008). However, consistent with a limited tonic role of actin polymerization at the spine EZ, clathrin puncta are not disassembled or disrupted during latrunculin application (Blanpied, Scott et al. 2002), whereas AMPA receptors and PSD scaffold proteins are quickly lost (Zhou, Xiao et al. 2001; Kuriu, Inoue et al. 2006). Our results are thus consistent with the idea that actin polymerization at the EZ is either highly transient during endocytosis (Merrifield, Feldman et al. 2002) or even negatively regulated in spine subregions (Rocca, Martin et al. 2008). PALM offers the possibility to resolve whether actin de/polymerization during induction of long-term depression occurs at the synapse, at the EZ, or at intervening points of the membrane traversed by receptors destined for endocytosis.

Platinum replica electron microscopy recently identified the presence of the Arp2/3 branching nucleator and a network rather than a bundle of filaments at the point of emergence of the spine from the shaft (Korobova and Svitkina 2009), suggesting that filament organization within spine necks is not a simple bundle. Our results confirm and extend these observations by providing live-cell measurements indicating that mature spine necks contain a complex filament organization of mixed directionality. The molecular basis for this remains to be determined, but functionally, the mixed orientation of neck filaments suggests that myosins which translocate to either the barbed end or pointed end of actin filaments could mediate vesicular traffic both to and from the spine head (Osterweil, Wells et al. 2005; Correia, Bassani et al. 2008; Wang, Edwards et al. 2008).

Regulation of filament length through depolymerization is mediated by cytosolic proteins that are unlikely to discriminate between filaments emanating from different, distant locations. On the other hand, there are a number of mechanisms by which active spatial regulation of polymerization would allow filaments of unique length or structure to be organized at discrete locations. At the synapse, for instance, cortactin (Uruno, Liu et al. 2001; Hering and Sheng 2003) and Abp1 (Haeckel, Ahuja et al. 2008) interact with the PSD protein Shank through SH3 domains and activate the Arp2/3 complex. Thus, it will be essential to measure within the spine the distribution of proteins that control polymerization, the mechanisms of their positioning over both short and long time scales, and potential means of compartmentalizing regulatory signaling cascades.

Dynamics of spine filament organization

On average, the distance traveled by tracked actin molecules increased with time for only approximately 8 seconds, reaching a plateau near 200 nm, suggesting that the large majority of filaments are shorter than 200 nm. Consistent with this interpretation, both classical and more recent EM methods show a filamentous actin network which stretches throughout the spine head, but with few filaments extending unambiguously longer than 250 nm (Fifkova and Delay 1982; Rostaing, Real et al. 2006; Korobova and Svitkina 2009). Furthermore, immuno-EM localization of actin-binding proteins within dendritic spines shows that the branch regulator Arp2/3 concentrates within 100 nm of the spine plasma membrane (Racz and Weinberg 2008) the filament-severing protein cofilin concentrates within 200 nm of the plasma membrane (Racz and Weinberg 2006), suggesting tight regulation of filament dynamics near the membrane. Thus, one significant difference between the actin networks of dendritic spines and lamellipodia is the considerably shorter filament length that exists in the spine head. Because neural activity is well known to regulate spine actin dynamics (Star, Kwiatkowski et al. 2002; Okamoto, Nagai et al. 2004; Cingolani and Goda 2008; Honkura, Matsuzaki et al. 2008; Penzes, Cahill et al. 2008), one intriguing interpretation of this difference is that a network of short filaments optimizes both the temporal and spatial response characteristics of actin within the spine following receptor activation.

Filament dynamics in the spine interior were complex, with frequently high single molecule velocities yet little correlation of the local direction of motion. Interestingly, both photoactivation and particle tracking indicated that few filaments penetrate from the spine head into the spine neck. This suggests that the deep interior of the spine near the spine neck represents a zone of depolymerization where filaments converge from broadly distributed regions of the spine head and neck. One potential implication of such an organization is that depolymerization of filaments at this point would offer coordinated regulatory control over both spine morphology and diverse actin functions in the spine. The actin severing protein cofilin is enriched in spines (Racz and Weinberg 2006), and with its regulators LIM kinase and slingshot is known to exert powerful control over spine morphology (Meng, Zhang et al. 2002) during long-term depression (Zhou, Homma et al. 2004; Wang, Yang et al. 2007) and potentiation (Rex, Chen et al. 2009). Such control may be facilitated by attacking filaments at this key organizational point.

Single-molecule tracking of intracellular proteins

The high contrast ratio of activated to non-activated fluorescence of mEos2 (Shroff, Galbraith et al. 2007) has allowed us to track single molecules with very high precision in the x-y plane. Spine geometry thus permitted determination of molecular motion with highest confidence along the spine's most peripheral membrane, where internally directed flow is parallel to the plane of focus. In addition, spine necks are thin enough to be contained within the illuminated volume, and the predominant flow towards the head is unlikely to be contaminated by 3d ambiguity. Within the spine central core,

filament orientation is clearly more complex and irregular, but is also more difficult to determine unambiguously due to the existence of axially oriented filaments in which molecular velocity will be underestimated. Future advances in tracking tools may allow detailed analysis of molecules in three dimensions. Accurate 3d tracking of molecule motion within living spines or other cell regions will complement other emerging 3d super-resolution techniques such as STED (Nagerl, Willig et al. 2008), though creating volumetric instead of planar maps through optical and analytical strategies for 3d localization will naturally require a dramatic increase in the total number of molecules tracked, at the expense of temporal resolution.

Our results demonstrate that single-molecule tracking offers the potential to dramatically facilitate analysis of signaling molecules, scaffolds, and other critical proteins whose dynamic behavior has remained obscure due to intricate cell morphology and highly compartmentalized function. Antibody-based methods to track single proteins in the plasma membrane have been remarkably successful (Sako, Minoghchi et al. 2000; Borgdorff and Choquet 2002; Ehlers, Heine et al. 2007). However, tracking intracellular proteins has presented a very steep challenge, because antibodies are generally not suitable to label single proteins within cells whereas bulk-expressed GFP-tagged proteins cannot easily be discriminated as single molecules. Massively parallel, dual-probe (Subach, Patterson et al. 2009), single-molecule tracking with PALM appears to provide a general tool for mapping the dynamics of key constituents in synapses and other small domains of many cell types.

4. Regulation of spine actin dynamics by Cortactin

Disruption of ongoing actin polymerization leads to a loss of synaptic AMPA receptor currents (Allison, Gelfand et al. 1998; Zhou, Xiao et al. 2001) coupled with a rapid and selective loss of actin-dependent scaffolding molecules from the PSD. This implies that interactions between filamentous actin and the postsynaptic scaffold are required for maintaining the composition and/or architecture of the synapse. Furthermore, the enhancement of actin polymerization near the PSD implies that molecular mechanisms exist to regulate filament assembly at the postsynaptic density. Such a mechanism would require proximity to the PSD as well as the ability to bind to and/or influence the polymerization or structure of growing actin filaments. A number of actin-binding molecules exist at the postsynaptic density, including Abp1, cortactin, CamKII, and alpha-actinin. Two of these molecules, cortactin and Abp1, have the ability to bind to PSD scaffold protein Shank through SH3 domain dependent interactions. Both proteins further bind actin and Arp2/3, an important cellular regulator of branch nucleation. Cortactin, and more recently Abp1 has been shown to play a critical role in the determination of spine number and morphology (Hering and Sheng 2003; Hotulainen, Llano et al. 2009).

In this study, I sought to examine the hypothesis that cortactin regulates the spatial distribution of branched filament nucleation near the PSD. I predicted that cortactin would localize to the PSD in the absence of polymerized actin in an SH3 domain dependent manner. I further predicted that mutations disrupting the interaction between cortactin and shank would alter the stability of the spine actin network. If

cortactin functions as a molecular link between the PSD and the actin cytoskeleton, then disrupting the interaction between cortactin and shank would alter the stability of shank at the PSD, as well as altering the recruitment of polymerized actin to larger spines. Finally, I predicted that disrupting the link between the PSD and the actin cytoskeleton would disrupt the association of large PSDs with larger spines.

Methods

Photoactivation experiments: Single spines of neurons were photoactivated with a titanium:sapphire pulsed laser tuned to 820 nm. Photoactivation was calibrated so that nearly 100% of photoactivateable GFP was photoconverted in a single photoactivation step. Spines were selected based on red fluorescence from co-expressed tdTomato. A second photoactivation step was included at the end of experiments. Only spines that photoactivated to within 30% of the initial photoactivation levels were analyzed. Other confocal experiments were conducted on an Olympus IX81 inverted microscope with a spinning disc confocal (Yokagawa) and a Hamamatsu Orca-ER camera.

Results

I reasoned that cortactin may influence spine actin dynamics. To directly test this prediction I co-expressed actin-paGFP and either full length or a truncation mutant lacking an SH3 domain (cortactin-ΔSH3). Individual spines were selected and timecourse of fluorescence loss following photoactivation of the actin in single spines was measured . In control neurons expressing red fluorescent protein tdTomato, actin-paGFP rapidly left spines with a timecourse fit well by a single exponential **(Figure 4.1A)**. Although

spines expressing full-length cortactin showed similar actin turnover rates as control spines, actin-paGFP turnover was dramatically increased in spines of neurons expressing cortactin-ΔSH3 (**Figure 4.1B**).

Figure 4.1: Photoactivated PA-GFP tagged actin molecules display rapid turnover kinetics in dendritic spines

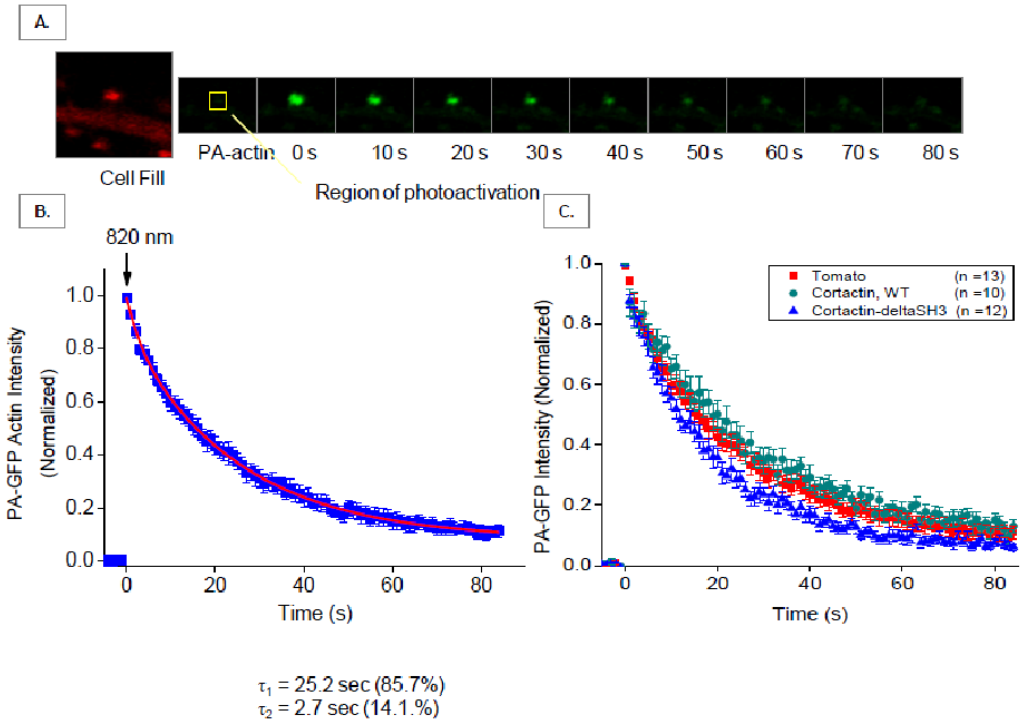

(A) Cells were transfected with tdTomato cell fill and photoactivateable-GFP tagged actin. Following photoactivation, targeted spines emitted green fluorescence, which rapidly decreased with a principle time constant of ~25 seconds **(B)**. A smaller fraction (14.1%) left the spine with a much faster time constant of 2.7 seconds. **(C)** To evaluate the role of cortactin in regulating actin turnover, we transfected photoactiveatable GFP tagged actin and either full length cortactin or a truncated mutant lacking the -SH3 domain. Transfection of the truncated mutant resulted in more rapid loss of photoactivated actin from dendritic spines (tomato n = 13, wt cortactin n = 10, cortactin-deltaSH3 n = 12).

I reasoned that the presence of binding interactions with shank might stabilize cortactin in the spine. To test this prediction, I expressed photoactivatable GFP fused to wild type cortactin or cortactin-ΔSH3 (**Figure 4.2B**). Photoactivated cortactin-ΔSH3-paGFP exited the spine more rapidly than either full-length or phospho null cortactin(W22A). Furthermore, a significantly smaller fraction of the activated cortactin-ΔSH3-paGFP remained at the end of 100 seconds.

The relative instability of cortactin-ΔSH3could be due either to the destabilization of the actin cytoskeleton or due to the loss of interactions at the PSD. To distinguish between these possibilities I expressed fluorescently tagged SH3 fragment of cortactin, which lacks the ability to interact with the actin cytoskeleton. The SH3 fragment was targeted to spines (**Figure 4.2B**). Thus, the SH3 domain of cortactin interacts with binding partners in the spine.

I reasoned that the increased turnover rates in spines expressing cortactin-deltaSH3 could be due to loss of localization to the PSD or other binding partners, and that expression of the SH3 domain alone could work as a dominant negative on endogenous cortactin within the spine, displacing it from the PSD or other sites where it may localize in an SH3 domain-dependent manner. I measured actin-paGFP turnover in spines of neurons expressing either the SH3 domain or control spines expressing tdTomato as a cell fill (**Figure 4.2C**). As in neurons expressing cortactin-deltaSH3, the rate of actin turnover was increased by the SH3 domain alone, suggesting that SH3

domain specific interactions are indeed critical for the proper function of cortactin on the spine cytoskeleton.

Figure 4.2: The Role of Cortactin SH3 domain in mediating actin-independent interactions within spines

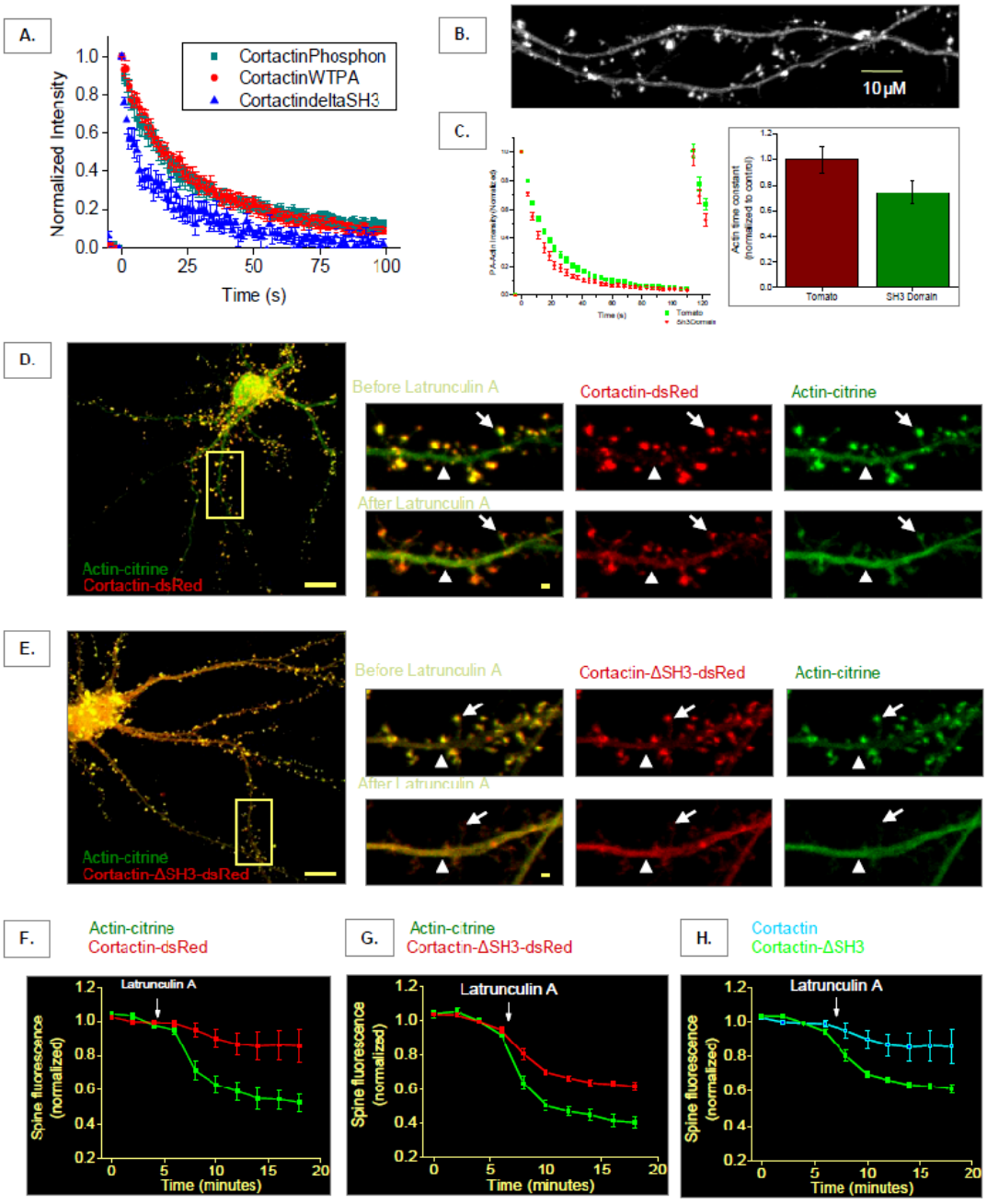

(A) To examine the role of –SH3 domain interactions in stabilizing cortactin within dendritic spines, I co-transfected neurons with tdTomato and photoactivateable GFP tagged cortactin. Photoactivation was targeted to individual spines and fluorescence was measured following photoactivation. Full length cortactin-paGFP fluorescence

disappeared rapidly from the spine. A cortactin phosphorylation mutant behaved similarly to full-length cortactin. In contrast, the –SH3 domain-lacking cortactin was lost rapidly from the spine. **(B)** To examine the sites of potential SH3 domain interactions within spines, I expressed the SH3 domain of cortactin tagged with dsRed. Fluorescence was detected in a punctuate pattern with numerous puncta corresponding to spines. **(C)** To determine the effect of SH3 domain interacting proteins in stabilizing the spine actin cytoskeleton, I co-transfected neurons with actin-paGFP and the SH3 domain of cortactin (n = 14 of each). Actin-paGFP turned over significantly faster within spines of neurons also expressing the cortactin SH3 domain. To examine the role of the SH3 domain in stabilizing cortactin within dendritic spines in the absence of polymerized actin, we co-expressed actin-citrine and either full-length cortactin **(D)** or cortactin-deltaSH3 **(E)**. Following several frames to establish baseline, latrunculin A was applied to depolymerized the actin cytoskeleton. Following actin depolymerization, actin-citrine was rapidly lost from the spinehead **(D-H)**. Wild type cortactin fluorescence also decreased, but to a lesser degree than actin loss **(D,F,H)**. Compared to wild type cortactin, a much greater proportion of truncated cortactin **(E,G,H)** was lost following actin depolymerization.

These findings suggested that cortactin is localized to dendritic spines both through interactions with the actin cytoskeleton and SH3-dependent interactions with proteins such as Shank. To directly define the relative degree to which each of these mechanisms mediate spine-targeting, I designed an experiment in which neurons expressing both actin-citrine and cortactin-dsRed or cortactin-deltaSH3-dsRed were imaged by confocal microscopy before and after the application of actin-polymerization inhibitor latrunculin (**Figure 3.2D-H**). Latrunculin treatment caused a rapid loss of green actin fluorescence from spines. Spines expressing full-length cortactin (**Figure 3.2D,F,H**) lost approximately 50% of their actin fluorescence within 15 minutes of latrunculin application. Interestingly, this loss of actin from the spine was coupled to a loss of a mere 10% of cortactin fluorescence. In sharp contrast, while spines of neurons expressing cortactin-deltaSH3 lost about 60% of the original green actin fluorescence, the red fluorescence from cortactin-deltaSH3 dropped to 60% of the original level (**Figure**

3.2E,G,H). These findings suggest that whereas cortactin-deltaSH3 depends on the actin cytoskeleton for localization to spines, full-length cortactin can interact with other binding partners within dendritic spines.

Discussion

The spine actin cytoskeleton is a dynamic, constantly changing structure and yet this ongoing, active recycling of the individual polymerized molecules within the network of filaments is critical for the stability of the composition and structure of the postsynaptic density. The timescale in which AMPA receptors and especially the latrunculin-sensitive subset of postsynaptic scaffolding molecules are lost following inhibition of actin polymerization by latrunculin implies that functional interaction between the cytoskeleton and the postsynaptic density occurs directly at the synapse. Moreover, it implies that the required filaments are not static structures. Instead, it appears that dynamic, polymerizing subsynaptic or perisynaptic actin filaments are a critical component of the synapse.

The spine actin cytoskeleton is polarized (Honkura, Matsuzaki et al. 2008; Hotulainen, Llano et al. 2009; Frost, Shroff et al. 2010) and polymerization is regulated at discrete locations within the spine, including the PSD (Frost, Shroff et al. 2010). Despite the abundance of actin binding molecules at the synapse, there is a paucity of information regarding the mechanisms involved in the regulation of actin polymerization at this location, or for that matter in the spine as a whole. Our data is consistent with a model in

which cortactin acts as a linker between the PSD and the actin cytoskeleton, regulating the elaboration of branching actin networks near the synapse.

Cortactin is targeted to spines, where it acts to stabilize the actin cytoskeleton in an SH3 domain dependent manner. Expression of cortactin-ΔSH3 destabilized spine actin networks. Furthermore, cortactin-ΔSH3 itself turned over more rapidly within the spine, suggesting fewer stable interactions within the spine. That the cortactin SH3 domain was targeted to spines suggests the presence of mechanisms by which cortactin is targeted to spines independent of polymerized actin filaments, such as Shank. Further supporting the role of the SH3 domain in the targeting of cortactin to spines was the finding that cortactin remained in spines following latrunculin in an SH3 domain dependent manner. Future studies will directly test the role of shank-cortactin interactions.

A number of other actin binding molecules are emerging as potential regulators of actin polymerization at the postsynaptic density, including CamKII (Okamoto, Narayanan et al. 2007; Okamoto, Bosch et al. 2009)and Abp1 (Hotulainen, Llano et al. 2009). CamKII bundling of actin filaments has been demonstrated in vitro, and expression of activation mutants of CamKII alter the stability of the spine actin network in cultured neurons. However, although CamKII exists in large quantities within the PSD (Chen, Vinade et al. 2005) there is the potential that it is extrasynaptic CaMKIIβ alone that stabilizes the actin network. Thus it is not clear that synaptic CamKII functions in the regulation of the actin cytoskeleton. Abp1 has been shown to alter spine morphology through an SH3 domain and shank dependent mechanism. Like cortactin, Abp1 also

binds F-actin and the Arp2/3 complex. Thus, Abp1 and cortactin have apparently overlapping or competing responsibilities at the synapse. It will be important in future studies to elucidate the relative roles of these two proteins in regulating actin polymerization at the synapse, particularly during synaptic plasticity.

5. Discussion

The spine actin network is essential for the function of the synapse, stabilizing scaffold molecules and glutamate receptors within the postsynaptic density. Disruption of ongoing actin polymerization within the neuron has previously been shown to affect synaptic function within minutes; however the location of functional actin filaments, and indeed the mechanism by which they exert a stabilizing effect on synaptic structures has not been investigated. Prior studies have been hampered by the small spatial scale of dendritic spines, and fundamental limitations of light microscopy.

In this study, I have demonstrated that PALM microscopy is capable of resolving molecular motion with fine precision. Using confocal microscopy, as well as PALM, I demonstrated that the motion of polymerized actin molecules within spines is polarized, resulting in their motion from the membrane toward the central core of the spine. Importantly, velocity varied, with discrete foci of high velocity flow originating from locations that were distributed across the spine membrane with the highest velocity flow associated with the PSD. My results are consistent with a model in which actin polymerization is independently upregulated at specific subdomains of the spine membrane, driving enhanced motion of polymerized molecules on filaments originating at these points.

Importantly, actin filaments originating at the the synapse displayed higer velocity flow in relation to the endocytic zone and elsewhere in the spine. This suggests that polymerization of actin networks is selectively upregulated at the synapse. Although this

does not rule out the possibility that actin networks distant from the PSD may exert effects on receptor trafficking or motion through the spine neck, the existence of polymerizing filaments directly at the synapse does support the hypothesis that a functional interaction exists between the PSD scaffold and the cytoskeleton. I propose that this interaction has bidirectional effects in that the PSD may directly regulate filament structure, and that the cytoskeleton may in turn directly influence the composition and function of the PSD.

This idea is supported by a growing body of evidence. First, the rapid loss of scaffolding molecules following depolymerization of the actin cytoskeleton (Kuriu, Inoue et al. 2006) suggests a direct effect on scaffold stability. Mechanisms involving protein trafficking or insertion into cellular membranes would likely occur over longer timescales. Furthermore, actin polymerization has direct effects both on PSD morphological plasticity (Blanpied, Kerr et al. 2008), and the motion of receptors within the PSD (Kerr, unpublished).

It remains puzzling how a cytoskeleton that is constantly moving and readjusting can be a stabilizing force on PSD composition and simultaneously drive morphological plasticity of the scaffolds. The nature of the interaction between actin filaments and the PSD remains unknown. The force vectors exerted on the PSD by polymerizing actin networks undoubtedly depend on the orientation of the individual filaments, the location of assembly, the distribution of sites at which PSD associated actin binding proteins interact with the actin network, and the affinity with which the actin binding proteins

interact with both the PSD and the cytoskeleton. It is possible that actin may exert axial force on scaffolds at the base of the PSD, thereby promoting their interactions with PSD molecules more proximal to the synaptic cleft. Similarly, inward force at the lateral edges of the PSD may compress the scaffolding molecules, preventing their lateral release from the synapse. Conversely, laterally oriented filaments along the bottom extent of the PSD could provide sheer force theoretically stabilizing the PSD again by pushing molecules from the lateral edge of the PSD toward the center. Intricate branching networks oriented in this manner could potentially provide a web preventing the escape of large PSD scaffolding molecules.

6. **Future Directions**

In this work I developed techniques allowing the measurement of the distribution and behavior of intracellular proteins within living neurons with previously unattainable precision and applied these techniques in the description of the structure and regulation of the actin cytoskeleton within individual dendritic spines. Ongoing experiments will utilize these techniques to investigate the structure and function of protein networks which support synaptic function both at the PSD and elsewhere within dendritic spines. Important questions remain regarding the mechanisms involved in the regulation of actin polymerization at the PSD, both by cortactin and other actin binding proteins known to be present at or near the synapse (See Appendix). I will focus this discussion into three parts: regulation of the synaptic structure and function by actin and its regulatory

molecules, regulation of protein trafficking by the actin cytoskeleton, and further work in optimizing super-resolution imaging techniques in the study of synaptic function.

The composition of both the scaffolding molecules present at the PSD and the receptors anchored within the synapse are regulated by ongoing actin polymerization, but the mechanisms by which actin functions in this regulation remains unknown. Ongoing studies will help elucidate the role of actin in affecting both the subsynaptic distribution of AMPAR and scaffolding molecules within the postsynaptic density. To test the role of actin binding proteins in the regulation of synaptic structure we plan to utilize mutations disrupting the interaction between cortactin and shank and measure the resulting changes in synaptic strength, composition, and size.

Actin may play roles in the trafficking of various proteins and cargo-laden vesicles to and from the synapse. Single molecule and single particle imaging techniques will be useful in studying the manner in which vesicles are transported from microtubule networks within the dendritic shaft into the spine, as well as the role of actin filaments in this process. Similarly, further investigations into the regulation of ongoing actin polymerization at sites of endocytosis will provide valuable clues about the mechanisms by which actin is regulated and functions during this process. Finally, actin structures are likely involved in the regulation of trafficking of both membrane proteins and receptors, as well as freely diffusing intracellular molecules, either by directly affecting the movement of these molecules through diffusional barriers or modulating the structure and/or content of the spine neck. Investigating the role of actin in modulating spine neck

geometry, while simultaneously monitoring the effect on protein motion across this potential barrier requires super-resolution imaging of living cells and may be accomplished using single-molecule tracking PALM. However, due to technical challenges of accurately measuring protein mobility within small bounded regions a more straightforward approach would be to utilize stimulated emission depletion (STED) microscopy to measure spine geometry with high reolution combined with FRAP or photoactivation to quantify the loss of target molecules from the spine head.

All of these studies will be greatly aided by further optimization of super-resolution techniques. Significant obstacles are currently posed by inadequate fluorophores for multicolor imaging, incompatibility of PALM with live tissue or slices, and speed/resolution trade-offs of three dimensional imaging and tracking. It is likely that the future will bring an increased selection of fluorophores with desirable characteristics: better green proteins for single molecule imaging, improved brightness/photon yield over currently available PA-TagRFP or mEos2, and far-red or blue proteins useful for three color imaging. Working with the molecules currently available it would be possible to perform 3 color super-resolution imaging using PA-CFP2 and PA-mCherry or PA-TagRFP coupled with far-red quantum dots or dyes targeted to surface proteins. These experiments are limited by low molecular yield or specificity of the third marker and are somewhat complicated by alignment procedures necessary to account for optical aberration or rotation of specific filters for each color.

Multidimensional PALM is possible, but limited by difficulty accounting for drift, and relatively small range in the z axis over which molecules can be reliable localized. Furthermore, the relative imprecision of localization in the z axis may be limiting in its usefulness in single particle tracking of photoconvertible proteins, due to their relatively low photon yield. Furthermore, the need to collect multiplanar images may be a significant time-loss in live cell experiments. Thus, the development of novel methods for multiplanar simultaneous acquisition and improved z-resolution will be invaluable to the application of these techniques to the study of neuronal function in living cells.

7. Appendix

A number of actin-binding proteins exist within the PSD. Many, including cortactin and Abp1, may participate in the elaboration of branching actin networks. Following is a discussion of PSD associated actin binding proteins and their known effects on synaptic function (also see figure 5.1 for a discussion of general mechanisms by which actin binding proteins may actively or passively influence filament structure).

Figure 5.1: Mechanisms of spatially restricting actin regulation.

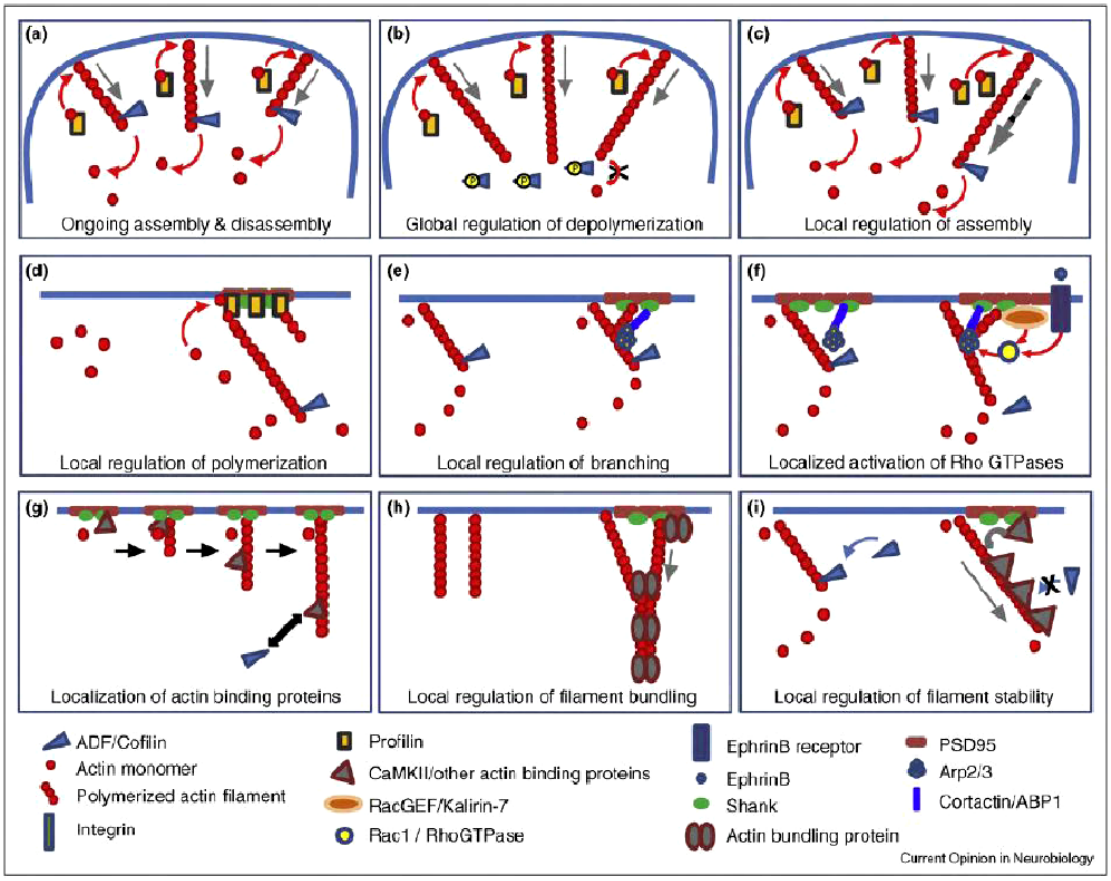

(a) Treadmilling of actin mediated by addition of monomers at filament barbed ends (red arrow) and depolymerization by cofilin (blue wedge) at or near filament pointed ends. Polymerized actin molecules and binding proteins flow along the active filament as monomers are added. Gray arrows indicate direction and rate of flow. **(b)** The pointed end of many filaments probably lie deep in the spine interior, and depolymerizing molecules are free to diffuse in the cytoplasm. Thus, even localized activation of signalling pathways near the spine membrane is likely to result in a widespread alteration of filament structure. For example, regulation of cofilin activity (by phosphorylation — yellow circle). **(c)** Conversely, sites of ongoing monomer incorporation near the spine membrane are likely to be important sites for localized regulation of filament structure, because rates of monomer incorporation may be controlled by anchored or membrane-associated factors. **(d)** Sites of assembly require profilin (yellow boxes), which is enriched near the PSD. This represents one known example of a potentially larger strategy for spatial regulation. **(e)** Spatial pattern of branch formation is determined by localization of the Arp2/3 complex (blue complex), which has binding partners Abp1 and cortactin that bind the PSD scaffold Shank. **(f)** Localization of signaling molecules including Kalirin-7, a RhoGEF which binds PSD-95, may be responsible for the spatial

segregation of downstream actin regulatory pathways. **(g)** A number of actin-binding proteins such as CaMKII are localized at the PSD through specific binding to PSD scaffolds. Their ability to bind to and be transported away from the membrane by a growing actin filament may be a mechanism for controlling the number and composition of signalling molecules at the PSD. In addition, these molecules compete with other actin-binding proteins for sites on the growing filament. **(h)** A number of molecules, including CaMKII and alpha-actinin, are localized at the synapse, and through association of multiple actin-binding domains, have the ability to bundle actin filaments. **(i)** Actin-binding proteins compete for binding sites on growing filaments. Thus, the preferential decoration of filaments near the synapse with molecules such as CaMKII or cortactin may represent a protective mechanism which allows growing filaments to penetrate more deeply into the spine interior before they are severed by cofilin.

Cortactin and Abp1

Cortactin is an 61 kDa F-actin binding protein that localizes to the lamellipodium and other sites of dynamic actin assembly where it is thought to enhance actin assembly through activation of the Arp2/3 complex (Weed, Karginov et al. 2000). Cortactin binds F-actin through the 4^{th} of 6 tandem repeat regions, and the Arp2/3 complex through an N terminal acidic region. Src-phosphorylated cortactin forms a complex with N-WASP and WIP(WASP interacting protein) through adaptor protein Nck (Tehrani, Tomasevic et al. 2007). Thus cortactin facilitates the activation of Arp2/3 by WASP and may direct the nucleation of new branches within the cell.

The fact that cortactin also interacts with PSD scaffolding molecule shank (Naisbitt, Kim et al. 1999) suggests that it, like Abp1, may coordinate the spatial distribution of new branch formation to sites near the PSD. Cortactin is targeted to spines, in a manner primarily reported to be dependent on the actin and arp2/3 binding (Hering and Sheng 2003), although the latter could be potentially explained by decreased concentration in F-

actin due to lack of Arp2/3 activation. The observation that the SH3 domain was not involved in spine targeting would indicate that the cortactin-shank interaction is not important physiologically, although I have observed both expression of SH3-tomato in spines as well as a stable core of cortactin that remains in spines following depolymerization of the actin cytoskeleton by latrunculin A, suggesting that cortactin does indeed interact with some stable proteins in the spine such as shank. Further supporting this notion, using EM tomography, Rostaing et al (2006) demonstrated that cortactin localized to the cytoplasmic face of the PSD at similar distances from the synaptic cleft as shank. The same study also found that cortactin and actin were translocated out of spines following the application of 50 uM NMDA, although it is difficult to assign causality to cortactin since so much of its spine targeting was determined by the presence of F-actin.

How might cortactin influence affect cytoskeletal structure and interaction with the PSD? It is interesting to suppose that specific molecules such as cortactin mediate force generated at circumscribed portions of the PSD. The PSD scaffolding molecule Shank has been localized by EM at the edge of the PSD (Valtschanoff and Weinberg 2001), where the synaptic fraction of spine cortactin is also found (Racz and Weinberg 2004). Thus, cortactin may be primarily responsible for regulating PSD-cytoskeletal interactions at this region. The behavior of PSD associated cortactin following binding to an actin filament is unknown. It is possible that on binding a growing actin filament, cortactin may stimulate the Arp2/3 complex to initiate branch nucleation while remaining

bound to the PSD, or it may dissociate from the PSD and travel with the growing filament.

Abp1 is another protein which may coordinate actin structures near the PSD through interactions with the F-actin and Shank (Haeckel, Ahuja et al. 2008). Interestingly, whereas overexpression of cortactin, which directly complexes with both Arp2/3 and WASP led to longer spines with no change in spine head size (Hering and Sheng 2003) overexpression of Abp1, which activates the Arp2/3 complex only indirectly through release of WASP autoinhibition, dramatically increases the length and complexity specifically of mushroom spines (Haeckel, Ahuja et al. 2008). This is particularly interesting since it suggests that overexpression of Abp1 leads to an increase in stable filaments traversing the neck. Whereas the spine head area was not quantified in the Abp1 study, overexpression of mutant forms of cortactin possessing the ability to bind actin but lacking the SH3 domain resulted in long, thin spines. One possible explanation for the difference in the effects of the two proteins is a tighter spatial regulation of actin filament behavior by cortactin, with a more promiscuous spread of Abp1-activated WASP. Conversely, Abp1 has a strong preference for binding to newly formed filaments (Kessels, Engqvist-Goldstein et al. 2001). As this preference may be mediated by affinity for ATP-actin, and as the time constant for conversion to ADP-actin is on the order of seconds, it is possible that Abp1 actually remains associated with actin filaments very near the PSD. Regardless, as the two proteins bind the same target at the PSD, the possibility that they work in competition for binding sites within the PSD is intriguing.

As these two proteins remain likely candidates for signaling the organization of specific actin structures near the PSD, and as these proteins may play principle roles linking the postsynaptic density to the actin cytoskeleton, it will be important to test whether they mediate the stabilizing effects of the dynamic actin cytoskeleton on the PSD. Does elimination of these molecules interfere with anchoring of AMPA or NMDA (Rosenmund and Westbrook 1993) receptors at the synapse or the stability of actin-dependent PSD scaffolding molecules such as Shank? Finally, is ongoing PSD restructuring dependent on tethering of the actin cytoskeleton to the PSD through molecules such as cortactin and Abp1?

Coronin

Coronins are a conserved group of actin binding proteins that bind actin and interact with the Arp2/3 complex (Uetrecht and Bear 2006). Coronin 1a was first discovered as a 57 kDa protein that immunoprecipitated with actin-myosin complexes (de Hostos, Bradtke et al. 1991) and formed crown like clusters and is necessary for phagocytosis in yeast (Maniak, Rauchenberger et al. 1995). In mammalian cells, the coronins re targeted to the leading edge of migrating cells where they interact with both slingshot and the Arp2/3 complex (Cai, Marshall et al. 2007). Whereas PKC phosphorylated coronin is inactive and allows Arp2/3 mediated actin assembly to proceed unhindered, dephosphorylation by slingshot leads to attenuation of Arp2/3 mediated actin assembly. Furthermore, binding of Arp2/3 by coronin destabilizes and alters the angle of Arp2/3 nucleated branch points (Cai, Makhov et al. 2008). Simultaneously, coronin is responsible for the recruitment of slingshot to the leading edge, and thus supports

activating dephosphorylation of cofilin by slingshot. Taken together these data suggest that localized activation of coronin may mediate the delicate balance between polymerization and depolymerization in dynamic actin networks. Although they are abundantly expressed in neurons of the brain, the role of coronins in the brain is virtually unstudied (Hasse, Rosentreter et al. 2005).

Alpha-actinin

Alpha-actinin is an actin bundling protein which forms a dimer with actin binding domain at each end, which allows it to crosslink and bundle actin filaments (Sjoblom, Salmazo et al. 2008). In dendritic spines, alpha-actinin is localized at the PSD where it binds competitively with Ca^{2+}-CaM to the NMDA receptor, and is likely to attenuate calcium mediated inactivation of the NMDA receptor (Wyszynski, Lin et al. 1997; Wyszynski, Kharazia et al. 1998). In addition, displacement of alpha-actinin from the C terminus of the NR1 subunit is necessary for binding of autophosphorylated CAMKII (Merrill, Malik et al. 2007). It is also found at the spine apparatus where it binds synaptopodin and is likely to be partially responsible for the thick sheets of polymerized actin observed in this location (Wyszynski, Kharazia et al. 1998; Capani, Martone et al. 2001; Kremerskothen, Plaas et al. 2005). Expressed alpha-actinin localizes to spines require both actin-binding and the spectrin repeat region. Furthermore, overexpression of alpha-actinin increases the length and density of dendritic spines in a manner that required both the actin binding domain and the spectrin repeat region, which is responsible for the binding to NMDA receptors (Nakagawa, Engler et al. 2004). Although all these studies implicate a role for alpha-actinin in linking synaptic NMDA

receptor signaling to polymerizing actin, the observation that only a small fraction of alpha-actinin immunoprecipitates with the NMDA receptor (Merrill, Malik et al. 2007) make this difficult to test directly.

Formin/Diaphonous

The formin family consists of 15 members, of which diaphanous is the best characterized (Schonichen and Geyer 2010). They range in size from 120-220 kDa which function as dimers (Chesarone and Goode 2009; Chesarone, DuPage et al. 2010) to bind actin-profilin complexes through C-terminal interactions. A flanking region in the C terminus also binds a number of plus end microtubule binding proteins, including End Binding Protein 1 (EB1). Formins stimulate the rapid nucleation of straight actin filaments which may grow at rates exceeding 1 um/s. To maintain continued stimulation of nucleation at the barbed end, formins therefore function as molecular motors which travel processively toward the barbed end of actin filaments, simultaneously catalyzing the addition of new monomers (Higashida, Miyoshi et al. 2004) and preventing the access of capping proteins.

A number of formins contain Rho binding domains, through which they act downstream of Rho signaling. One family member, Delphilin has two PDZ domains through which it may interact instead with the Glutamate Receptor delta2 subunit (Miyagi, Yamashita et al. 2002), through which at least one isoform is targeted to postsynaptic sites (Matsuda, Matsuda et al. 2006; Matsuda, Matsuda et al. 2006). A longer isoform localizes to the soma and dendritic shaft and may associate with recycling

endosomes, thus mediating interactions with the actin cytoskeleton and microtubules. Phosphorylation of Serine 1 and Threonine 2 regulates the interaction between Delphilin and the glutamate receptor, and thus this interaction may be regulated in an activity-dependent manner (Sonoda, Mochizuki et al. 2006). Consistent with a possible role of these family members in receptor cycling and endocytosis, another member of the Formin family Daam1 is localizes in a punctuate pattern along the dendrite, soma, and spines (Salomon, Haber et al. 2008), and is involved in the endocytosis of EphB receptors (Kida, Sato et al. 2007). Formins are likely to be involved in processes requiring extremely high velocity actin filament nucleation, so it is intriguing that they may be involved in endocytosis through rapid bursts of polymerization that may push or pull an internalized vesicle away from the membrane, clearing the endocytic zone. mDia2 localizes to the tip of filopodia and to spine heads of mature spines. Knockdown of this protein leads to a decrease in the density of filopodia and thin spines (Hotulainen, Llano et al. 2009), suggesting that it is important in the formation of protrusions with specific actin structures, namely those protrusions with a high density of long unbranched filaments, and that its importance is diminished in spines containing elaborate branched networks under the control of the Arp2/3 complex. It is possible that these structures are maintained by actin flow of higher velocity than that present in mature spines, although this has not been directly compared.

Synaptopodin

Synaptopodin is a dual alpha-actinin and actin binding protein expressed at high levels in neurons where it appears to be important in anchoring of endoplasmic

reticulum-like organelles such as the spine apparatus (Deller, Korte et al. 2003) and the cisternal organelle of the axon initial segment (Bas Orth, Schultz et al. 2007). Although the function of both these organelles is largely mysterious, the spine apparatus represents a specific domain within the head of many mushroom spines which is associated with thick sheets of bundled actin filaments (Capani, 2004). Synaptopodin expression is required for the existence of the spine apparatus, which normally lies in close proximity or may be directly connected to the PSD. The fact that synaptopodin-lacking mice show deficits in the expression of long term potentiation thus implies that putative calcium release or other function of the spine apparatus may be involved in LTP induction or expression. Synaptopodin is localized primarily in large spines (Vlachos, Korkotian et al. 2009) which exhibit enhanced AMPAR responses to glutamate uncaging than synaptopodin-lacking spines. Finally, caffeine stimulation of cultured neurons has been shown to elicit intracellular rises in calcium near the sites of the spine apparatus and an associated recruitment of AMPA receptors, providing evidence that it acts as a reservoir for calcium that may be released through activated Ryanodine Receptors. Interestingly, the same study demonstrated that synaptopodin containing spines were resistant to the effects of latrunculin, suggesting that the spine apparatus may be associated with a stable core (Honkura, Matsuzaki et al. 2008) of F-Actin. If the spine apparatus is involved in plasticity induction, the association of such a stable pool with the spine apparatus may explain the fact that spines with large stable pools may give rise to more robust spine enlargement during LTP induction protocols.

Drebrin

Drebrin is an actin-binding protein expressed strongly in the brain where it targets to spines (Hayashi, Ishikawa et al. 1996). It has been reported to have a myriad of effects on spine morphology and plasticity mediated through interactions with a number of actin binding proteins including myosin, tropomyosin (Ishikawa, Hayashi et al. 1994; Hayashi, Ishikawa et al. 1996), alpha-actinin, gelsolin (Hayashi, Ishikawa et al. 1996), profilin (Hayashi and Shirao 1999), Ras (Biou et Matus, 2008), and other proteins. Overexpression of wild type drebrin leads to lengthening of spines (Hayashi and Shirao 1999), and may destabilize mature spines in a ras dependent manner (Biou, Brinkhaus et al. 2008). Overexpression of Drebrin in the latter study resulted in dendrites with a large proportion of thin dendritic filopodia, whereas drebrin knockdown resulted in an increased percentage of spines with globular heads. On the other hand, another study reported that drebrin was responsible for PSD clustering and the conversion of filopodia into spines (Takahashi, Sekino et al. 2003). The precise mechanism whereby drebrin regulates the spine actin cytoskeleton remains poorly understood, and may involve its inhibition of myosin, which may have direct effects on spine morphology (Ryu, Liu et al. 2006) or indirect effects on synapse maturation through inhibition of myosin-delivered cargo (Correia, Bassani et al. 2008; Wang, Edwards et al. 2008). The differences in the reported effects of drebrin are likely due to differences in expression levels as low levels of protein may still remain under active regulation by endogenous upstream signaling pathways, whereas higher levels of drebrin (or any actin binding protein) has the ability to bind more actin filaments in a non-specific way, displacing other actin binding proteins or affecting the gross structure of the actin network.

CamKII-beta

The role of CamKII in the regulation of synaptic function and plasticity is enormous. CamKII forms a dodecameric barrel-shaped complex that measures 20 nm tall. It is densely localized to synapses, where it localizes principally in a single layer on the cytoplasmic face of the postsynaptic density (Petersen, Chen et al. 2003), through interactions with densin and the long cytoplasmic tail of NMDA channels. These CamKII molecules are thus ideally positioned to influence the function of synaptic NMDA receptors and scaffolding molecules while simultaneously bridging the PSD to the actin cytoskeleton through beta subunits contained in the complex.

CamKII beta is an actin binding protein which can bind both F-actin (O'Leary, Lasda et al. 2006; Okamoto, Narayanan et al. 2007; Lin and Redmond 2008)Sanabria et Waxham, 2009) and G-actin (Sanabria, Swulius et al. 2009). Only the beta isoform associates with actin structures, and this association is influenced by alternately sliced isoforms (O'Leary, Lasda et al. 2006), although the dodecameric structure of CamKII dictates that most complexes will contain both alpha and beta isoforms and therefore possess at least some actin-binding ability. CamKII beta bundles and stabilizes actin filaments in vitro and in living cells (Fink, Bayer et al. 2003; Okamoto, Narayanan et al. 2007; Lin and Redmond 2008; Okamoto, Bosch et al. 2009). In spines, CamKII beta knockdown leads to a lengthening of protrusions, which may be rescued by kinase dead mutants of CamKII. Overexpression of CamKII or mutants containing the actin binding domain and have the ability to oligomerize stabilize actin dynamics measured by FRAP (Okamoto, Bosch et al. 2009). Taken together, these observations suggest that a: bundling

requires only oligomerization of the CamKII actin binding domains, and b: CamKII alpha kinase activity is sufficient to compensate for the loss of CamKII beta kinase activity. However, the kinase activity is important in the regulation of actin bundling by CamKII as activation and autophosphorylation of CamKII by calcium/calmodulin was shown to inhibit the bundling activity of CamKII on actin filaments *in vitro*. CamKII beta expression also has been shown to stabilize other actin structures, including filopodia. Interestingly, it was shown in this study that constitutively active CamKII (T287D) stabilizes actin dynamics to similar degrees as wild type CamKII, whereas a phosphorylation null mutant (T287A) destabilized actin turnover in these structures (Andersen, Li et al. 2005). This evidence is supported by the stimulation of new protrusions by injection of autophoshorylated CamKII (Jourdain, Fukunaga et al. 2003). Taken together, these studies suggest the possibility that CamKII may stabilize actin dynamics in spines or other structures through mechanisms distinct from its bundling activity, perhaps through sequestration of monomers or through capping activity.

CamKII translocates into spines following NMDA receptor stimulation (Shen and Meyer 1999),and interestingly CamKII alpha recruitment precedes recruitment of CamKII beta, suggesting that the two isoforms have different binding partners and may play distinct functional roles within the spine. CamKII kinase activity is necessary for NMDA and integrin-signalling mediated spine remodeling (Shi and Ethell 2006), and chronic blockade of network activity coupled with actin-depolymerization may result in loss of CamKII from spines (Ahmed, Zha et al. 2006), again suggesting that CamKII-actin interactions are functionally relevant. However, the true site and nature of CamKII

mediated influences on actin structures remains to be fully understood. Is the primary role of CamKII beta – actin binding to link the actin cytoskeleton to the postsynaptic scaffold? Or does CamKII mediate effects on actin structure at sites other than the PSD. Finally, as most of the studies on the effect of CamKII on actin dynamics in neurons have been performed using expression of proteins, it will be important to examine the acute effects of blocking or activating CamKII kinase activity on the actin cytoskeleton.

Myosins

The myosins are a large family of actin-based motor proteins whose activities, coordinated with the cytoskeleton, function in a wide range of functions including the production of contractile force and processive transport of cargo. Myosins possess two actin binding "heads" which allow them to move "hand over hand" along polymerized actin filaments (Yildiz, Forkey et al. 2003). In addition, myosin II can oligomerize through interactions of a coiled coil domain, allowing them to generate contractile force through actions on multiple actin filaments (Woolner and Bement 2009). Most myosins move toward the plus (barbed) end of actin filaments; myosin VI is an unconventional motor whose movement is directed toward the minus (pointed) end (Menetrey, Bahloul et al. 2005). A number of myosins have been implicated in the regulation of synaptic function, including nonmuscle myosin IIb (Naisbitt, Valtschanoff et al. 2000; Ryu, Liu et al. 2006) Myosin Va (Takagishi and Murata 2006; Correia, Bassani et al. 2008; Lise, Srivastava et al. 2009) but see (Petralia, Wang et al. 2001), myosin Vb (Wang, Edwards

et al. 2008), and myosin VI. The latter, which moves away from the sites of actin polymerization, is implicated in playing a role in endocytosis. Defects in stimulus—induced AMPAR internalization coupled with the ability of myosin VI to interact with AP-2 and SAP97 suggest that they may help to pull AMPAR containing endosomes away from the endocytic zone (Osterweil, Wells et al. 2005).

Myosin Va is mutated in the human hereditary neurological disease, Griscelli syndrome type 1; Mice carrying this mutation lack a spine apparatus and display deficits in the induction of LTP and LTD (Takagishi and Murata 2006). Thus, it is possible that myosin Va plays a role in the transport or anchoring of smooth ER or other organelles within spines. Another observation suggesting a tethering role was the finding that expression of myosin Va dominant-negative enhanced the exocytosis of dense core vesicles in neurons (Bittins, Eichler et al. 2009). As myosin V processes toward the plus end of actin filaments, and thus presumably toward the extracellular membrane, and because the depolymerization of actin filaments with latrunculin mimicked the effect of dominant negative myosin Va, it was concluded that myosin Va normally functions to tether dense core vesicles to actin structures away from the membrane. Another study, examining the role of myosin Va in delivery of recycling endosomes, used the same dominant negative fragment of myosin Va and observed deficits in synaptic delivery of GluR1 during LTP. Furthermore, myosin Va interacts with Rab11 (a marker of recycling endosomes), and expression of the dominant negative myosin Va tail decreased the incidence of Rab11 puncta in spines (Correia, Bassani et al. 2008). Although the authors concluded that myosin Va actively transports recycling endosomes into spines during

LTP, it cannot be ruled out that myosin 5a actually serves as a tether, preventing endocytosed vesicles from leaving the spine. Evidence that another member of the myosin V family, myosin Vb, is involved in endosome trafficking has also been reported. Myosin Vb also interacts with Rab11, and appears to traffic with transferrin receptor-containing endosomes (Wang, Edwards et al. 2008).

It is thus possible that both motors interact with recycling endosomes, perhaps at distinct points in the recycling process. The ATPase activity and actin-binding of both proteins is activated by calcium (Li, Jung et al. 2006; Wang, Edwards et al. 2008), and slows the processive motion of myosin Va on F-actin (Krementsov, Krementsova et al. 2004). The plus end polarity of myosin V raises the possibility that calcium influx at the synapse may result in stable myosin Va or Vb-actin complexes at the base of the spine that may be carried into the spine head by treadmilling of filaments directed into the spine head. On the other hand, calcium-bound myosins in the spine head could be driven to the base of the spine by the same mechanism, depending on the orientation of actin filaments in the neck. It is possible that once there, they could associate with recycling endosomes, and [assuming steep enough gradient of calcium concentration between the spine head and dendritic shaft] processivly move back into the spine head along the same filaments (Wang, Edwards et al. 2008). Neither mechanism is completely satisfying as they fail to explain a) the positioning of recycling endosomes at the base of spines under basal conditions or b) are vesicles directly transported to the spine membrane by either of these motors or do the myosins disengage from their cargo in the spine head, allowing them to reach their target (presumably syntaxin-4 rich exocytic zone (Kennedy, Davidson

et al. 2010) unaided. Taken together however, they do reveal a strong an important role for actin filaments in the spine neck, and open the possibility that regulation of filament orientation may be an important factor driving cargo delivery into and out of spines.

In contrast to the proposed roles of other myosins in delivering or anchoring cargo stores to sites near the synapse, myosin II is thought to play a structural role directly impacting the cytoskeletal network (Ryu, Liu et al. 2006). Inhibition of myosin II activity by blebistatin causes a rapid restructuring of the shape of mushroom spines, with the appearance of numerous filopodia-like processes which protrude from the spine head. Thus, similarly to its roles in the lamellipodia of migrating cells or in growth cone, myosin II is thought to form a contractile core in the center of spines, cross-linking filaments, regulating the tension of the actin network, and perhaps regulating disassembly (Medeiros, Burnette et al. 2006).

Spire/ WH2 Homology Domain containing proteins

The discovery of the Arp2/3 complex and the formin family of actin filament nucleators provided a mechanism for cells to catalyze the assembly of new filaments from freely diffusing monomers, a process that occurs orders of magnitude too slowly in the absence of nucleating factors. With the discovery of a third family of actin nucleators, the WH2 homology Domain proteins, it is clear that they are not alone. The first members of the group, spire, was shown to nucleate the formation of unbranched filaments from pyrene-labeled G-actin (Quinlan, Heuser et al. 2005). Spire contains 4 WH2 domains, which are all necessary for maximal filament assembly. The protein also

contains an N terminal Kinase non-catalytic C lone domain (KIND) domain, a Spir-box which may be a target of Rab GTPases, and an FYVE zinc finger motif at its c-terminus which directs it to subcellular membrane compartments. Spire interacts with formins through a c-terminal spir-interactive motif, and may inhibit formin mediated actin nucleation (Chhabra and Higgs 2007). Spir-1 is expressed primarily in the forebrain, where it displays strong staining in the pyramidal cell layer of the hippocampus and the pyramidal cell layer of the cerebellum (Schumacher, Borawski et al. 2004). Obviously, much work will need to be performed to elucidate the potential roles of this new family of actin filament nucleators at the synapse.

The vast numbers of regulatory mechanisms that exist with single spines provide an actin cytoskeleton that is an intricate and highly organized structure. Although much is known about the biochemical function of various actin binding molecules on actin polymerization in vitro or in other biological systems, little is known about how they interact within spines and at the synapse. Much work remains to determine how actin polymerization is regulated on fine spatial scales within the spine, and how these processes may be modulated in response to external input or synaptic stimuli.

8. References

Ackermann, M. and A. Matus (2003). "Activity-induced targeting of profilin and stabilization of dendritic spine morphology." Nat Neurosci **6**(11): 1194-1200.

Ahmed, R., X. M. Zha, et al. (2006). "Synaptic activity and F-actin coordinately regulate CaMKIIalpha localization to dendritic postsynaptic sites in developing hippocampal slices." Molecular and cellular neurosciences **31**(1): 37-51.

Allison, D. W., A. S. Chervin, et al. (2000). "Postsynaptic scaffolds of excitatory and inhibitory synapses in hippocampal neurons: maintenance of core components independent of actin filaments and microtubules." J Neurosci **20**(12): 4545-4554.

Allison, D. W., V. I. Gelfand, et al. (1998). "Role of actin in anchoring postsynaptic receptors in cultured hippocampal neurons: differential attachment of NMDA versus AMPA receptors." J Neurosci **18**(7): 2423-2436.

Andersen, R., Y. Li, et al. (2005). "Calcium/calmodulin-dependent protein kinase II alters structural plasticity and cytoskeletal dynamics in Drosophila." The Journal of neuroscience : the official journal of the Society for Neuroscience **25**(39): 8878-8888.

Ashby, M. C., S. R. Maier, et al. (2006). "Lateral diffusion drives constitutive exchange of AMPA receptors at dendritic spines and is regulated by spine morphology." J Neurosci **26**(26): 7046-7055.

Bagal, A. A., J. P. Kao, et al. (2005). "Long-term potentiation of exogenous glutamate responses at single dendritic spines." Proc Natl Acad Sci U S A **102**(40): 14434-14439.

Band, A. M., H. Ali, et al. (2002). "Endogenous plasma membrane t-SNARE syntaxin 4 is present in rab11 positive endosomal membranes and associates with cortical actin cytoskeleton." FEBS Lett **531**(3): 513-519.

Barria, A., V. Derkach, et al. (1997). "Identification of the Ca2+/calmodulin-dependent protein kinase II regulatory phosphorylation site in the alpha-amino-3-hydroxyl-5-methyl-4-isoxazole-propionate-type glutamate receptor." The Journal of biological chemistry **272**(52): 32727-32730.

Barria, A., D. Muller, et al. (1997). "Regulatory phosphorylation of AMPA-type glutamate receptors by CaM-KII during long-term potentiation." Science **276**(5321): 2042-2045.

Bas Orth, C., C. Schultz, et al. (2007). "Loss of the cisternal organelle in the axon initial segment of cortical neurons in synaptopodin-deficient mice." The Journal of comparative neurology **504**(5): 441-449.

Bats, C., L. Groc, et al. (2007). "The interaction between Stargazin and PSD-95 regulates AMPA receptor surface trafficking." Neuron **53**(5): 719-734.

Belyantseva, I. A., B. J. Perrin, et al. (2009). "Gamma-actin is required for cytoskeletal maintenance but not development." Proceedings of the National Academy of Sciences of the United States of America **106**(24): 9703-9708.

Betzig, E., G. H. Patterson, et al. (2006). "Imaging Intracellular Fluorescent Proteins at Nanometer Resolution." Science **313**(5793): 1642-1645.

Biou, V., H. Brinkhaus, et al. (2008). "Interactions between drebrin and Ras regulate dendritic spine plasticity." The European journal of neuroscience **27**(11): 2847-2859.

Bittins, C. M., T. W. Eichler, et al. (2009). "Expression of the dominant-negative tail of myosin Va enhances exocytosis of large dense core vesicles in neurons." Cellular and molecular neurobiology **29**(4): 597-608.

Blanchoin, L., K. J. Amann, et al. (2000). "Direct observation of dendritic actin filament networks nucleated by Arp2/3 complex and WASP/Scar proteins." Nature **404**(6781): 1007-1011.

Blanchoin, L. and T. D. Pollard (2002). "Hydrolysis of ATP by polymerized actin depends on the bound divalent cation but not profilin." Biochemistry **41**(2): 597-602.

Blanpied, T. A., J. M. Kerr, et al. (2008). "Structural plasticity with preserved topology in the postsynaptic protein network." Proc Natl Acad Sci U S A **105**(34): 12587-12592.

Blanpied, T. A., D. B. Scott, et al. (2002). "Dynamics and regulation of clathrin coats at specialized endocytic zones of dendrites and spines." Neuron **36**(3): 435-449.

Blanpied, T. A., D. B. Scott, et al. (2002). "Regulation and dynamics of clathrin at specialized endocytic zones in dendrites and spines." Neuron **36**(3): 435-449.

Bloodgood, B. L. and B. L. Sabatini (2005). "Neuronal activity regulates diffusion across the neck of dendritic spines." Science **310**(5749): 866-869.

Borgdorff, A. J. and D. Choquet (2002). "Regulation of AMPA receptor lateral movements." Nature **417**(6889): 649-653.

Bramham, C. R. and D. G. Wells (2007). "Dendritic mRNA: transport, translation and function." Nat Rev Neurosci **8**(10): 776-789.

Bredt, D. S. and R. A. Nicoll (2003). "AMPA receptor trafficking at excitatory synapses." Neuron **40**(2): 361-379.

Caceres, A., M. R. Payne, et al. (1983). "Immunocytochemical Localization of Actin and Microtubule-Associated Protein MAP2 in Dendritic Spines." Proceedings of the National Academy of Sciences **80**(6): 1738-1742.

Cai, L., A. M. Makhov, et al. (2008). "Coronin 1B antagonizes cortactin and remodels Arp2/3-containing actin branches in lamellipodia." Cell **134**(5): 828-842.

Cai, L., T. W. Marshall, et al. (2007). "Coronin 1B coordinates Arp2/3 complex and cofilin activities at the leading edge." Cell **128**(5): 915-929.

Capani, F., M. E. Martone, et al. (2001). "Selective localization of high concentrations of F-actin in subpopulations of dendritic spines in rat central nervous system: a three-dimensional electron microscopic study." J Comp Neurol **435**(2): 156-170.

Carlier, M. F., V. Laurent, et al. (1997). "Actin depolymerizing factor (ADF/cofilin) enhances the rate of filament turnover: implication in actin-based motility." The Journal of cell biology **136**(6): 1307-1322.

Carlier, M. F. and D. Pantaloni (1986). "Direct evidence for ADP-Pi-F-actin as the major intermediate in ATP-actin polymerization. Rate of dissociation of Pi from actin filaments." Biochemistry **25**(24): 7789-7792.

Carlisle, H. J., P. Manzerra, et al. (2008). "SynGAP regulates steady-state and activity-dependent phosphorylation of cofilin." The Journal of neuroscience : the official journal of the Society for Neuroscience **28**(50): 13673-13683.

Carlsson, L., L. E. Nystrom, et al. (1977). "Actin polymerizability is influenced by profilin, a low molecular weight protein in non-muscle cells." Journal of molecular biology **115**(3): 465-483.

Chen, X., L. Vinade, et al. (2005). "Mass of the postsynaptic density and enumeration of three key molecules." Proc Natl Acad Sci U S A **102**(32): 11551-11556.

Chesarone, M. A., A. G. DuPage, et al. (2010). "Unleashing formins to remodel the actin and microtubule cytoskeletons." Nature reviews. Molecular cell biology **11**(1): 62-74.

Chesarone, M. A. and B. L. Goode (2009). "Actin nucleation and elongation factors: mechanisms and interplay." Current opinion in cell biology **21**(1): 28-37.

Chhabra, E. S. and H. N. Higgs (2007). "The many faces of actin: matching assembly factors with cellular structures." Nature cell biology **9**(10): 1110-1121.

Cingolani, L. A. and Y. Goda (2008). "Actin in action: the interplay between the actin cytoskeleton and synaptic efficacy." Nat Rev Neurosci **9**(5): 344-356.

Correia, S. S., S. Bassani, et al. (2008). "Motor protein-dependent transport of AMPA receptors into spines during long-term potentiation." Nat Neurosci **11**(4): 457-466.

Danuser, G. and C. M. Waterman-Storer (2006). "Quantitative fluorescent speckle microscopy of cytoskeleton dynamics." Annu Rev Biophys Biomol Struct **35**: 361-387.

de Hostos, E. L., B. Bradtke, et al. (1991). "Coronin, an actin binding protein of Dictyostelium discoideum localized to cell surface projections, has sequence similarities to G protein beta subunits." The EMBO journal **10**(13): 4097-4104.

Dell'Acqua, M. L., K. E. Smith, et al. (2006). "Regulation of neuronal PKA signaling through AKAP targeting dynamics." European Journal Of Cell Biology **85**(7): 627-633.

Deller, T., M. Korte, et al. (2003). "Synaptopodin-deficient mice lack a spine apparatus and show deficits in synaptic plasticity." Proc Natl Acad Sci U S A **100**(18): 10494-10499.

Deller, T., C. B. Orth, et al. (2007). "A role for synaptopodin and the spine apparatus in hippocampal synaptic plasticity." Ann Anat **189**(1): 5-16.

Ding, J. B., K. T. Takasaki, et al. (2009). "Supraresolution imaging in brain slices using stimulated-emission depletion two-photon laser scanning microscopy." Neuron **63**(4): 429-437.

Ehlers, M. D., M. Heine, et al. (2007). "Diffusional trapping of GluR1 AMPA receptors by input-specific synaptic activity." Neuron **54**(3): 447-460.

Ehrlich, I., M. Klein, et al. (2007). "PSD-95 is required for activity-driven synapse stabilization." Proc Natl Acad Sci U S A **104**(10): 4176-4181.

Ehrlich, I. and R. Malinow (2004). "Postsynaptic density 95 controls AMPA receptor incorporation during long-term potentiation and experience-driven synaptic plasticity." J Neurosci **24**(4): 916-927.

Emptage, N., T. V. Bliss, et al. (1999). "Single synaptic events evoke NMDA receptor-mediated release of calcium from internal stores in hippocampal dendritic spines." Neuron **22**(1): 115-124.

Engqvist-Goldstein, A. E. and D. G. Drubin (2003). "Actin Assembly and Endocytosis: From Yeast to Mammals." Annu Rev Cell Dev Biol **19**: 287-332.

Esteban, J. A., S. H. Shi, et al. (2003). "PKA phosphorylation of AMPA receptor subunits controls synaptic trafficking underlying plasticity." Nat Neurosci **6**(2): 136-143.

Fifkova, E. and R. J. Delay (1982). "Cytoplasmic actin in neuronal processes as a possible mediator of synaptic plasticity." J Cell Biol **95**(1): 345-350.

Fink, C. C., K. U. Bayer, et al. (2003). "Selective regulation of neurite extension and synapse formation by the beta but not the alpha isoform of CaMKII." Neuron **39**(2): 283-297.

Fischer, M., S. Kaech, et al. (1998). "Rapid actin-based plasticity in dendritic spines." Neuron **20**(5): 847-854.

Fischer, M., S. Kaech, et al. (2000). "Glutamate receptors regulate actin-based plasticity in dendritic spines." Nat Neurosci **3**(9): 887-894.

Frischknecht, R., M. Heine, et al. (2009). "Brain extracellular matrix affects AMPA receptor lateral mobility and short-term synaptic plasticity." Nat Neurosci **12**(7): 897-904.

Frost, N. A. and T. A. Blanpied (2008). "Spatial organization of actin polymerization within single dendritic spines." Soc Neurosci Abs.

Frost, N. A., H. Shroff, et al. (2010). "Single-molecule discrimination of discrete perisynaptic and distributed sites of actin filament assembly within dendritic spines." Neuron **67**(1): 86-99.

Fukazawa, Y., Y. Saitoh, et al. (2003). "Hippocampal LTP Is Accompanied by Enhanced F-Actin Content within the Dendritic Spine that Is Essential for Late LTP Maintenance In Vivo." Neuron **38**(3): 447-460.

Fukunaga, K., D. Muller, et al. (1995). "Increased phosphorylation of Ca2+/calmodulin-dependent protein kinase II and its endogenous substrates in the induction of long-term potentiation." The Journal of biological chemistry **270**(11): 6119-6124.

Fukunaga, K., L. Stoppini, et al. (1993). "Long-term potentiation is associated with an increased activity of Ca2+/calmodulin-dependent protein kinase II." The Journal of biological chemistry **268**(11): 7863-7867.

Galbraith, C. G., K. M. Yamada, et al. (2007). "Polymerizing actin fibers position integrins primed to probe for adhesion sites." Science **315**(5814): 992-995.

Ghosh, M., X. Song, et al. (2004). "Cofilin promotes actin polymerization and defines the direction of cell motility." Science **304**(5671): 743-746.

Goldschmidt-Clermont, P. J., M. I. Furman, et al. (1992). "The control of actin nucleotide exchange by thymosin beta 4 and profilin. A potential regulatory mechanism for actin polymerization in cells." Molecular biology of the cell **3**(9): 1015-1024.

Goldschmidt-Clermont, P. J., L. M. Machesky, et al. (1990). "The actin-binding protein profilin binds to PIP2 and inhibits its hydrolysis by phospholipase C." Science **247**(4950): 1575-1578.

Gray, N. W., R. M. Weimer, et al. (2006). "Rapid Redistribution of Synaptic PSD-95 in the Neocortex In Vivo." PLoS Biol **4**(11).

Greenfield, D., A. L. McEvoy, et al. (2009). "Self-organization of the Escherichia coli chemotaxis network imaged with super-resolution light microscopy." PLoS biology **7**(6): e1000137.

Gu, J., C. W. Lee, et al. (2010). "ADF/cofilin-mediated actin dynamics regulate AMPA receptor trafficking during synaptic plasticity." Nature neuroscience **13**(10): 1208-1215.

Haeckel, A., R. Ahuja, et al. (2008). "The actin-binding protein Abp1 controls dendritic spine morphology and is important for spine head and synapse formation." J Neurosci **28**(40): 10031-10044.

Harris, K. M. and J. K. Stevens (1988). "Dendritic spines of rat cerebellar Purkinje cells: serial electron microscopy with reference to their biophysical characteristics." J Neurosci **8**(12): 4455-4469.

Harris, K. M. and J. K. Stevens (1989). "Dendritic spines of CA 1 pyramidal cells in the rat hippocampus: serial electron microscopy with reference to their biophysical characteristics." J Neurosci **9**(8): 2982-2997.

Harvey, C. D. and K. Svoboda (2007). "Locally dynamic synaptic learning rules in pyramidal neuron dendrites." Nature **450**(7173): 1195.

Harvey, C. D., R. Yasuda, et al. (2008). "The spread of Ras activity triggered by activation of a single dendritic spine." Science **321**(5885): 136-140.

Hasse, A., A. Rosentreter, et al. (2005). "Coronin 3 and its role in murine brain morphogenesis." Eur J Neurosci **21**(5): 1155-1168.

Hasson, T. (2003). "Myosin VI: two distinct roles in endocytosis." J Cell Sci **116**(Pt 17): 3453-3461.

Hayashi, K., R. Ishikawa, et al. (1996). "Modulatory Role of Drebrin on the Cytoskeleton within Dendritic Spines in the Rat Cerebral Cortex." J. Neurosci. **16**(22): 7161-7170.

Hayashi, K. and T. Shirao (1999). "Change in the Shape of Dendritic Spines Caused by Overexpression of Drebrin in Cultured Cortical Neurons." J. Neurosci. **19**(10): 3918-3925.

Hayashi, Y., S. H. Shi, et al. (2000). "Driving AMPA receptors into synapses by LTP and CaMKII: requirement for GluR1 and PDZ domain interaction." Science **287**(5461): 2262-2267.

Heine, M., L. Groc, et al. (2008). "Surface mobility of postsynaptic AMPARs tunes synaptic transmission." Science **320**(5873): 201-205.

Hering, H. and M. Sheng (2003). "Activity-dependent redistribution and essential role of cortactin in dendritic spine morphogenesis." J Neurosci **23**(37): 11759-11769.

Hess, S. T., T. P. Girirajan, et al. (2006). "Ultra-high resolution imaging by fluorescence photoactivation localization microscopy." Biophys J **91**(11): 4258-4272.

Hess, S. T., T. J. Gould, et al. (2007). "Dynamic clustered distribution of hemagglutinin resolved at 40 nm in living cell membranes discriminates between raft theories." Proc Natl Acad Sci U S A **104**(44): 17370-17375.

Higashida, C., T. Miyoshi, et al. (2004). "Actin Polymerization-Driven Molecular Movement of mDia1 in Living Cells." Science **303**(5666): 2007 - 2010.

Honkura, N., M. Matsuzaki, et al. (2008). "The subspine organization of actin fibers regulates the structure and plasticity of dendritic spines." Neuron **57**(5): 719-729.

Horne, E. A. and M. L. Dell'Acqua (2007). "Phospholipase C is required for changes in postsynaptic structure and function associated with NMDA receptor-dependent long-term depression." The Journal of neuroscience : the official journal of the Society for Neuroscience **27**(13): 3523-3534.

Hotulainen, P. and C. C. Hoogenraad (2010). "Actin in dendritic spines: connecting dynamics to function." J. Cell Biol. **xx**: xxx-yyy.

Hotulainen, P. and P. Lappalainen (2006). "Stress fibers are generated by two distinct actin assembly mechanisms in motile cells." The Journal of cell biology **173**(3): 383-394.

Hotulainen, P., O. Llano, et al. (2009). "Defining mechanisms of actin polymerization and depolymerization during dendritic spine morphogenesis." J Cell Biol **185**(2): 323-339.

Ishikawa, R., K. Hayashi, et al. (1994). "Drebrin, a development-associated brain protein from rat embryo, causes the dissociation of tropomyosin from actin filaments." The Journal of biological chemistry **269**(47): 29928-29933.

Jewell, J. L., W. Luo, et al. (2008). "Filamentous actin regulates insulin exocytosis through direct interaction with Syntaxin 4." J Biol Chem **283**(16): 10716-10726.

Jourdain, P., K. Fukunaga, et al. (2003). "Calcium/calmodulin-dependent protein kinase II contributes to activity-dependent filopodia growth and spine formation." The Journal of neuroscience : the official journal of the Society for Neuroscience **23**(33): 10645-10649.

Kaech, S., M. Fischer, et al. (1997). "Isoform specificity in the relationship of actin to dendritic spines." The Journal of neuroscience : the official journal of the Society for Neuroscience **17**(24): 9565-9572.

Kaksonen, M., C. P. Toret, et al. (2006). "Harnessing actin dynamics for clathrin-mediated endocytosis." Nat Rev Mol Cell Biol **7**(6): 404-414.

Kennedy, M. J., I. G. Davidson, et al. (2010). "Syntaxin-4 Defines a Domain for Activity-Dependent Exocytosis in Dendritic Spines." Cell **141**(3): 524-535.

Kessels, M. M., A. E. Engqvist-Goldstein, et al. (2001). "Mammalian Abp1, a signal-responsive F-actin-binding protein, links the actin cytoskeleton to endocytosis via the GTPase dynamin." J Cell Biol **153**(2): 351-366.

Kida, Y. S., T. Sato, et al. (2007). "Daam1 regulates the endocytosis of EphB during the convergent extension of the zebrafish notochord." Proceedings of the National Academy of Sciences of the United States of America **104**(16): 6708-6713.

Kim, C. H. and J. E. Lisman (1999). "A role of actin filament in synaptic transmission and long-term potentiation." J Neurosci **19**(11): 4314-4324.

Kim, Y., J. Y. Sung, et al. (2006). "Phosphorylation of WAVE1 regulates actin polymerization and dendritic spine morphology." Nature **442**(7104): 814-817.

Kolodziej, S. J., A. Hudmon, et al. (2000). "Three-dimensional reconstructions of calcium/calmodulin-dependent (CaM) kinase IIalpha and truncated CaM kinase IIalpha reveal a unique organization for its structural core and functional domains." The Journal of biological chemistry **275**(19): 14354-14359.

Kopec, C. D., E. Real, et al. (2007). "GluR1 links structural and functional plasticity at excitatory synapses." J Neurosci **27**(50): 13706-13718.

Korobova, F. and T. Svitkina (2009). "Molecular Architecture of Synaptic Actin Cytoskeleton in Hippocampal Neurons Reveals a Mechanism of Dendritic Spine Morphogenesis." Mol Biol Cell.

Krementsov, D. N., E. B. Krementsova, et al. (2004). "Myosin V: regulation by calcium, calmodulin, and the tail domain." The Journal of cell biology **164**(6): 877-886.

Kremerskothen, J., C. Plaas, et al. (2005). "Synaptopodin, a molecule involved in the formation of the dendritic spine apparatus, is a dual actin/alpha-actinin binding protein." J Neurochem **92**(3): 597-606.

Krucker, T., G. R. Siggins, et al. (2000). "Dynamic actin filaments are required for stable long-term potentiation (LTP) in area CA1 of the hippocampus." Proc Natl Acad Sci U S A **97**(12): 6856-6861.

Kueh, H. Y. and T. J. Mitchison (2009). "Structural plasticity in actin and tubulin polymer dynamics." Science **325**(5943): 960-963.

Kuriu, T., A. Inoue, et al. (2006). "Differential Control of Postsynaptic Density Scaffolds via Actin-Dependent and -Independent Mechanisms." J. Neurosci. **26**(29): 7693-7706.

Landis, D. M. and T. S. Reese (1983). "Cytoplasmic organization in cerebellar dendritic spines." J Cell Biol **97**(4): 1169-1178.

Lee, H. K., M. Barbarosie, et al. (2000). "Regulation of distinct AMPA receptor phosphorylation sites during bidirectional synaptic plasticity." Nature **405**(6789): 955-959.

Lee, M. C., R. Yasuda, et al. (2010). "Metaplasticity at single glutamatergic synapses." Neuron **66**(6): 859-870.

Lee, S. J., Y. Escobedo-Lozoya, et al. (2009). "Activation of CaMKII in single dendritic spines during long-term potentiation." Nature **458**(7236): 299-304.

Lee, S. J. and R. Yasuda (2009). "Spatiotemporal Regulation of Signaling in and out of Dendritic Spines: CaMKII and Ras." The open neuroscience journal **3**: 117-127.

Li, X. D., H. S. Jung, et al. (2006). "The globular tail domain of myosin Va functions as an inhibitor of the myosin Va motor." The Journal of biological chemistry **281**(31): 21789-21798.

Lin, D. T., Y. Makino, et al. (2009). "Regulation of AMPA receptor extrasynaptic insertion by 4.1N, phosphorylation and palmitoylation." Nat Neurosci **12**(7): 879-887.

Lin, Y. C. and L. Redmond (2008). "CaMKIIbeta binding to stable F-actin in vivo regulates F-actin filament stability." Proc Natl Acad Sci U S A **105**(41): 15791-15796.

Lise, M. F., D. P. Srivastava, et al. (2009). "Myosin-Va-interacting protein, RILPL2, controls cell shape and neuronal morphogenesis via Rac signaling." J Cell Sci **122**(Pt 20): 3810-3821.

Lisman, J., H. Schulman, et al. (2002). "The molecular basis of CaMKII function in synaptic and behavioural memory." Nat Rev Neurosci **3**(3): 175-190.

Lisman, J. E. (1985). "A mechanism for memory storage insensitive to molecular turnover: a bistable autophosphorylating kinase." Proc Natl Acad Sci U S A **82**(9): 3055-3057.

Lisman, J. E. and A. M. Zhabotinsky (2001). "A model of synaptic memory: a CaMKII/PP1 switch that potentiates transmission by organizing an AMPA receptor anchoring assembly." Neuron **31**(2): 191-201.

Liu, G., S. Choi, et al. (1999). "Variability of neurotransmitter concentration and nonsaturation of postsynaptic AMPA receptors at synapses in hippocampal cultures and slices." Neuron **22**(2): 395-409.

Loisel, T. P., R. Boujemaa, et al. (1999). "Reconstitution of actin-based motility of Listeria and Shigella using pure proteins." Nature **401**(6753): 613-616.

Low, S. H., A. Vasanji, et al. (2006). "Syntaxins 3 and 4 are concentrated in separate clusters on the plasma membrane before the establishment of cell polarity." Mol Biol Cell **17**(2): 977-989.

Lu, J., T. D. Helton, et al. (2007). "Postsynaptic positioning of endocytic zones and AMPA receptor cycling by physical coupling of dynamin-3 to homer." Neuron **55**(6): 874-889.

Lynch, G., J. Larson, et al. (1983). "Intracellular injections of EGTA block induction of hippocampal long-term potentiation." Nature **305**(5936): 719-721.

Ma, L., R. Rohatgi, et al. (1998). "The Arp2/3 complex mediates actin polymerization induced by the small GTP-binding protein Cdc42." Proceedings of the National Academy of Sciences of the United States of America **95**(26): 15362-15367.

MacAskill, A. F. and J. T. Kittler (2010). "Control of mitochondrial transport and localization in neurons." Trends Cell Biol **20**(2): 102-112.

Machesky, L. M., S. J. Atkinson, et al. (1994). "Purification of a cortical complex containing two unconventional actins from Acanthamoeba by affinity chromatography on profilin-agarose." The Journal of cell biology **127**(1): 107-115.

Majewska, A., A. Tashiro, et al. (2000). "Regulation of spine calcium dynamics by rapid spine motility." J Neurosci **20**(22): 8262-8268.

Makino, H. and R. Malinow (2009). "AMPA receptor incorporation into synapses during LTP: the role of lateral movement and exocytosis." Neuron **64**(3): 381-390.

Malenka, R. C. and M. F. Bear (2004). "LTP and LTD: an embarrassment of riches." Neuron **44**(1): 5-21.

Malenka, R. C., J. A. Kauer, et al. (1989). "An essential role for postsynaptic calmodulin and protein kinase activity in long-term potentiation." Nature **340**(6234): 554-557.

Malinow, R., H. Schulman, et al. (1989). "Inhibition of postsynaptic PKC or CaMKII blocks induction but not expression of LTP." Science **245**(4920): 862-866.

Malinow, R. and R. W. Tsien (1990). "Identifying and localizing protein kinases necessary for LTP." Adv Exp Med Biol **268**: 301-305.

Malinow, R. and R. W. Tsien (1991). "Long-term potentiation: postsynaptic activation of Ca(2+)-dependent protein kinases with subsequent presynaptic enhancement." Prog Brain Res **89**: 271-289.

Malleret, G., J. M. Alarcon, et al. (2010). "Bidirectional regulation of hippocampal long-term synaptic plasticity and its influence on opposing forms of memory." The Journal of neuroscience : the official journal of the Society for Neuroscience **30**(10): 3813-3825.

Mammoto, A., T. Sasaki, et al. (1998). "Interactions of drebrin and gephyrin with profilin." Biochemical and biophysical research communications **243**(1): 86-89.

Maniak, M., R. Rauchenberger, et al. (1995). "Coronin involved in phagocytosis: dynamics of particle-induced relocalization visualized by a green fluorescent protein Tag." Cell **83**(6): 915-924.

Manley, S., J. M. Gillette, et al. (2008). "High-density mapping of single-molecule trajectories with photoactivated localization microscopy." Nat Methods **5**(2): 155-157.

Matsuda, K., S. Matsuda, et al. (2006). "Characterization of the delta2 glutamate receptor-binding protein delphilin: Splicing variants with differential

palmitoylation and an additional PDZ domain." The Journal of biological chemistry **281**(35): 25577-25587.
Matsuda, S., K. Matsuda, et al. (2006). "A new motif necessary and sufficient for stable localization of the delta2 glutamate receptors at postsynaptic spines." The Journal of biological chemistry **281**(25): 17501-17509.
Matsuzaki, M., N. Honkura, et al. (2004). "Structural basis of long-term potentiation in single dendritic spines." Nature **429**(6993): 761-766.
Matus, A. (2000). "Actin-based plasticity in dendritic spines." Science **290**(5492): 754-758.
McAllister, A. K. and C. F. Stevens (2000). "Nonsaturation of AMPA and NMDA receptors at hippocampal synapses." PNAS **97**(11): 6173-6178.
McKinney, S. A., C. S. Murphy, et al. (2009). "A bright and photostable photoconvertible fluorescent protein." Nat Methods **6**(2): 131-133.
Medeiros, N. A., D. T. Burnette, et al. (2006). "Myosin II functions in actin-bundle turnover in neuronal growth cones." Nat Cell Biol **8**: 216-226.
Menetrey, J., A. Bahloul, et al. (2005). "The structure of the myosin VI motor reveals the mechanism of directionality reversal." Nature **435**(7043): 779-785.
Meng, Y., Y. Zhang, et al. (2002). "Abnormal spine morphology and enhanced LTP in LIMK-1 knockout mice." Neuron **35**(1): 121-133.
Merrifield, C. J., M. E. Feldman, et al. (2002). "Imaging actin and dynamin recruitment during invagination of single clathrin-coated pits." Nat Cell Biol **4**(9): 691-698.
Merrill, M. A., Z. Malik, et al. (2007). "Displacement of alpha-actinin from the NMDA receptor NR1 C0 domain By Ca2+/calmodulin promotes CaMKII binding." Biochemistry **46**(29): 8485-8497.
Miki, H. and T. Takenawa (2003). "Regulation of actin dynamics by WASP family proteins." Journal of biochemistry **134**(3): 309-313.
Miller, P., A. M. Zhabotinsky, et al. (2005). "The stability of a stochastic CaMKII switch: dependence on the number of enzyme molecules and protein turnover." PLoS Biol **3**(4): e107.
Minerbi, A., R. Kahana, et al. (2009). "Long-term relationships between synaptic tenacity, synaptic remodeling, and network activity." PLoS Biol **7**(6): e1000136.
Miyagi, Y., T. Yamashita, et al. (2002). "Delphilin: a novel PDZ and formin homology domain-containing protein that synaptically colocalizes and interacts with glutamate receptor delta 2 subunit." J Neurosci **22**(3): 803-814.
Morin, M., K. E. Bryan, et al. (2009). "In vivo and in vitro effects of two novel gamma-actin (ACTG1) mutations that cause DFNA20/26 hearing impairment." Human molecular genetics **18**(16): 3075-3089.
Morishita, W., H. Marie, et al. (2005). "Distinct triggering and expression mechanisms underlie LTD of AMPA and NMDA synaptic responses." Nat Neurosci **8**(8): 1043-1050.
Nagerl, U. V., K. I. Willig, et al. (2008). "Live-cell imaging of dendritic spines by STED microscopy." Proc Natl Acad Sci U S A **105**(48): 18982-18987.
Naisbitt, S., E. Kim, et al. (1999). "Shank, a novel family of postsynaptic density proteins that binds to the NMDA receptor/PSD-95/GKAP complex and cortactin." Neuron **23**(3): 569-582.

Naisbitt, S., J. Valtschanoff, et al. (2000). "Interaction of the postsynaptic density-95/guanylate kinase domain-associated protein complex with a light chain of myosin-V and dynein." J Neurosci **20**(12): 4524-4534.

Nakagawa, T., J. A. Engler, et al. (2004). "The dynamic turnover and functional roles of alpha-actinin in dendritic spines." Neuropharmacology **47**(5): 734-745.

Neuhoff, H., M. Sassoe-Pognetto, et al. (2005). "The actin-binding protein profilin I is localized at synaptic sites in an activity-regulated manner." Eur J Neurosci **21**(1): 15-25.

Newpher, T. M. and M. D. Ehlers (2009). "Spine microdomains for postsynaptic signaling and plasticity." Trends Cell Biol.

Nolen, B. J., N. Tomasevic, et al. (2009). "Characterization of two classes of small molecule inhibitors of Arp2/3 complex." Nature **460**(7258): 1031-1034.

O'Leary, H., E. Lasda, et al. (2006). "CaMKIIbeta association with the actin cytoskeleton is regulated by alternative splicing." Molecular biology of the cell **17**(11): 4656-4665.

Okamoto, K., M. Bosch, et al. (2009). "The roles of CaMKII and F-actin in the structural plasticity of dendritic spines: a potential molecular identity of a synaptic tag?" Physiology (Bethesda) **24**: 357-366.

Okamoto, K., T. Nagai, et al. (2004). "Rapid and persistent modulation of actin dynamics regulates postsynaptic reorganization underlying bidirectional plasticity." Nat Neurosci **7**(10): 1104-1112.

Okamoto, K., R. Narayanan, et al. (2007). "The role of CaMKII as an F-actin-bundling protein crucial for maintenance of dendritic spine structure." Proc Natl Acad Sci U S A **104**(15): 6418-6423.

Opazo, P., S. Labrecque, et al. (2010). "CaMKII triggers the diffusional trapping of surface AMPARs through phosphorylation of stargazin." Neuron **67**(2): 239-252.

Osterweil, E., D. G. Wells, et al. (2005). "A role for myosin VI in postsynaptic structure and glutamate receptor endocytosis." J Cell Biol **168**(2): 329-338.

Otmakhov, N., L. C. Griffith, et al. (1997). "Postsynaptic inhibitors of calcium/calmodulin-dependent protein kinase type II block induction but not maintenance of pairing-induced long-term potentiation." J Neurosci **17**(14): 5357-5365.

Pak, D. T., S. Yang, et al. (2001). "Regulation of dendritic spine morphology by SPAR, a PSD-95-associated RapGAP." Neuron **31**(2): 289-303.

Pantaloni, D., R. Boujemaa, et al. (2000). "The Arp2/3 complex branches filament barbed ends: functional antagonism with capping proteins." Nat Cell Biol **2**(7): 385-391.

Park, M., E. C. Penick, et al. (2004). "Recycling endosomes supply AMPA receptors for LTP." Science **305**(5692): 1972-1975.

Park, M., J. M. Salgado, et al. (2006). "Plasticity-induced growth of dendritic spines by exocytic trafficking from recycling endosomes." Neuron **52**(5): 817-830.

Patterson, G. H. and J. Lippincott-Schwartz (2002). "A photoactivatable GFP for selective photolabeling of proteins and cells." Science **297**(5588): 1873-1877.

Penzes, P., M. E. Cahill, et al. (2008). "Convergent CaMK and RacGEF signals control dendritic structure and function." Trends Cell Biol **18**(9): 405-413.

Petersen, J. D., X. Chen, et al. (2003). "Distribution of postsynaptic density (PSD)-95 and Ca2+/calmodulin-dependent protein kinase II at the PSD." J Neurosci **23**(35): 11270-11278.

Petralia, R. S., Y.-X. Wang, et al. (2001). "Glutamate receptor targeting in the postsynaptic spine involves mechanisms that are independent of myosin Va." European Journal of Neuroscience **13**(9): 1722-1732.

Pollard, T. D. and G. G. Borisy (2003). "Cellular motility driven by assembly and disassembly of actin filaments." Cell **112**(4): 453-465.

Quinlan, M. E., J. E. Heuser, et al. (2005). "Drosophila Spire is an actin nucleation factor." Nature **433**(7024): 382-388.

Racz, B., T. A. Blanpied, et al. (2004). "Lateral organization of endocytic machinery in dendritic spines." Nat Neurosci **7**(9): 917-918.

Racz, B. and R. J. Weinberg (2004). "The subcellular organization of cortactin in hippocampus." J Neurosci **24**(46): 10310-10317.

Racz, B. and R. J. Weinberg (2006). "Spatial organization of cofilin in dendritic spines." Neuroscience **138**(2): 447.

Racz, B. and R. J. Weinberg (2008). "Organization of the Arp2/3 complex in hippocampal spines." J Neurosci **28**(22): 5654-5659.

Raghavachari, S. and J. E. Lisman (2004). "Properties of quantal transmission at CA1 synapses." J Neurophysiol **92**(4): 2456-2467.

Reisler, E. and E. H. Egelman (2007). "Actin structure and function: what we still do not understand." The Journal of biological chemistry **282**(50): 36133-36137.

Renner, M., D. Choquet, et al. (2009). "Control of the postsynaptic membrane viscosity." J Neurosci **29**(9): 2926-2937.

Rex, C. S., L. Y. Chen, et al. (2009). "Different Rho GTPase-dependent signaling pathways initiate sequential steps in the consolidation of long-term potentiation." J Cell Biol **186**(1): 85-97.

Richards, D. A., V. De Paola, et al. (2004). "AMPA-receptor activation regulates the diffusion of a membrane marker in parallel with dendritic spine motility in the mouse hippocampus." J Physiol **558**(Pt 2): 503-512.

Rizzo, M. A., G. H. Springer, et al. (2004). "An improved cyan fluorescent protein variant useful for FRET." **22**(4): 445-449.

Rocca, D. L., S. Martin, et al. (2008). "Inhibition of Arp2/3-mediated actin polymerization by PICK1 regulates neuronal morphology and AMPA receptor endocytosis." Nat Cell Biol **10**(3): 259-271.

Rohatgi, R., L. Ma, et al. (1999). "The interaction between N-WASP and the Arp2/3 complex links Cdc42-dependent signals to actin assembly." Cell **97**(2): 221-231.

Rosenmund, C. and G. L. Westbrook (1993). "Rundown of N-methyl-D-aspartate channels during whole-cell recording in rat hippocampal neurons: role of Ca2+ and ATP." J Physiol **470**: 705-729.

Rostaing, P., E. Real, et al. (2006). "Analysis of synaptic ultrastructure without fixative using high-pressure freezing and tomography." Eur J Neurosci **24**(12): 3463-3474.

Ryu, J., L. Liu, et al. (2006). "A critical role for myosin IIb in dendritic spine morphology and synaptic function." Neuron **49**(2): 175-182.

Sako, Y., S. Minoghchi, et al. (2000). "Single-molecule imaging of EGFR signalling on the surface of living cells." Nat Cell Biol **2**(3): 168-172.
Salomon, S. N., M. Haber, et al. (2008). "Localization of the Diaphanous-related formin Daam1 to neuronal dendrites." Neuroscience letters **447**(1): 62-67.
Sanabria, H., M. T. Swulius, et al. (2009). "{beta}CaMKII regulates actin assembly and structure." The Journal of biological chemistry **284**(15): 9770-9780.
Santamaria, F., J. Gonzalez, et al. (2010). "Quantifying the effects of elastic collisions and non-covalent binding on glutamate receptor trafficking in the post-synaptic density." PLoS Comput Biol **6**(5): e1000780.
Santamaria, F., S. Wils, et al. (2006). "Anomalous diffusion in Purkinje cell dendrites caused by spines." Neuron **52**(4): 635-648.
Saxton, M. J. (1993). "Lateral diffusion in an archipelago. Single-particle diffusion." Biophysical journal **64**(6): 1766-1780.
Saxton, M. J. and K. Jacobson (1997). "Single-particle tracking: Applications to membrane dynamics." Annual Review of Biophysics and Biomolecular Structure **26**(1): 373-399.
Schaefer, A. W., N. Kabir, et al. (2002). "Filopodia and actin arcs guide the assembly and transport of two populations of microtubules with unique dynamic parameters in neuronal growth cones." J Cell Biol **158**(1): 139-152.
Schonichen, A. and M. Geyer (2010). "Fifteen formins for an actin filament: a molecular view on the regulation of human formins." Biochimica et biophysica acta **1803**(2): 152-163.
Schumacher, N., J. M. Borawski, et al. (2004). "Overlapping expression pattern of the actin organizers Spir-1 and formin-2 in the developing mouse nervous system and the adult brain." Gene Expr Patterns **4**(3): 249-255.
Sdrulla, A. D. and D. J. Linden (2007). "Double dissociation between long-term depression and dendritic spine morphology in cerebellar Purkinje cells." Nat Neurosci **10**(5): 546-548.
Shen, K. and T. Meyer (1999). "Dynamic control of CaMKII translocation and localization in hippocampal neurons by NMDA receptor stimulation." Science **284**(5411): 162-166.
Shi, Y. and I. M. Ethell (2006). "Integrins control dendritic spine plasticity in hippocampal neurons through NMDA receptor and Ca2+/calmodulin-dependent protein kinase II-mediated actin reorganization." The Journal of neuroscience : the official journal of the Society for Neuroscience **26**(6): 1813-1822.
Shroff, H., C. G. Galbraith, et al. (2008). "Live-cell photoactivated localization microscopy of nanoscale adhesion dynamics." Nat Methods **5**(5): 417-423.
Shroff, H., C. G. Galbraith, et al. (2007). "Dual-color superresolution imaging of genetically expressed probes within individual adhesion complexes." Proc Natl Acad Sci U S A **104**(51): 20308-20313.
Shtengel, G., J. A. Galbraith, et al. (2009). "Interferometric fluorescent super-resolution microscopy resolves 3D cellular ultrastructure." Proceedings of the National Academy of Sciences of the United States of America **106**(9): 3125-3130.
Sjoblom, B., A. Salmazo, et al. (2008). "Alpha-actinin structure and regulation." Cellular and molecular life sciences : CMLS **65**(17): 2688-2701.

Sonoda, T., C. Mochizuki, et al. (2006). "Binding of glutamate receptor delta2 to its scaffold protein, Delphilin, is regulated by PKA." Biochemical and biophysical research communications **350**(3): 748-752.

Spacek, J. (1985). "Three-dimensional analysis of dendritic spines. II. Spine apparatus and other cytoplasmic components." Anat Embryol (Berl) **171**(2): 235-243.

Spacek, J. and K. M. Harris (1997). "Three-dimensional organization of smooth endoplasmic reticulum in hippocampal CA1 dendrites and dendritic spines of the immature and mature rat." J Neurosci **17**(1): 190-203.

Star, E. N., D. J. Kwiatkowski, et al. (2002). "Rapid turnover of actin in dendritic spines and its regulation by activity." Nat Neurosci **5**(3): 239-246.

Subach, F. V., G. H. Patterson, et al. (2009). "Photoactivatable mCherry for high-resolution two-color fluorescence microscopy." Nat Methods **6**(2): 153-159.

Svitkina, T. M. and G. G. Borisy (1999). "Arp2/3 complex and actin depolymerizing factor/cofilin in dendritic organization and treadmilling of actin filament array in lamellipodia." The Journal of cell biology **145**(5): 1009-1026.

Svitkina, T. M., E. A. Bulanova, et al. (2003). "Mechanism of filopodia initiation by reorganization of a dendritic network." The Journal of cell biology **160**(3): 409-421.

Svoboda, K., D. W. Tank, et al. (1996). "Direct measurement of coupling between dendritic spines and shafts." Science **272**(5262): 716-719.

Tada, T. and M. Sheng (2006). "Molecular mechanisms of dendritic spine morphogenesis." Curr Opin Neurobiol **16**(1): 95-101.

Takagishi, Y. and Y. Murata (2006). "Myosin Va mutation in rats is an animal model for the human hereditary neurological disease, Griscelli syndrome type 1." Annals of the New York Academy of Sciences **1086**: 66-80.

Takahashi, H., Y. Sekino, et al. (2003). "Drebrin-Dependent Actin Clustering in Dendritic Filopodia Governs Synaptic Targeting of Postsynaptic Density-95 and Dendritic Spine Morphogenesis." J. Neurosci. **23**(16): 6586-6595.

Tardin, C., L. Cognet, et al. (2003). "Direct imaging of lateral movements of AMPA receptors inside synapses." Embo J **22**(18): 4656-4665.

Tatavarty, V., E. J. Kim, et al. (2009). "Investigating sub-spine actin dynamics in rat hippocampal neurons with super-resolution optical imaging." PLoS One **4**(11): e7724.

Tehrani, S., N. Tomasevic, et al. (2007). "Src phosphorylation of cortactin enhances actin assembly." Proc Natl Acad Sci U S A **104**(29): 11933-11938.

Terry-Lorenzo, R. T., D. W. Roadcap, et al. (2005). "Neurabin/Protein phosphatase-1 complex regulates dendritic spine morphogenesis and maturation." Mol Biol Cell **16**(5): 2349-2362.

Thompson, R. E., D. R. Larson, et al. (2002). "Precise nanometer localization analysis for individual fluorescent probes." Biophys J **82**(5): 2775-2783.

Triller, A. and D. Choquet (2008). "New concepts in synaptic biology derived from single-molecule imaging." Neuron **59**(3): 359-374.

Tsuriel, S., R. Geva, et al. (2006). "Local sharing as a predominant determinant of synaptic matrix molecular dynamics." PLoS Biol **4**(9): e271.

Uetrecht, A. C. and J. E. Bear (2006). "Coronins: the return of the crown." Trends in cell biology **16**(8): 421-426.

Urban, E., S. Jacob, et al. (2010). "Electron tomography reveals unbranched networks of actin filaments in lamellipodia." Nat Cell Biol **12**(5): 429-435.
Uruno, T., J. Liu, et al. (2001). "Activation of Arp2/3 complex-mediated actin polymerization by cortactin." Nat Cell Biol **3**(3): 259-266.
Valtschanoff, J. G. and R. J. Weinberg (2001). "Laminar organization of the NMDA receptor complex within the postsynaptic density." J Neurosci **21**(4): 1211-1217.
Vlachos, A., E. Korkotian, et al. (2009). "Synaptopodin regulates plasticity of dendritic spines in hippocampal neurons." J Neurosci **29**(4): 1017-1033.
Wang, X. B., Y. Yang, et al. (2007). "Independent expression of synaptic and morphological plasticity associated with long-term depression." J Neurosci **27**(45): 12419-12429.
Wang, Z., J. G. Edwards, et al. (2008). "Myosin Vb mobilizes recycling endosomes and AMPA receptors for postsynaptic plasticity." Cell **135**(3): 535-548.
Watanabe, N. and T. J. Mitchison (2002). "Single-Molecule Speckle Analysis of Actin Filament Turnover in Lamellipodia." Science **295**: 1083-1087.
Wear, M. A., A. Yamashita, et al. (2003). "How capping protein binds the barbed end of the actin filament." Current biology : CB **13**(17): 1531-1537.
Weed, S. A., A. V. Karginov, et al. (2000). "Cortactin localization to sites of actin assembly in lamellipodia requires interactions with F-actin and the Arp2/3 complex." J Cell Biol **151**(1): 29-40.
Wegner, A. M., C. A. Nebhan, et al. (2008). "N-wasp and the arp2/3 complex are critical regulators of actin in the development of dendritic spines and synapses." J Biol Chem **283**(23): 15912-15920.
Welch, J. M., D. Wang, et al. (2004). "Differential mRNA expression and protein localization of the SAP90/PSD-95-associated proteins (SAPAPs) in the nervous system of the mouse." J Comp Neurol **472**(1): 24-39.
Welch, M. D., J. Rosenblatt, et al. (1998). "Interaction of human Arp2/3 complex and the Listeria monocytogenes ActA protein in actin filament nucleation." Science **281**(5373): 105-108.
Woolner, S. and W. M. Bement (2009). "Unconventional myosins acting unconventionally." Trends in cell biology **19**(6): 245-252.
Wyszynski, M., V. Kharazia, et al. (1998). "Differential regional expression and ultrastructural localization of alpha-actinin-2, a putative NMDA receptor-anchoring protein, in rat brain." J Neurosci **18**(4): 1383-1392.
Wyszynski, M., J. Lin, et al. (1997). "Competitive binding of alpha-actinin and calmodulin to the NMDA receptor." Nature **385**(6615): 439-442.
Yang, N., O. Higuchi, et al. (1998). "Cytoplasmic localization of LIM-kinase 1 is directed by a short sequence within the PDZ domain." Experimental cell research **241**(1): 242-252.
Yang, N., O. Higuchi, et al. (1998). "Cofilin phosphorylation by LIM-kinase 1 and its role in Rac-mediated actin reorganization." Nature **393**(6687): 809-812.
Yang, Y., X. B. Wang, et al. (2008). "Delivery of AMPA receptors to perisynaptic sites precedes the full expression of long-term potentiation." Proc Natl Acad Sci U S A **105**(32): 11388-11393.

Yarar, D., C. M. Waterman-Storer, et al. (2005). "A Dynamic Actin Cytoskeleton Functions at Multiple Stages of Clathrin-mediated Endocytosis." Mol. Biol. Cell **16**(2): 964-975.

Yildiz, A., J. N. Forkey, et al. (2003). "Myosin V walks hand-over-hand: single fluorophore imaging with 1.5-nm localization." Science **300**(5628): 2061-2065.

Yudowski, G. A., M. A. Puthenveedu, et al. (2007). "Real-time imaging of discrete exocytic events mediating surface delivery of AMPA receptors." J Neurosci **27**(41): 11112-11121.

Yuen, E. Y., W. Liu, et al. (2010). "Regulation of AMPA Receptor Channels and Synaptic Plasticity by Cofilin Phosphatase Slingshot in Cortical Neurons." J Physiol **xx**: xx.

Zhang, W. and D. L. Benson (2001). "Stages of synapse development defined by dependence on F-actin." J Neurosci **21**(14): 5169-5181.

Zhou, Q., K. J. Homma, et al. (2004). "Shrinkage of dendritic spines associated with long-term depression of hippocampal synapses." Neuron **44**(5): 749-757.

Zhou, Q., M. Xiao, et al. (2001). "Contribution of cytoskeleton to the internalization of AMPA receptors." Proc Natl Acad Sci U S A **98**(3): 1261-1266.

Zhu, M., T. Yang, et al. (2003). "Mutations in the gamma-actin gene (ACTG1) are associated with dominant progressive deafness (DFNA20/26)." American journal of human genetics **73**(5): 1082-1091.